DEVELOPMENT OF SHORT PULSE ERBIUM-YTTERBIUM AND THULIUM-YTTERBIUM CO-DOPED CLADDING PUMPED FIBER LASERS

IBRAHIM MUHAMMAD BABAR

INSTIUTE OF GRADUATE STUDIES
UNIVERSITY OF MALAYA
KUALA LUMPUR

2017

DEVELOPMENT OF SHORT PULSE ERBIUM-YTTERBIUM AND THULIUM-YTTERBIUM CO-DOPED CLADDING PUMPED FIBER LASER

IBRAHIM MUHAMMAD BABAR

THESIS SUBMITTED IN FULFILMENT OF THE REQUIREMENTS FOR THE DEGREE OF DOCTOR OF PHILOSOPHY

INSTITUTE OF GRADUATE STUDIES
UNIVERSITY OF MALAYA
KUALA LUMPUR

2017

UNIVERSITY OF MALAYA

ORIGINAL LITERARY WORK DECLARATION

Name of Candidate: Ibrahim Muhammad Babar

Matric No: HHE130003

Name of Degree: Doctor of Philosophy

Title of Project Paper/Research Report/Dissertation/Thesis ("this Work"):

DEVELOPMENT OF SHORT PULSE ERBIUM-YTTERBIUM AND THULIUM-YTTERBIUM CO-DOPED CLADDING PUMPED FIBER LASERS.

Field of Study: Physics

I do solemnly and sincerely declare that:

(1) I am the sole author/writer of this Work;
(2) This Work is original;
(3) Any use of any work in which copyright exists was done by way of fair dealing and for permitted purposes and any excerpt or extract from, or reference to or reproduction of any copyright work has been disclosed expressly and sufficiently and the title of the Work and its authorship have been acknowledged in this Work;
(4) I do not have any actual knowledge nor do I ought reasonably to know that the making of this work constitutes an infringement of any copyright work;
(5) I hereby assign all and every rights in the copyright to this Work to the University of Malaya ("UM"), who henceforth shall be owner of the copyright in this Work and that any reproduction or use in any form or by any means whatsoever is prohibited without the written consent of UM having been first had and obtained;
(6) I am fully aware that if in the course of making this Work I have infringed any copyright whether intentionally or otherwise, I may be subject to legal action or any other action as may be determined by UM.

Candidate's Signature Date:

Subscribed and solemnly declared before,

Witness's Signature Date:

Name:

Designation:

ABSTRACT

This research work focuses on the development of fiber lasers operating in both continuous wave (CW) and short pulse modes by using two differentYtterbium co-doped double-clad fibers; Erbium-Ytterbium co-doped fiber (EYDF) and Thulium-Ytterbium co-doped fiber (TYDF) as a gain medium. Both fibers are characterized in both linear and ring cavity configurations by using cladding pumping technique with different fiber lengths. In linear configuration, the EYDF laser operates at 1545.6 nm with slope efficiency of 18.4% at the optimum length of 5m. With the ring configuration, the EYDFL operates at lower efficiency of 4.6%. The TYDF laser (TYDFL) achieves the maximum slope efficiency of 0.88% operating at 1961.4 nm when the gain medium is fixed at 10 m. A multi-wavelength TYDFL operating at 2 μm region is also demonstrated based on nonlinear polarization rotation (NPR) effect. The laser generated triple-wavelength outputs at 1982.12 nm, 1986.69 nm and 1991.26 nm. Q-switched EYDFL is demonstrated by employing Molybdenum disulfide (MoS_2) polyvinyl alcohol (PVA) film as saturable absorber (SA). The laser operates at around 1563 nm with repetition rate in the range of 6.4 kHz to 113.4 kHz as the pump power is varied from 100 to 1250 mW. Q-switched TYDFL is demonstrated by utilizing multi-walled carbon nanotubes PVA film as SA. The laser operates at 1977.5 nm with pulse repetition rate from 18.8 to 50.6 kHz, and corresponding pulse width from 8.6 to 1.0 μs, by varying the pump power from 1591.3 to 2261.5 mW. Finally, EYDFL and TYDFL operating in mode-locking mode are demonstrated by using a graphene PVA film based SA. The EYDFL operates at about 1562.5 nm with repetition rate of 0.92 MHz and pulse width of 387 ns. The mode-locked TYDFL operates around 1942.95 nm with repetition rate of 11.76 MHz when the fiber is pumped from 1487 to 1964 mW. The EYDF and TYDF lasers operate in eye-safe regions of 1.5 and 2 μm, respectively and

thus they find potential applications in optical communication, spectroscopy, material processing, metrology and medicine.

ABSTRAK

Kerja penyelidikan ini tertumpu kepada pembangunan laser gentian yang beroperasi di dalam gelombang berterusan dan juga gelombang denyutan pendek melalui penggunaan dua jenis fiber terdop Ytterbium dua-lapisan. Fiber tersebut ialah fiber terdop-bersama Erbium-Ytterbium (EYDF) dan fiber terdop-bersama Thulium-Ytterbium (TYDF) yang bertindak sebagai medium pertambahan. Kedua-dua gentian ini telah dikaji di dalam konfigurasi linear dan konfigurasi bulatan menggunakan teknik pengepaman berlapis melalui beberapa panjang gentian yang berbeza. Di dalam konfigurasi linear, laser EYDF beroperasi pada panjang gelombang 1545.6 nm dengan kadar kecekapan 18.4% menggunakan kepanjangan gentian optimum 5 m. Apabila menggunakan konfigurasi bulatan, kecekapan laser EYDFL telah menurun pada kadar 4.6%. Bagi laser TYDF pula, kadar kecekapan tertinggi yang direkodkan ialah 0.88% pada panjang gelombang 1961.4 nm menggunakan gentian dengan kepanjangan 10 m. Laser TYDFL juga menghasilkan banyak cabang gelombang pada julat 2 μm melalui kesan putaran polarisasi linear (NPR) iaitu pada panjang gelombang 1982.12, 1986.69 dan 1991.26 nm. Laser suis-Q EYDFL dijana dengan menggunakan kepingan Molybdenum disulfida (MoS_2) yang dihoskan oleh polyvinyl alkohol (PVA) sebagai penyerap tertepu (SA) dimana ia telah menghasilkan laser pada panjang gelombang 1563 nm dengan julat denyutan dari 6.4 hingga 113.4 kHz berdasarkan perubahan kuasa pam dari 100 hingga 1250 mW. Laser suis-Q TYDFL pula dihasilkan dengan menggunakan karbon bertiub nano yang berlapis-lapis sebagai SA dimana laser tersebut beroperasi pada panjang gelombang 1977.5 nm. Kadar denyutan yang direkodkan ialah dari 18.8 hingga 50.6 kHz manakala lebar denyutan pula adalah dari 8.6 hingga 1.0 μs berdasarkan perubahan kuasa pam dari 1591.3 to 2261.5 mW. Akhir sekali, laser mod-mengunci EYDFL dan TYDFL dihasilkan dengan menggunakan kepingan PVA grafin sebagai SA. Laser mod-

mengunci EYDFL beroperasi pada panjang gelombang 1562.5 nm dengan kadar denyutan 0.92 MHz dan lebar denyutan 387 ns manakala laser mod-mengunci TYDFL pula beroperasi pada panjang gelombang 1942.95 nm dengan kadar denyutan 11.76 MHz berdasarkan perubahan kuasa pam dari 1487 hingga 1964 mW. Laser EYDF dan TYDF beroperasi di dalam julat panjang gelombang yang selamat untuk mata manusia iaitu pada 1.5 dan 2 μm. Oleh itu, laser-laser ini berpotensi untuk digunakan dalam bidang komunikasi, spektroskopi, pemprosesan bahan, metrology dan perubatan.

ACKNOWLEDGEMENTS

All praises are to the Almighty Allah (swt) for providing me this opportunity and granting me the capability to proceed successfully. I would like to thank my supervisor Prof. Dr. Sulaiman Wadi Harun, who has not only been patient and tolerant to me in my quest of seeking knowledge, but also generous in sharing his knowledge, expertise and experience in the field of Photonics. I managed to complete this thesis with his invaluable guidance and encouragement.

I would like to thank my second supervisor Professor Dr. Ulung Datuk Harith Ahmad for his willingness to undertake supervision in my experimental work, guidance and support to accomplish this task. I have been fortunate to work under them who cared about my developments both as a researcher and as a person.

My appreciation also goes to all those people who helped me to complete this research work here at the Photonics Research Centre, University Malaya. It is a pleasure to thank them.

I would like to thank my parents and family for their continuous encouragement and support during the course of this work and my stay away from them. Especially to my late father who passed away recently in the month of August, 2016 for his support, encouragement, motivation and appreciation of my work and decision to pursue Ph.D. studies.

TABLE OF CONTENTS

LIST OF FIGURES

LIST OF SYMBOLS AND ABBREVIATIONS

Al_2O_3	Aluminium Oxide
AlGaAs	Aluminium Gallium Arsenide
CNT	Carbon nanotubes
Cr:YAG	Chromium doped Yttrium Aluminum Garnet
CVD	chemical vapor deposition
CW	Continuous-wave
DIAL	Differential absorption Lidar
DMF	Dimethylformamide
DS	Dissipative soliton
EDF	Erbium-doped fiber
EDFL	Erbium-doped fiber laser
Er^{3+}	Erbium ion
ESA	Excited-state absorption
ESA	Excited state absorption
EYDFL	Erbium-Ytterbium doped fiber laser
FWM	Four-wave mixing
GHz	Gigahertz
GVD	Group velocity dispersion
InGaAs	Indium Gallium Arsenide
KLM	Kerr-lens mode-locking
LASER	Light Amplification by the Stimulated Emission of Radiation
Lidar	Light Detection And Ranging
LMA	large mode area
LPE	Liquid phase exfoliation
MHz	Megahertz
MMC	Multimode combiner
MOPA	Master oscillator power amplifier

MoS_2	Molybdenum di Sulfide
MWCNT	Multi walled carbon nanotube
NA	Numerical aperture
Nd:YAG	Neodymium-doped Yttrium Aluminium garnet
Nd:YLF	Neodymium-doped Yttrium Lithium Fluoride
NLSE	Nonlinear Schrodinger equation
NPR	Nonlinear polarization rotation
OPM	Optical power meter
OSA	Optical spectrum analyser
OSNR	Optical to signal noise ratio
P_2O_5	Phosphorus Pentoxide
PC	Polarization controller
PVA	Poly Vinyl Alcohol
RF	Radio frequency
SA	Saturable absorber
SESAM	Semiconductor saturable absorption mirror
SMF	Single mode fiber
SNR	Signal to noise ratio
SPM	Self-phase modulation
SPM	Self-phase modulation PC
TBP	Time Bandwidth Product
TDF	Thulium-doped fiber
TDFL	Thulium (Tm^{3+}) doped fiber lasers
THz	Terahertz
Tm_2O_3	Thulium Oxide
Tm^{3+}	Thulium ion
TMD	Transition metal dichalcogenides
TYDFL	Thulium-Ytterbium doped fiber laser

UV	Ultraviolet
Y_2O_3	Yttrium Oxide
Yb	Ytterbium
Yb_2O_3	Ytterbium Oxide
Yb^{3+}	Ytterbium ion
YDF	Ytterbium-doped fiber
YDFL	Ytterbium-doped fiber laser
$\alpha(\lambda)$	Absorption coefficient
$g(\lambda)$	Gain coefficient
β_2	Group velocity dispersion parameter
$sech^2$	Hyperbolic-secant-squared

CHAPTER 1: INTRODUCTION

1.1 Background

Light Amplification by the Stimulated Emission of Radiation (LASER) is a powerful source of photons that have been used in many applications. It works based on stimulated emission where the amplification of light is achievable under condition of population inversion. Where electrons encounter pump electrons and lose energy by emitting an exactly same photon through stimulated emission. In addition to the gain media, another essential component of the laser is optical cavity (resonator) in which the light can be oscillated and get amplified. As long as the gain is larger than the losses, the power of the light in the laser cavity quickly rises. Significant power output is thus achieved only above the so-called laser threshold that is the power where the small-signal gain is just sufficient to compensate the cavity loss.

Fiber lasers have been becoming a promising alternative to the conventional solid-state laser systems due to their advantages such as compact size, superior beam quality and reliability, lower maintenance, high electrical efficiency, great output power, mobility, low cost and ruggedness. The first fiber laser was demonstrated by Elias Snitzer in 1963 and its commercial devices were first appeared in the market in the late 1980s. These lasers used single-mode diode pumping and attracted users because of their large gains and the feasibility of single-mode continuous-wave (CW) lasing for many transitions of rare-earth ions, not achievable in the conventional crystal based laser system. They are capable to emit a few tens of milliwatts of power by using a specialized optical fiber doped with rare earth elements such as Ytterbium, Erbium and Thulium as the gain medium. These rare-earth elements have many advantages such as simple energy levels, high quantum efficiency, long life time at high level and a wide absorption spectrum. These advantages have led to the development of high power

fiber lasers (Halder et al., 2012; Pal et al., 2010; Simpson et al., 2008) for many applications such as medicine, industry, military, communication and etc. (KINCADE, 2005; Mary et al., 2014; Mingareev et al., 2012).

In the late 1980s, a double-clad fiber was introduced for high power fiber laser applications (Snitzer et al., 1988). This fiber has a core surrounded by two cladding layers. The core is doped with active dopant material that functions to guide and amplify the signal light. The pump light guided by the inner cladding is used to provide the energy needed to allow amplification and lasing in the core of the fiber. In order to confine the light into the core, the outer cladding must have lower refractive index, compared to the core (Sen et al., 2015). Double-clad fiber is advantageous compared to that of the standard single-clad fiber because it has low dispersion over a much wider wavelength range.

The most commonly developed fiber laser uses rare earth material named Ytterbium, which is doped in the core of active fiber. The Ytterbium-doped fiber (YDF) serves as a highly efficient gain medium to operate in the 1 μm band. It can offer high power conversion efficiencies and larger power levels than erbium-doped fiber lasers (EDFLs). Therefore, Ytterbium-doped fiber laser (YDFL) is now used extensively in industrial, medical, and high quality imaging applications. In addition, Ytterbium has acquired a prominent role in the form of the trivalent ion Yb^{3+}, which is used as a laser-active dopant in a variety of host materials. Particularly, double-clad YDF based fiber lasers have attracted extensive attention and have been widely investigated for several reasons. First, YDFLs have a broad bandwidth which is larger than 150 nm; this large fluorescence spectral range is well adapted for tunable laser application. Second, they have high efficiency up to 90%, because the laser operates based on a quasi-three-level energy system that can avoid any pump or signal excited-state absorption (ESA). Third, Yb^{3+} ion presents a large absorption cross-section within 850 to 1070 nm, allowing for a

low-cost commercially available laser diode as the pump source (M. Fermann et al., 1988).

However, other than emission at 1 μm band, Ytterbium also can be used as the sensitized element for Erbium and Thulium for the emission band at 1.5 μm and 2 μm. These bands would also give several industry applications such as in area of communication, remote sensing and biomedical applications. Yb^{3+} has the advantage to present only two multiplets: the ground-state level $^2F_{7/2}$ and the excited-state level $^2F_{5/2}$, corresponding the highly efficient absorption in the range of 900-1000 nm (Pask et al., 1995). This particular energy level structure is highly desirable for efficient absorption of commercially available laser diodes emitting around 900-980 nm and avoiding any undesirable ESA under intense optical pumping. Based on the above consideration, ytterbium co-doping in erbium and Thulium doped fiber is investigated and become an interest area of research. In this work, various fiber lasers operating in CW, Q-switching and mode-locking modes are proposed and demonstrated using Erbium-Ytterbium and Thulium-Ytterbium co-doped fibers as a gain medium to operate at 1550 nm and 1900 nm region, respectively. All the fiber lasers are based on a low cost multimode pumping.

1.2 Problem Statement

Lasers operating in CW or quasi-CW mode have limited optical output power, depending on the maximum available pump power. The laser peak output power can be improved by concentrating the available energy in a single, short optical pulse, or in a periodic sequence of optical pulses as in a Q-switched fiber laser. Q-switching is a technique that enables the generation of an optical pulse at repetition rate in kHz region and pulse width in a range of microseconds to nanoseconds by sudden switching of the cavity loss. Compared to CW fiber lasers, high-peak-power *Q*-switched fiber lasers are

practically useful in numerous applications, such as range finding, remote sensing, industrial processing and medicine (El-Sherif & King, 2003; Nayar et al., 1998; Nettleton et al., 2000). Although Q-switching does not produce the ultra-short pulses as in mode-locked lasers, it has several advantages such as inexpensive, easy to implement and efficient in extracting energy stored in upper laser level.

On the other hand, mode-locked laser is obtained based on phase locking of many longitudinal modes of laser beam in which photons from all modes are absorbed and released simultaneously at the end of complete one round-trip of the oscillating photons(Haus, 2000). Compared to the Q-switched laser, the repetition rate of mode-locked laser is higher (MHz) and it depends on the laser cavity length that determines its one round-trip time. Mode-locked lasers have attracted a lot of attention in recent years since they could provide ultra-short pulses, which are important for many applications (Jung et al., 2015; Mary et al., 2014; Nishizawa, 2014).

The Q-switched and mode-locked fiber lasers can be realized by either active or passive techniques. The active technique is based on an active loss modulation by using mechanical, electro-optic or acousto-optic based modulators. However, such techniques require complicated electronic circuits and have limited gain bandwidth. The attention then moves towards the passive techniques which have simpler configuration, low cost, more compact in size and reliable operation without high voltages. Moreover, passive technique is more convenient where the cavity design can be simplified to eliminate the need for external electronics.

The passive Q-switched and mode-locked fiber lasers can be achieved by utilizing saturable absorbers (SAs) inside the laser cavity. There are various kind of SAs developed such as carbon nanotubes (CNTs), semiconductor saturable absorption mirror (SESAM) and ion-doped crystals. SESAM have been chosen commercially to generate passive mode-locked laser since it possesses higher stability and flexibility, but it has

certain drawbacks such as higher cost to implement and limited range of optical response. Therefore, numerous works have been carried out by researchers to discover alternative lower cost SA materials.

Recently a great interest have also been given on the development of both solid state and fiber lasers operating in 2 micron region because of its wide applications in medicine, remote sensing, Light Detection and Ranging (LIDAR), range finding, and molecular spectroscopy (Baudelet et al., 2010; Eichhorn, 2010; Opsommer et al., 2001). The strong absorption by water and thus strong absorption by human tissues at 2 μm also nominate it as an ideal wavelength for biological and medical applications including laser angioplasty in the coronary arteries, ophthalmic procedures, arthroscopy, laparoscopic cholecystectomy and refractive surgeries. In addition, other features of 2 μm laser such as the lower atmospheric absorption, smaller scattering and "eye-safe" property make the wavelength desirable for material processing, ranging, low altitude wind shear and remote sensing, which includes Doppler Lidar (Light Detection And Ra nging) wind sensing and water vapor profiling by differential absorption Lidar (DIAL). Such wavelength is also an ideal pump source for mid-infrared optical material. The 2 μm laser can be realized using a Thulium-doped fiber (TDF) as the gain medium. Most of the commercial TDF is based on single-clad structure or core pumping approach.

Recently carbon nanotubes and graphene are normally used as the SA for the *Q*-switched fiber lasers. These SAs are a comparatively simple and cost effective alternative compared to SESAM. This is due to their inherent advantages, including good compatibility with optical fibers, low saturation intensity, fast recovery time, and wide operating bandwidth, while the other types of crystal and semiconductor based SAs cannot be used for all fiber laser structure due to their relatively big volume. However, most of the current works are focusing on Erbium-doped fiber lasers (EDFLs) based on single mode pumping. There are still a lack of research works on Q-switching

and mode-locking both in 1.5 micron and 2 micron regions using a double-clad active fiber. In this work, low cost multi wall carbon nanotube (MWCNT), Graphene and Molybdenum di Sulfide ($MoS_{2)}$ based SAs are developed for Q-switching and mode-locking applications in Yb co-doped fiber lasers. The lasers are based on low cost multimode pumping.

1.3 Research Objectives

The main objective of this research is to design and construct efficient and low cost Q-switched and mode-locked fiber lasers using double clad Erbium-Ytterbium doped fiber (EYDF) and double clad Thulium-Ytterbium doped fiber (TYDF) as the gain medium to operate in 1.5 and 2.0 μm regions, respectively. This can be achieved by performing the following tasks;

1) To demonstrate CW fiber laser using a double-clad EYDF and TYDF as the gain medium to operate at 1.5 and 2 micron region, respectively. A cladding pumping approach is used in this study.
2) To fabricate and characterize various types of passive saturable absorbers based on MoS_2, multi-walled carbon nanotubes (MWCNTs) and graphene.
3) To demonstrate Q-switched double clad Erbium-Ytterbium co-doped fiber laser (EYDFL) and double clad Thulium-Ytterbium co-doped fiber laser (TYDFL) by using a simple fabricated passive SA in conjunction with a low cost multimode pumping.
4) To demonstrate new passively mode-locked fiber lasers using double-clad EYDF and TYDF as a gain medium in conjunction with multimode pumping.

1.4 Organization of the thesis

This thesis is organized into five chapters which comprehensively demonstrate the development of CW, Q-switched and mode-locked fiber lasers operating in 1.5 and 2.0 μm region using double-clad Erbium-Ytterbium and Thulium-Ytterbium co-doped fibers as the gain medium. Chapter 1 gives a brief description on the background of the study. The motivation and objective of this study are also highlighted. Chapter 2 furnishes a detailed literature on the basic theory of optical fibers, fiber lasers and dynamics of Q-switched and mode-locked fiber lasers. It includes description of double-clad fiber structure along with some details of Erbium-Ytterbium and Thulium-Ytterbium co-doped double clad fibers.

Chapter 3 presents a thorough study on both EYDFL and TYDFL operating in CW mode based on low cost cladding pumping by utilizing a double-clad fiber as a gain medium. The performance and optimization of both fiber lasers are investigated for both linear and ring configuration. Multi-wavelength fiber lasers are also demonstrated based on both gain media.

In chapter 4, new passively Q-switched fiber lasers are demonstrated using EYDF and TYDF as a gain medium to operate at 1550 nm and 1900 nm region, respectively. Passively Q-switched ring-cavity EYDFLs are demonstrated using nonlinear polarization rotation technique and few-layer MoS_2 based SA. On the other hand, Q-switched TYDFL is demonstrated using homemade MWCNTs based SA. Both MoS_2 and MWCNTs are embedded into Poly Vinyl Alcohol (PVA) film, which is then sandwiched between two fiber ferrules and incorporated into a laser ring cavity for Q-switching pulse generation.

Chapter 5 aims to develop new passively mode-locked fiber lasers using double-clad EYDF and TYDF as a gain medium to operate at 1550 nm and 1900 nm region, respectively. It uses a newly developed graphene embedded into PVA as the mode-

locker between two fiber ferules. Finally, Chapter 6 summarizes the findings for this Ph.D work and future outlook.

CHAPTER 2: LITERATURE REVIEW

2.1 Introduction

The development of the LASER (Light Amplification by Stimulated Emission of Radiation) was the first important step in the establishment of the fiber optics industry. Fiber lasers have gone through intense development in the last two decades since they are compact, reliable and environmentally stable compared to their bulk counterparts. They are ideally suited in many applications such as material processing, telecommunications, spectroscopy and medicine (Bouma et al., 1998; Henderson et al., 1993; J. Liu, Wang, et al., 2012; Polder & Bruce, 2012; Sorokina et al., 2014; Spiers et al., 2011). Despite the progress already made by fiber lasers, there is still much room for the development of new lasers intended for specific applications. The objective of this thesis is to develop low cost pulsed fiber lasers operating at 1.5 μm and 2.0 μm spectral regions using an Erbium-Ytterbium co-doped fiber (EYDF) and Thulium-Ytterbium co-doped fiber (TYDF), respectively as the gain medium in conjunction with a newly developed passive saturable absorber. There are a number of interesting principles that come into play in the operation of the Q-switched and model-locked fiber lasers. This chapter briefly introduces the main principles relevant to understand the operation of such lasers.

2.2 Optical fibers

The material of choice for fiber lasers and fiber amplifiers is glass fibers, doped with laser-active rare earth ions (in the fiber core). These ions absorb pump light, mostly at a shorter wavelength than the laser or amplifier wavelength (except in up conversion lasers), which excites them into some metastable levels to produce light amplification through stimulated emission. Such doped fiber is normally referred to active fiber,

which serves as gain medium to provide high gain efficiency, resulting mainly from the strong optical confinement in the fiber's waveguide structure (D. R. Paschotta).

The chemical composition of the host glass of the fiber core strongly influences the performance and practical applications of an active fiber. Due to limited transparency range of host glass certain laser transitions may exclude, for example mid-infrared lasers are difficult to obtain with silicate fibers, which are strongly absorbing for wavelengths above 2 μm. Moreover glass composition limits the maximum concentration of the dopant ions that can be incorporated without excessive clustering, which would result in quenching effects and an increase in propagation losses. It also effects optical transitions of the rare earth ions, particularly, the emission and absorption cross sections, absorption and emission bandwidth, total transition rates and thus the metastable level lifetimes, etc. The rate constants for energy transfers between different ions also depend on the chemical composition. To a large extent the maximum phonon energy of the host glass determines the rate of multi-phonon emission processes, thus the speed of non-radiative transfers between certain levels. This effect can be strong: certain levels may be long-lived (multiple milliseconds) in heavy-metal fluoride glasses, but very short-lived (few microseconds) in silicate glasses.

In rare-earth doped fibers, one rarely uses pure silicate glass, but the glass modified by some additional dopants like aluminum, germanium or phosphorous. These dopants, such as aluminum improve the solubility of rare earth ions and thus allow higher concentration of these ions without quenching of the upper state life time. Others effect refractive index, spectral shape of the optical transitions or the rate of energy transfers (Digonnet, 2001b).

Recently, the interest in co-doped fibers is also increasing to improve efficiency of laser performances. These fibers are doped with two different kinds of rare earth ions, for example EYDF is doped with both erbium and ytterbium ions. It possesses normally

a significantly higher concentration of ytterbium. When pumped with 980 nm laser diode, most of the pump light is absorbed by ytterbium ions (called sensitizer ions), bringing these into their excited states. From there, the energy can be efficiently transferred to the erbium ions non-radiatively, to lase in the 1.5-μm spectral region. Compared with purely erbium-doped fibers, EYDFs offer much higher pump absorption per unit length and can therefore is used for fiber devices with much shorter lengths. For the energy transfer to be efficient, the doping concentrations have to be well balanced, and the core composition must be suitable. Co-dopants can also be used for quenching the lower-state population in gain systems with self-terminating laser transitions. For example, praseodymium co-doping allows for relatively efficient operation of 2.7-μm erbium fiber lasers.

Besides all the properties of a passive (un-doped) optical fiber, such as the guiding properties (effective mode area, numerical aperture, cut-off wavelength, bend losses), nonlinearities, etc., the active fiber also have several other properties that are required for photon generation and amplification. One of the important parameters is the rare-earth doping concentration, specified in ppm wt. (parts per million by weight). A higher doping concentration permits efficient pump absorption in a shorter length and thus reduces the effect of nonlinearities in high peak power devices. But, it can also lead to concentration quenching. Wavelength-dependent effective absorption, emission cross sections, excited state absorption (ESA) cross sections and upper-state lifetime are required for calculating the wavelength tuning behavior, power efficiency, etc. Also parameters for quantifying the speed of energy transfer processes are important particularly for co-doped fibers.

Giles parameters such as the absorption coefficient $\alpha(\lambda)$ of the fiber with all laser-active ions in the ground state, and the gain coefficient $g(\lambda)$ for the fiber with all laser-active ions in the upper laser level are also important. These parameters depend on

the doping concentration, effective mode area and effective cross sections. A variety of measurement techniques are used for measuring these parameters. Such as absorption cross sections (for known doping concentrations) can be found using White-light absorption spectra. Fluorescence spectra are used to obtain Emission cross sections. Upper-state lifetimes are generally obtained from fluorescence measurements with pulsed pumping, and ESA parameters can be obtained in experiments with a modulated pump power. These parameters are used in laser and amplifier models based on rate equations, to predict or check the performance of fiber laser or amplifier devices, the effect of possible modifications, etc. (D. R. Paschotta).

2.3 Double-clad fiber

To overcome the three limitations (small core radius, larger attenuation, and dispersion) of high speed transmission, a new type of optical fiber called double-clad optical fiber is proposed. It consists of three layers of optical material instead of the usual two. The inner-most layer is called the core, surrounded by the inner cladding while the inner cladding is surrounded by the outer cladding. All the three layers are made of materials with different refractive indices. The typical refractive index profiles are shown in Fig. 2.1. Generally the outer cladding is made of a polymer material rather

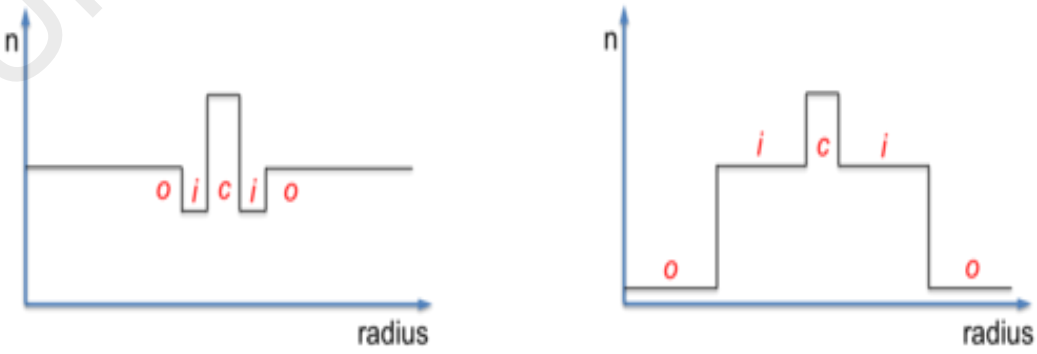

Figure 2.1: Typical refractive index profiles of double clad optical fiber (encyclopedia).

than glass. In most cases the inner cladding has a higher refractive index than the outer cladding. This enables the inner cladding to guide light by total internal reflection in the same manner the core does, but for a different range of wavelengths. Also the inner cladding has larger area and higher numerical aperture so that it can support large number of modes. This enables laser diodes, which possess high power but low brightness, to be used as the optical pump sources.

The pump light can be easily coupled into the large inner cladding, and propagates through the inner cladding while the signal propagates in the smaller core. The doped core gradually absorbs the cladding light as it propagates, driving the amplification process. This pumping scheme is often called cladding pumping, which is an alternative to the conventional core pumping, in which the pump light is coupled into the small core. This pumping scheme has revolutionized the design of fiber amplifiers and lasers (Po et al., 1989). Using this method, modern fiber lasers can produce continuous power up to several kilowatts, while the signal light in the core maintains near diffraction-limited beam quality (Y. e. Jeong et al., 2004).

The shape of the cladding is very important, especially when the core diameter is small compared to the size of the inner cladding. Circular symmetry in a double-clad fiber seems to be the worst solution for a fiber laser; in this case, many modes of the light in the cladding miss the core and hence cannot be used to pump it (Bedö et al., 1993). The shape of the inner cladding is normally non-circular to achieve better absorption of the pump in the doped core region. Fig. 2.2 shows different inner clad shapes of rare-earth-doped fibers. Thus, cladding-pumped fiber lasers can be treated as devices to generate diffraction-limited single-mode laser output using multimode pump lasers. With large size inner cladding, very high pump powers can be launched into a double-clad fiber. However, the core size limits the output power to a certain level due to the onset of optical damage and thermal effects (Upadhyaya, 2014).

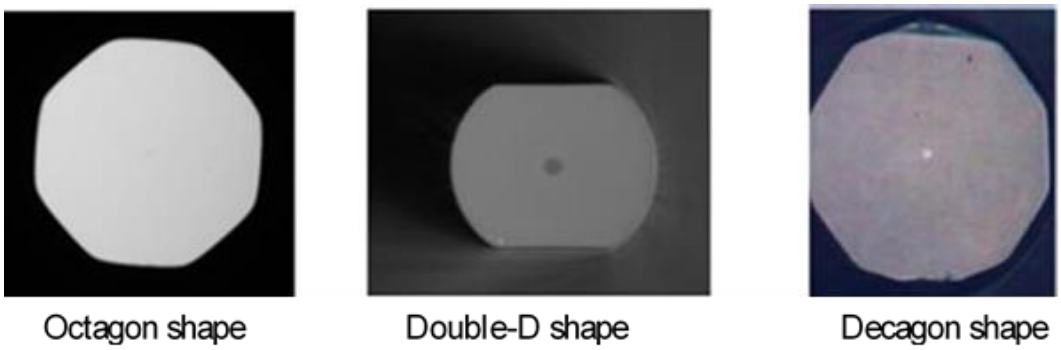

Figure 2.2: Cross-sectional images of a few inner cladding shapes used in double-clad fiber lasers (a) Octagon (b) double-D (c) Decagon (Sen et al., 2015).

2.4 Ytterbium co-doped fiber

Rare earth doped fiber lasers have been co-doped with Ytterbium (Yb) to generate more efficient sources. Ytterbium is one of the most versatile laser ions in a silica-based host. Sensitization of rare earth fibers by Yb^{3+} shows several advantages. First, silica based glasses can be heavily doped with Yb^{3+}, it facilitates strong absorption of the pump light, thereby greatly reducing the fiber length requirement. Yb^{3+} does not introduce absorption bands at longer wavelengths, so that a higher concentration does not affect the fiber loss at the laser wavelength. Barnes et al. (1989) has compared the output power characteristic of an EYDF laser (EYDFL) with a singly Erbium-doped silica fiber laser. It was found that the EYDFL exhibited a slightly lower threshold and higher slope efficiency (against launched pump power) than the conventional EDF laser (Barnes et al., 1989).

Secondly, a higher concentration of Yb^{3+} reduces the mean distance between ions and thus facilitates energy transfer between them without the effect of concentration quenching. Thirdly, the absorption band of Yb^{3+} is very broad (M. Fermann et al., 1988) and provides a wide range of possible pump wavelengths, typically about 300 nm, stretches from below 850 nm to above 1070 nm as shown in Fig. 2.3. Fig. 2.3 shows the absorption and emission cross-section of an Ytterbium fiber

(Pask et al., 1995). The absorption and emission spectra are attributed to the $^2F_{7/2} \rightarrow {}^2F_{5/2}$ transition as illustrated in the inset of Fig. 2.3. Yb doped silica fibers can thus be pumped with a wide selection of solid-state lasers, including, Aluminium Gallium Arsenide (AlGaAs) (800–850 nm) and Indium Gallium Arsenide (InGaAs) (980 nm) laser diodes, and Neodymium-doped Yttrium Lithium Fluoride (Nd:YLF) (1047 nm) and Neodymium-doped Yttrium Aluminium garnet (Nd:YAG) (1064 nm) lasers. This broad pump band also relaxes considerably both the requirements for pump wavelength and its stability with temperature. The fourth advantage is that Yb^{3+} likely to improve the output power stability with temperature of the fiber laser. Because of its broad absorption band, it can sustain the variation in the pump wavelength from laser diode caused by temperature variation (Taccheo et al., 1998).

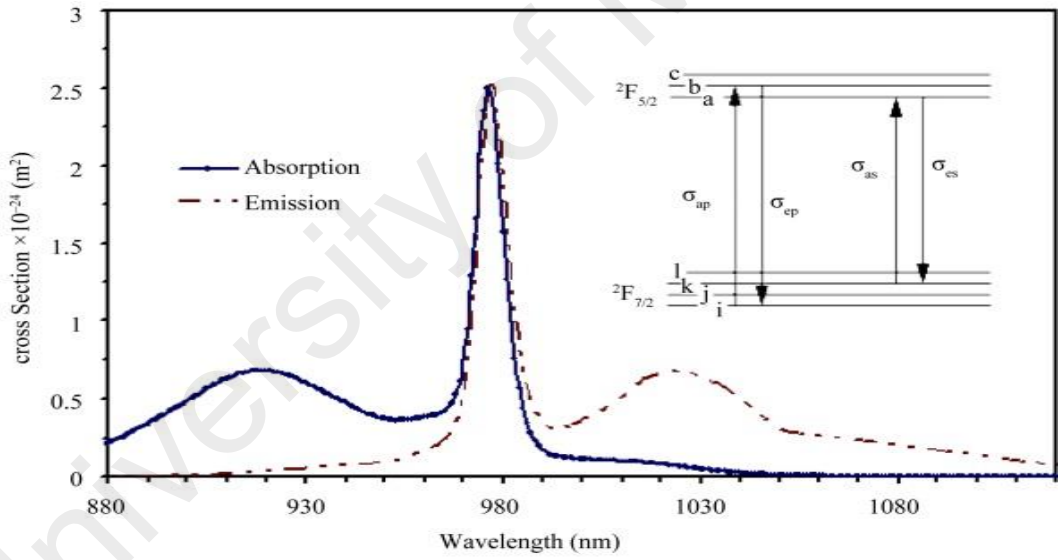

Figure 2.3: The absorption and emission cross-section of Yb ions. Inset shows an energy level diagram of the Ytterbium fiber (Pask et al., 1995).

As illustrated in the inset of Fig. 2.3, Yb^{3+} exhibits only a ground state ($^2F_{7/2}$) and a metastable state ($^2F_{5/2}$) spaced by approximately 10,000 cm^{-1}. All other levels are in the Ultraviolet (UV). The radiative lifetime of the $^2F_{5/2}$ state is typically in the range of 700–1400 μs, depending on the host (R Paschotta et al., 1997). The absence of higher energy levels greatly reduces the incidence of multi-phonon relaxation and ESA, and, therefore, should facilitate the development of high-power lasers. These combined

features allow for very strong pump absorption and very short fiber lasers. Owing to these properties, Ytterbium is co-doped with different rare earth ions in glass fibers. The idea is simple, the glass host is doped with a laser ion and co-doped, or sensitized, with a second ion that (1) absorbs strongly in a band not available to the laser ion, and (2) efficiently transfers its energy to the laser ion.

2.4.1 Erbium co-doping with Ytterbium

The working mechanism of EYDF is illustrated in Fig. 2.4. Absorption of a pump photon by an Yb^{3+} promotes an electron from ground state $^2F_{7/2}$ to the $^2F_{5/2}$ manifold, which is followed by efficient energy transfer from this level to the $^4I_{11/2}$ level of erbium and non-radiative decay to the upper laser level $^4I_{13/2}$. This process is efficient; the electron relaxes preferentially to the Er^{3+} upper laser level state, rather than back to the $^2F_{5/2}$ level of the Yb^{3+} ion. The energy transfer efficiency can be improved by co-doping with Phosphorus Pentoxide ($P_2O_{5)}$ (Mindly et al., 1993), which increases the non-radiative relaxation rate from the $^4I_{11/2}$ level to $^4I_{13/2}$ level and reduces energy transfer back to the Yb^{3+} donor (Grubb et al., 1991). In phosphate glasses, the transfer efficiency can be as high as 85%. Ytterbium co-doping is not only beneficial to Erbium doped double clad fibers but also with other fibers like Thulium doped double clad fiber.

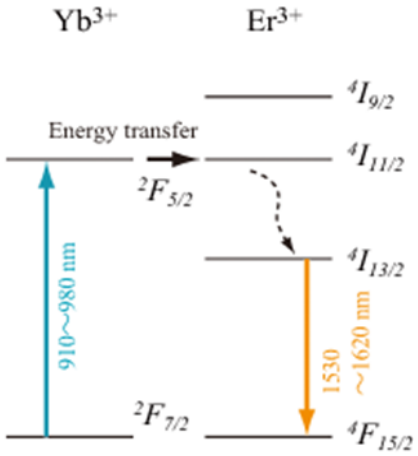

Figure 2.4: Ytterbium ion to Erbium ion energy transfer mechanism (Tanguy et al., 1998).

2.4.2 Thulium co-doping with Ytterbium

For Thulium ions, energy transition from $^3F_4$ to $^3H_6$ results in quantum efficiency near 2 μm due to cross-relaxation energy transfer between Thulium ions as shown in Fig. 2.5. During this process two ground-level Thulium ions are excited to the upper lasing level of $^3H_6$ by absorbing only one pump photon near 790 nm. This suggests that one excited Tm^{3+} ion at the $^3H_4$ level generates two Tm^{3+} ions at the $^3F_4$ upper laser level. However, commercial high power diodes required for the excitation in this wavelength range are difficult to obtain as well as very costly. Pumping Thulium-doped fibers at another pumping wavelength of 1200 nm or 1600 nm is complicated because semiconductor laser diodes with sufficient power are not commercially available. Another viable solution is to co-dope the Thulium fiber with Ytterbium ions so that it can be pumped by a commercially available laser diode operating within 905 to 980 nm. This is made possible by the energy transfer from Ytterbium to Thulium ions similar to the case of Yb^{3+} sensitized Er^{3+}-doped fibers (Pal et al., 2010).

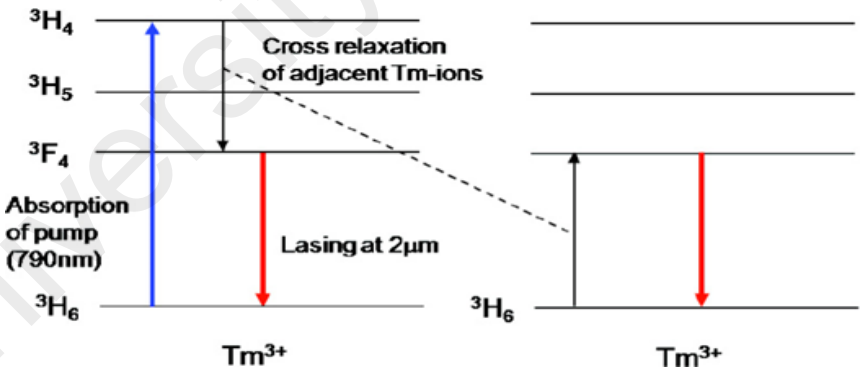

Figure 2.5: Cross relaxation energy transfer between Tm ions.

As shown in the Fig. 2.6, the sensitization of Tm^{3+} doped fibers with Yb^{3+} is possible due to $^3H_5$ level of Tm^{3+} which is quasi-resonant with the excited Yb^{3+} level ($^2F_{5/2}$). The up-conversion system has long been proposed based on Tm^{3+}-Yb^{3+} co-doped glass and fibers (Pal et al., 2010), but only more recently the concept is used for the 2- μm fiber laser application (Harun et al., 2011).

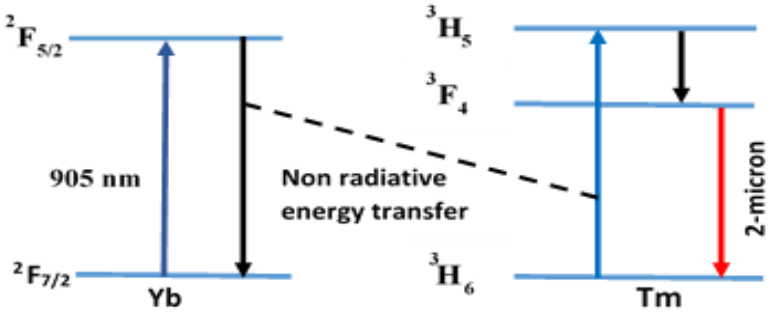

Figure 2.6: Ytterbium to Thulium energy transfer.

2.5 Q-switched lasers

Q-switching, also known as giant pulse formation or Q-spoiling, (Früngel, 2014) is a powerful technique by which a laser can be made to produce a pulsed output beam. This technique is capable of producing light pulses with extremely high (gigawatt) peak power, much higher than the continuous wave mode (constant output) operation of the laser. As compared to mode-locking, another technique for pulse generation with lasers, Q-switching leads to much lower pulse repetition rates, much higher pulse energies, and much longer pulse durations than it. Q-switching was first proposed in 1958 by Gordon Gould, (Taylor, 2002) and demonstrated in 1961 or 1962 by R.W. Hellwarth and F.J. McClung using electrically switched Kerr cell shutters in a ruby laser (McClung & Hellwarth, 1962).

A Q-switched pulse laser is achieved by putting some type of variable attenuator inside the laser's optical resonator. When the attenuator is functioning, light which leaves the gain medium does not return or cannot travel back and forth, this restricts the lasing, putting the optical cavity in low Q factor or high loss condition. A high Q factor represents low resonator losses per roundtrip. The variable attenuator is commonly known as "Q-switch".

First the laser medium is pumped while the Q-switch is set to prevent feedback of light into the gain medium (producing an optical resonator with low Q factor). This

produces a population inversion by losing pump energy through absorption by electrons, thus pumping electrons to higher energy level; this accumulates energy in the gain medium. But laser operation cannot yet begin, since there is no feedback from the resonator. As the rate of stimulated emission depends on the amount of light entering the medium, the amount of energy stored in the gain medium increases as the medium is pumped. Due to losses from spontaneous emission and other processes, the stored energy takes some time to reach some maximum level; the medium is said to be gain saturated. At this point, the Q-switch is quickly changed from low to high Q, allowing feedback and the process of optical amplification by stimulated emission to begin. Since large amount of energy already stored in the gain medium, the intensity of light in the laser resonator builds up very quickly; this also causes the energy stored in the medium to be depleted almost as quickly. This develops a short pulse of light output from the laser, known as a giant pulse, which may have very high peak intensity. Generally, several round trips are needed to completely depopulate the upper energy level and several more round trips to empty the optical cavity so the duration of the pulse is greater than one round trip. The peak power (the pulse energy divided by its duration) of these lasers can be in the megawatt range or even higher. There are two main techniques for Q-switching: active and passive.

2.5.1 Active Q-switching

In active Q-switching, the losses are modulated with an active control element so-called active Q-switcher, either by using an acousto-optic or electro-optic modulator. Fig. 2.7 shows the temporal evolution of gain and losses in an actively Q-switched laser. As shown in the figure, the pulse is formed shortly after an electrical trigger signal arrives. There is also mechanical type Q-switchers such as spinning mirrors, used as end mirrors of laser resonators. The pulse repetition rate can be controlled by the active

modulator in an actively Q-switched laser. Higher repetition rates lead to lower pulse energies. The switching time of the modulator can be much longer than the pulse duration, since it takes many resonator round trips for an intense pulse to be formed. If it is too long, however, may lead to double pulses or to certain instabilities.

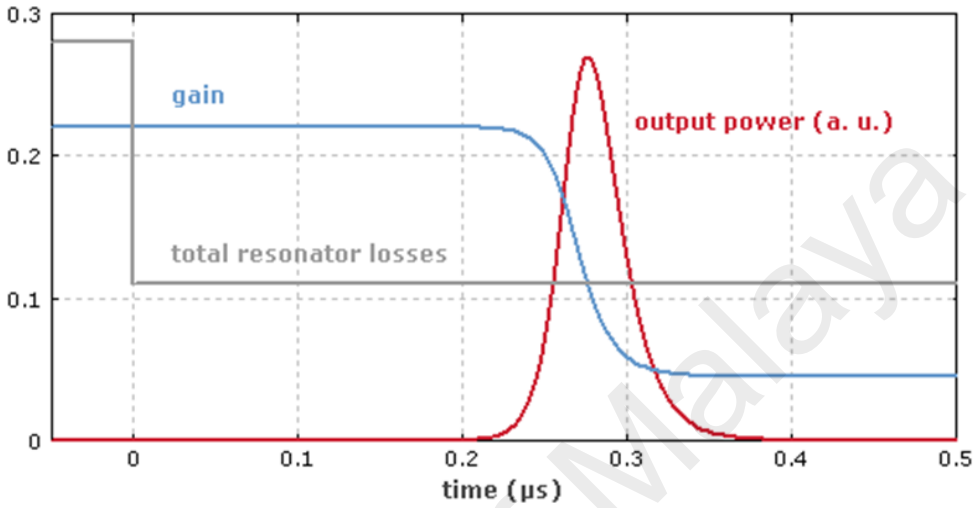

Figure 2.7: Temporal evolution of gain and losses in an actively Q-switched laser. The Q switch is activated at t = 0, the power starts to rise exponentially at this point, but becomes high only after ≈ 0.2 µs (D. R. Paschotta) .

2.5.2 Passive Q-switching

In passive Q-switching, the losses are modulated or controlled by optical cavity light, rather than some external electrical source. A saturable absorber device is normally used as a Q-switcher in this technique. The transmission of this device increases when the intensity of light exceeds some threshold. The material may be an ion-doped crystal like Cr:YAG (Chromium Doped Yttrium AIuminum Garnet), which is used for Q-switching of Nd:YAG (neodymium-doped Yttrium aluminium garnet) lasers, a bleachable dye, graphene mechanical exfoliation and PVA thin film, semiconductor saturable absorber mirrors (SESAM) and carbon nanotubes embedded in PVA thin films. Initially, the loss of the absorber is high, once a large amount of energy is stored in the gain medium, the laser power increases, it saturates the absorber, and light can pass through as there are no electrons in the ground state to absorb pumped

energy. As soon as the energy is depleted in the resonator the absorber recovers to its high-loss state before the gain recovers, so that the next pulse is delayed until the energy in the gain medium is fully replenished. In this way it works as an on off optical switch to generate pulses. The pulse repetition rate can only be controlled indirectly by varying the laser's pump power and the amount of saturable absorber in the cavity. For direct control of the repetition rate, a pulsed pump source is needed.

The recovery time of a saturable absorber is ideally longer than the pulse duration, to avoid unnecessary energy losses. However, it should be fast enough to prevent premature lasing when the gain recovers. Typically, a recovery time somewhere between the pulse duration and the upper-state lifetime of the gain medium is ideal. In principle, a saturable absorber may absorb only a minor fraction of the energy of the generated pulses, so that power efficiency of the laser doesn't reduces. It can be managed by keeping the saturation energy of the absorber well below that of the gain medium and by preventing non-saturable losses. However, significant non-saturable losses are often occurred in real absorbers, and practical limitations such as damage thresholds may make it impossible to strongly reduce the absorber's saturation energy by using strong focusing. Therefore, the power efficiency is in practice often significantly reduced (D. R. Paschotta).

Passive Q switching is simpler and cost-effective as compared to active one. It eliminates the modulator and its electronics. Moreover it is suitable for very high pulse repetition rates, but with lower pulse energies. External triggering of the pulses is not possible (except with an optical pulse from another source), also pulse energy and duration are often more or less independent of the pump power, which only determines the pulse repetition rate (D. R. Paschotta; Webb & Jones, 2004).

2.5.3 Passive Q-switching rate equations

The function of a passively Q-switched laser can be expressed numerically with a slight modification of the differential rate equations presented by Sevastru et.al. (2012). With these modifications the equations are valid for three level and quasi three level active mediums such as EYDF and TYDF, ring resonator unidirectional light propagation, continuous pumping, upper and ground state absorption of the saturable absorber and excluding the carrier concentration. The rate equations are;

$$\frac{d\emptyset}{dt} = \frac{\emptyset}{\tau_{rt}}\left(\sigma_g l_g N_g - \sigma_{sg} l_s N_{sg} - \sigma_{se} l_s N_{se} - \propto_{rt}\right) + S \tag{2.1}$$

$$\frac{dN_g}{dt} = -c\sigma_g l_g \emptyset N_g - \frac{N_g}{\tau_g} + R_p \tag{2.2}$$

$$\frac{dN_{sg}}{dt} = -\gamma_s c\sigma_{sg} l_s \emptyset N_{sg} + \frac{N_{se}}{\tau_{se}} \tag{2.3}$$

where

φ - photon density;

S - Spontaneous emission

N_g - the population inversion density of the gain medium;

N_{sg} - the population density of the SA ground absorbing state;

N_{se} - the population density of the SA excited absorbing state;

lg - the length of the gain medium;

l_a - the length or thickness of the SA;

c - the speed of light;

R_p - the pumping rate density of the active medium;

σ_g - the stimulated emission cross sectional area of the gain medium;

σ_{sg} - the ground state absorption cross section of the SA;

σ_{se} - the excited state absorption cross section of the SA;

τ_{rt} - the round trip transit time in the laser resonator;

τ_g - the lifetime of the upper laser level of the gain medium;

τ_{se} - the lifetime of the SA excited state;

P_P – Pump Power;

The round trip transit time of the laser resonator, parameter which appears in equation (2.1) is defined as:

$$\tau_{rt} = \frac{l_r}{c} \tag{2.4}$$

where l_r is the optical resonator length. The pumping rate density into the upper laser level rate, R_p [$Wcm^{-3}s^{-1}$], appearing in equation (2.2) is approximated as

$$R_p \approx \frac{P_p}{h\nu A_g l_g} \tag{2.5}$$

where A_g is the area of the fiber active medium core area and hν is the energy of a laser photon (Savastru et al., 2012; ZULKIFLI, 2015)).

Equations (2.1) and (2.2) describe the increase rate of photon density and the decrease rate of population inversion respectively. Equation 2.1 modeled the nonlinear passive Q-switching by including the product of population density at ground state $N_{sg,}$ with its ground state absorption cross section, $\sigma_{sg,}$ and the population density at the excited state, N_{se} with its excited state absorption cross section, $\sigma_{se,}$ of the saturable absorber. They put a decreasing effect on the photon density increase rate while the spontaneous emission, S can contribute to the increase rate of photon density.

Equation (2.2) specifically introduces parameters related to the gain medium (quasi-three level fiber gain medium) by including the pumping rate density, R_p which in turn proportionally relates to the pump power, P_p as defined in equation (2.5), considering continuous pump scheme. The equation states that the decrease rate of the population inversion increases as the population inversion density is increased with having the pumping rate of gain medium have an opposite impact to the decrease rate.

Equation (2.3) describes the behavior of the decrease rate of absorption at the

ground state of the SA, where the decrease rate is fast when the population density at the ground state of the SA, N_{sg} is large, the incident light intensity is high and the population density of the SA at the excited state, N_{se} is small.

2.5.4 Threshold condition for Passive Q-switching

An expression for the threshold condition for a passively Q-switched laser with saturable absorber can be derived with the help of the rate equation 2.1 described in the previous subsection. The expression can be developed at a transition time; that is when the laser system has high loss, t=0, to the laser system has net increment of photon density, t>0. At t=0, the net increment experienced by a photon in the laser resonator is zero, where rate equation, dØ/dt = 0, and subsequently must be increasing, where the derivative of rate equation, dØ/dt > 0 at t>0. This leads to the passively Q-switched threshold condition (Gupta & Ballato, 2006);

$$\alpha_r = \frac{\sigma_{sg} l_s}{\sigma_{gl} l_g} > \frac{N_s \sigma_{sg} + (\alpha_{rt}/l_s)}{N_s(\sigma_{sg} - \sigma_{se})} \qquad (2.6)$$

where Ns is the total population density of the SA which includes the population at the ground and excited states and α_{rt} is the resonator round-trip loss. The left hand side of the expression dictates that the absorption cross-section state of the SA, σ_{sg} must be greater than the stimulated emission cross-section area of the gain medium, σ_g to enable Q-switching. Meanwhile, the right hand side of the expression describes the ratio of the total round-trip loss to the saturable round trip loss at t = 0. In a system where the loss is dominated by SA ($\alpha_{rt,t}/\ \alpha_{rt,s} \approx 1$), expression of Equation (2.6) simplifies and states that the loss of the SA saturates more quickly than the gain of the gain medium and Q-switching can be initiated. In contrast, laser will tend to oscillate in CW regime when the expression (2.6) is unsatisfied.

Furthermore, the excited-state lifetime, τ_{se} of the SA should be long enough; to enable the right amount of depletion of the ground-state population density upon

illumination for Q-switching operation, the dynamics of this depletion has been described in the rate equation (2.3). In addition, the excited state absorption (ESA) cross section, σ_{se} must be considerably smaller than that of the ground-state, σ_{sg} to prevent the ESA effect and to enhance the saturable absorption of the ground state. The ESA effect can occur typically when the SA saturates (when the excited state becomes significantly populated via one-photon absorption) which lead to the possibility of these excited electrons being further photo-excited to another higher excited state. This effect will cause parasitic absorption at the high-intensity side of the Q-switched pulse transmission and form a source of loss in the laser resonator. Therefore, it is desirable to use a material of minimum σ_{se}/σ_{sg} ratio for good passively Q-switched laser performance (Burshtein et al., 1998).

2.5.5 Pulse build up process in a passively Q-switched laser

Fig. 2.8 shows the pulse build-up process for Q-switched laser with saturable absorber by considering a quasi-three level active medium and continuous pumping. In the figure, the loss curve represents the saturable absorption of the SA, along with nonsaturable loss from the resonator and the SA, whereas the gain curve represents the population inversion dynamics and the pulse curve represents the photon density dynamics. In this model, both SA and the gain medium contribute in modulating the Q-value of the laser resonator with continuous pumping through a laser diode, the resonator will continuously Q-switched producing a train of pulses. The SA creates loss (by absorbing light) thereby delaying laser generation due to the suppression of stimulated emission in the gain medium. This raised the population inversion or gain at a high amount. When the laser gain reaches the initial population inversion density value, N_{gi0}, that is where the gain exceeds the total resonator loss, the photon density or pulse will then start to build up from amplified spontaneous emission (ASE) noise

(Kashiwagi & Yamashita, 2010). After some time, the photon density will become large enough that it begins to saturate the SA, subsequently, the total resonator loss will be reduced dramatically and high intensity of light will be transmitted. Due to the pulse generation, the gain will start to reduce and a pulse peak is formed after it has reached the N_p value as shown in Fig. 2.8 (Dong, 2003).

Once the Q-switched laser begins to oscillate in the resonator, the population density at the ground state of SA and population inversion of the gain medium begin to change rapidly, where a train of pulses can be generated. It is noted that, for the second and subsequent pulses, the initial population inversion will be different by considering the residual population inversion density, N_{gf} (Dong, 2003; Savastru et al., 2012).

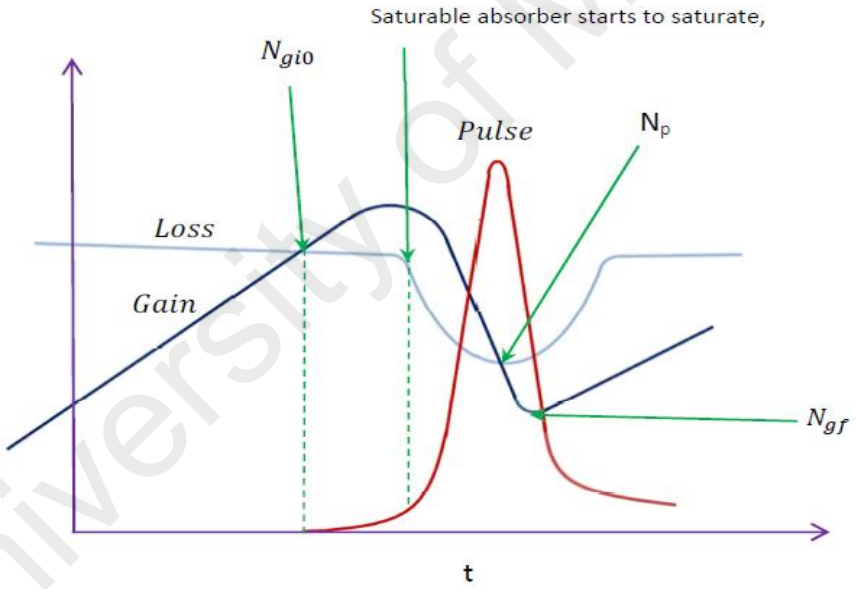

Figure 2.8: The first pulse build-up process for Q-switched laser with saturable absorber (ZULKIFLI, 2015).

2.5.6 Saturable absorber parameters for Q-switching

The most important properties of a saturable absorber device are the saturable absorption, nonsaturable absorption, saturation intensity, absorbing recovery time and absorption bandwidth. These properties are governed by the chemical composition and atomic arrangement of the material as well as the structure of the saturable absorber

device. Moreover, the properties can be combined and described in a simple two-level nonlinear saturable absorption coefficient as described in the following equation;

$$\alpha(I) = \frac{\alpha_s}{1+\frac{I}{I_s}} + \alpha_{ns} \quad (2.7)$$

where α_s is the saturable absorption, I is the incident light intensity, I_s is the saturation intensity, and α_{ns} is the nonsaturable absorption. It is noted that, due to normalization, the saturable absorption is also termed as modulation depth. The two components of non-linear absorption; saturable and nonsaturable absorption can also be expressed as a percentage of linear absorption (Bao et al., 2011; Xing et al., 2010).

On the other hand, the saturable absorption can also be expressed as,

$$\alpha_s = \sigma_{sg} N \quad (2.8)$$

where σ_{sg} and N are the absorption ground cross section and concentration of the material, respectively. The saturable absorption dictates the relative number of photons absorbed per unit distance from the saturable absorber material. If the saturable absorption coefficient is large, the photons are absorbed over a relatively short distance rather than deeper into the absorber, as described in Fig. 2.9. This figure shows the photon intensity, I_{v0} as a function of distance, x for two general values of absorption coefficient. It indicates that if the absorption coefficient is large, the photons are absorbed over relatively short distance with the photon intensity decreases exponentially with distance through the saturable absorber. Furthermore, the saturation intensity from equation (2.7) can be defined as the intensity required in a steady state to reduce the absorption into half of its unsaturated value,

$$I_s = \frac{hf}{\sigma_{sg}\tau_{se}} \quad (2.9)$$

where h is plank constant, f is the light frequency operation, σ_{sg} is the absorption cross section at the ground state of the SA, and τ_{se} is the excited state life time or the absorber recovery time. Equation (2.9) suggests that the longer the excited state life time before

recombination, the less continuous wave intensity is required to saturate the saturable absorber.

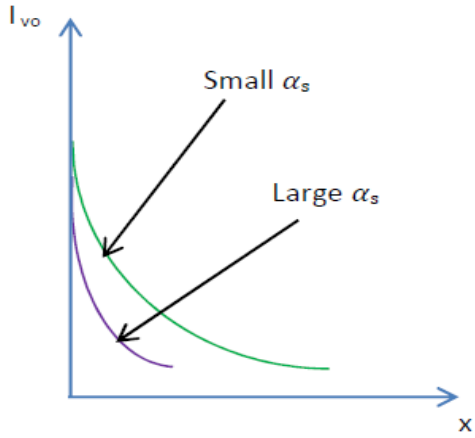

Figure 2.9: Photon intensity, Ivo versus distance, x for two different absorption coefficients (ZULKIFLI, 2015).

In order to demonstrate the absorption dynamics of the SA, Fig. 2.10 shows a plot of the normalized non-linear absorption at different normalized light intensity as described in equation (2.7). From the figure, when light intensity produced in the laser resonator is less than the saturation intensity ($I < I_s$) of the SA, the optical absorption is high and lasing is prevented.

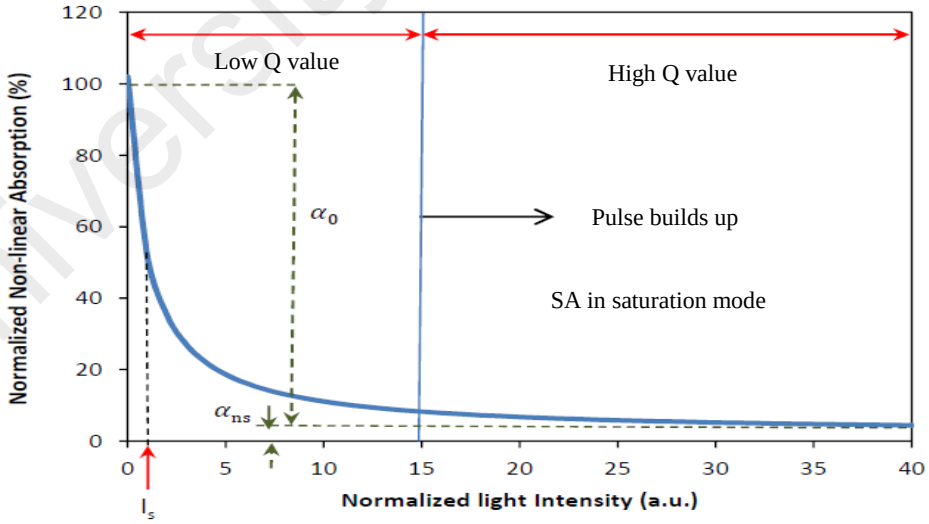

Figure 2.10: The non-linear saturable absorption dynamics as a function of light intensity in Q-switching (ZULKIFLI, 2015).

When the light intensity, $I \geq I_s$, the absorption decreases and transmissivity gradually becomes greater. Finally, when $I \gg I_s$ the absorption is saturated thus, the resonator is in high Q-value and Q-switched laser oscillation commence. However, the nonlinear

saturable absorption could not reach 0% as shown in the figure due to the non-saturable loss property, α_{ns} of the saturable absorber (ZULKIFLI, 2015).

2.6 Mode-locked lasers

In laser technology, mode-locking refers to a technique by which a laser can be made to generate pulses of extremely short duration, on the order of picoseconds (10^{-12} s) or femtoseconds (10^{-15} s). This is achieved by establishing a fixed-phase relationship between the longitudinal modes of the laser's resonant cavity. The laser is then referred as phase-locked or mode-locked. Interference between these modes causes the laser light to be produced as a train of pulses. In a simple laser, different modes oscillates independently, without a fixed relationship between each other, like a set of independent lasers all emitting light at slightly different frequencies. In lasers with few oscillating modes, interference between the modes produces beats in the laser output, leading to fluctuations in intensity; whereas in lasers with many thousands of modes, interference between modes tend to average to a near-constant output intensity. Fig. 2.11 shows the electric fields of five modes with random phase and the power of the total signal distributed in a random fashion.

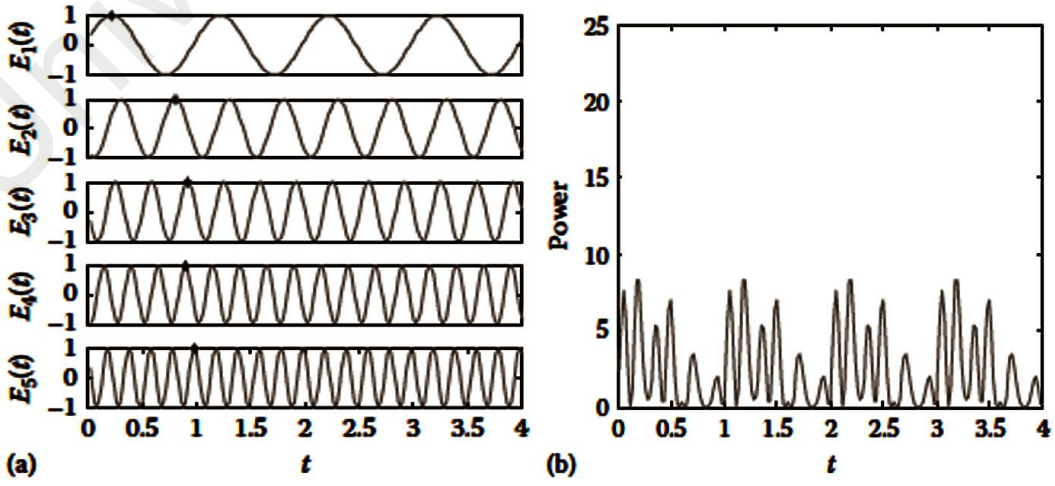

Figure 2.11: Plots of (a) electric field amplitudes of five individual modes of randomly distributed phases and (b) power of the total signal of a multi-longitudinal mode laser (Ngo., 2011).

On the other hand, if each mode operates with a fixed phase relationship between it and the other modes, all modes of the laser will periodically constructively interfere with one another, generating an intense burst or pulse of light instead of random or constant output intensity as shown in Fig. 2.12. Such a laser is termed as mode-locked or phase-locked laser. These pulses are separated in time by $\tau = 2L/c$, where τ is the time taken for the light to make exactly one round trip of the laser cavity, L is the length of laser cavity and c is speed of light. The frequency is exactly equal to the mode spacing of the laser, $\Delta\nu = 1/\tau$. The duration of each pulse is determined by the number of modes which are oscillating in phase. If there are N modes locked with a frequency separation $\Delta\nu$, the overall mode-locked bandwidth is $N\Delta\nu$, and the wider the bandwidth, the shorter the pulse duration of the laser.

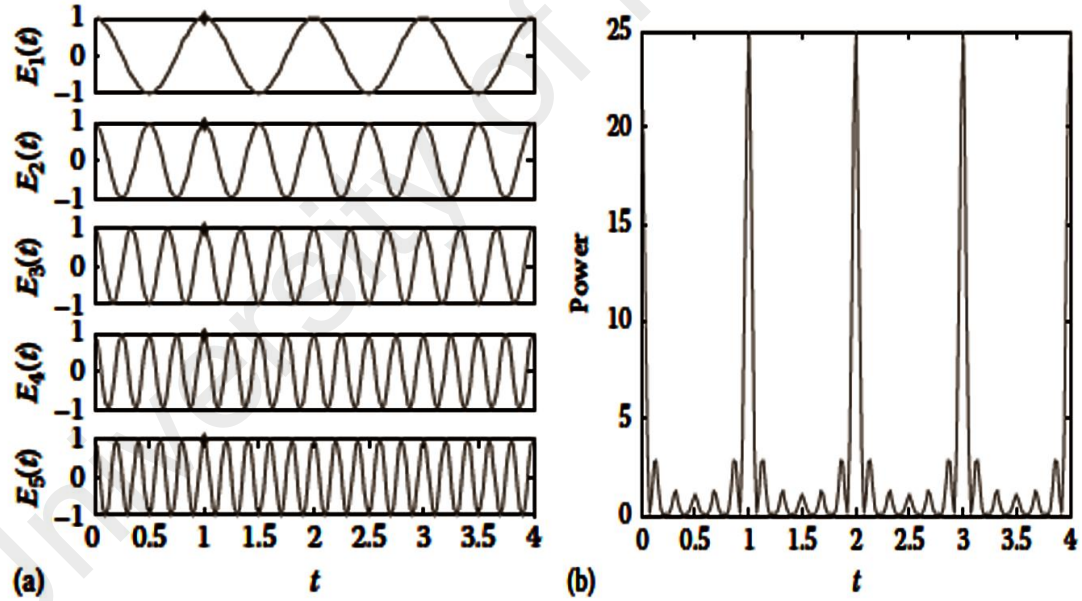

Figure 2.12: Plots of (a) Electrical field amplitudes of five in-phase individual modes and (b) the total power of a periodic pulse train (Ngo, 2011).

In practice, the actual pulse duration is determined by the shape of each pulse, which is determined by the amplitude and phase relationship of each longitudinal mode. For instance, a laser producing pulses with a Gaussian temporal shape, the minimum possible pulse duration Δt is given by the equation

$$\Delta t = \frac{0.441}{N\Delta\nu} \tag{2.10}$$

The value 0.441 is known as the 'time-bandwidth product' of the pulse, and varies depending on the pulse shape. Generally for ultra-short pulse lasers, a hyperbolic-secant-squared ($sech^2$) pulse shape is considered, giving a time-bandwidth product of 0.315. Using this equation, the minimum pulse duration can be calculated consistent with the measured laser spectral width (Ngo, 2011).

Mode-locked fiber lasers are capable of producing pulses with widths from close to 30 fs to 1 ns at repetition rates, ranging from less than 1 MHz to 100 GHz. This broad range along with compact size of optical fiber lasers is quite unique in laser technology, making them feasible for a large range of applications. As mode-locked fiber laser technology matured and these lasers became commercially available, they have been used in many different fields, such as laser radar, all-optical scanning delay lines, nonlinear frequency conversion, injection-seeding, two-photon microscopes, THz generation, and optical telecommunications, just to mention the most widely publicized areas. Undoubtedly, mode locked fiber lasers are a premier source of short optical pulses sharing equal position with semiconductor and solid-state lasers (Digonnet, 2001a).

2.6.1 Mode-locking methods

Mode-locked lasers can be produced by using either active or passive methods. In active mode-locking, the optical modulator such as acousto-optic modulator is used with the help of an external electrical signal, as a mode-locker. On the other hand, passive mode-locking doesn't need an external signal to operate (Martin E. Fermann, 2003). The mode-locking is achieved by modulating an intra-cavity light using some intra-cavity elements, such as nonlinear polarization rotation and saturable absorber.

Most of the passively mode-locked lasers are achieved using a saturable absorber since it allows the generation of much shorter (femtosecond) pulses. This is attributed to the saturable absorber used, which can modulate the resonator losses much faster than an electronic modulator: the shorter the pulse becomes, the faster the loss modulation, provided that the absorber has a sufficiently short recovery time. The pulse duration can be even well below the recovery time of the absorber.

There are also passive mode-locking schemes that do not depends on materials that directly display an intensity dependent absorption. In these methods, nonlinear optical effects in intra-cavity components are used to provide a method of selectively amplifying high-intensity light in the cavity, and attenuation of low-intensity light. One of the most successful schemes is called Kerr-lens mode-locking (KLM), also sometimes called "self-mode-locking". This technique uses a nonlinear optical process, the optical Kerr effect, which results in high-intensity light being focused differently from low-intensity light. By careful arrangement of an aperture in the laser cavity, this effect can be exploited to produce the equivalent of an ultra-fast response time saturable absorber.

2.6.2 Optical solitons

A fascinating manifestation of the fiber nonlinearity is the development of optical solitons, formed as a result of the interplay between the dispersive and nonlinear effects. Solitons describe special kinds of wave packets that can propagate undistorted over long distances through a fiber. Solitons have been discovered in many branches of physics. In the context of optical fibers, not only are solitons of fundamental interest but they have also found practical applications in the field of fiber-optic communications (Agrawal, 2007).

Consider the case that an optical pulse is launched into a fiber with $\beta_2<0$ (where β_2 is the group velocity dispersion parameter), anomalous dispersion. SPM (self-phase modulation) leads to lower frequency components at the leading edge of the pulse and higher frequency components at the trailing edge. In the anomalous dispersion regime, lower frequency components travel slower than higher frequency components. Therefore, the anomalous dispersion causes the leading edge of the pulse to slow down while the trailing edge travels faster. Effectively, anomalous dispersion compresses the pulse and undoes the frequency chirp induced by SPM. The pulse maintains the shape and width, along the entire length of the fiber, if the effects of SPM and GVD cancel out with each other. Such a pulse is called solitary wave pulse or soliton. The pulse that has the above property is the sech profile pulse, which is a solution of the nonlinear Schrodinger equation NLSE (Ngo, 2011).

Fig. 2.13 shows different types of mode-locked fiber lasers. The conventional soliton and stretched pulse are obtained in anomalous dispersion fiber laser setup, where the pulse shaping is mainly due to the natural balance between the anomalous dispersion and the fiber nonlinearity. On the other hand, Dissipative solitons (DSs) is obtained in the normal dispersion region due to the result of the combined effects among the cavity dispersion, fiber nonlinearity, gain and loss, and spectral filtering. Also the dissipative effects play a crucial part on the soliton shaping. Consequently, compared to conventional soliton and stretched soliton, DS has a relatively wider pulse duration and lower peak power (D. Li et al., 2015).

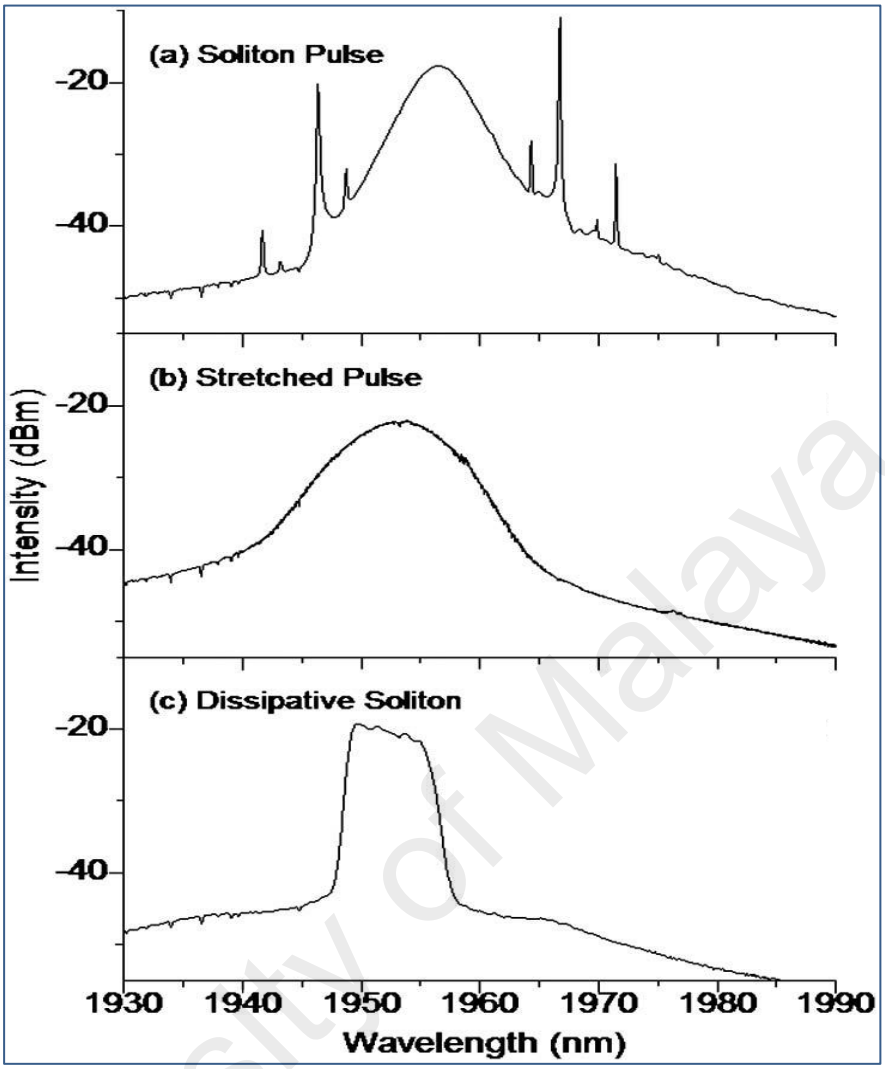

Figure 2.13: Different types of solitons.

2.7 Summary

This chapter describes some of the basic concepts regarding optical fibers and dynamics of Q-switched and mode-locked fiber lasers with the help of existing literature. It includes description of double clad fiber structure along with some details of doped fibers as Erbium-Ytterbium and Thulium-Ytterbium co-doped double clad fibers. Later it presents some details about Q-switching, its types and the necessary equations. It also includes a detailed description of mode-locked lasers, especially, passive mode-locked lasers along with a brief introduction of solitons, which are an integral part of the most mode-locked fiber lasers.

CHAPTER 3: YTTERBIUM CO-DOPED FIBER LASERS USING DOUBLE CLAD FIBER

3.1 Introduction

Development of fiber-based lasers utilizing Ytterbium co-doped fibers has continued over the past 20 years (Federighi & Di Pasquale, 1995; Grubb et al., 1992; Harun et al., 2008; Park et al., 1996; Sudo, 1997; Yahel & Hardy, 2003). Most of these lasers are based on Erbium-Ytterbium co-doped fibers (EYDF) and thus they operate at around 1550 nm region. Thanks to their eye-safety, they outperform the most popular solid state Nd:YAG or Yb-doped fiber lasers for wide range of applications ranging from scientific to military or medical. Co-doping of Erbium fiber with Ytterbium ions prevents the formation of Erbium clusters and effectively controls the upconversion from $^4I_{13/2}$; higher doping level can thus be used. The pair induced energy transfer from Ytterbium to erbium provides an efficient indirect pumping mechanism. Ytterbium ions, which have a high absorption at wavelengths between 900 and 1000 nm, absorb pump light and transfer their energy to erbium ions through a non-radiative cross-relaxation effect. The availability of high-power multimode pumps enables the demonstration of high power output by a cladding pumping technique. For instance, Jeong et al. (2005) presented a master oscillator power amplifier (MOPA) source based on Er-Yb co-doped large mode area (LMA) fiber with 151 W output power at 1563 nm (Y Jeong et al., 2005). Two years later the same group achieved 297 W continuous-wave (CW) output from a Er-Yb co-doped LMA fiber laser (Yoonchan Jeong et al., 2007). Such output power levels are unable to achieve when the conventional Yb-free, Erbium-doped fibers (EDFs) are used. Even with large diameter cores, the Erbium ions clustering effect is limiting the attainable output power to several tens of watts (Blixt et al., 1991; Myslinski et al., 1997; Nilsson et al., 1993).

On the other hand, Thulium (Tm)-doped fiber lasers (TDFLs) are useful for generating coherent emission in the "eye-safe" wavelength range. Their emission band extends over a wide range of wavelength from 1.6 μm to over 2 μm, and they can be efficiently pumped at ~790 nm, ~1200 nm, or ~1600 nm (Clarkson et al., 2002; Zen et al., 2013). These features make Tm^{3+} doped fiber lasers attractive for a variety of applications in defense (Eichhorn, 2010), medicine (Theisen-Kunde et al., 2007), spectroscopy (Baudelet et al., 2010), and material processing (Mingareev et al., 2012). Interest in the 2 μm lasers for medical field is mainly due to their radiation which has a strong absorption in water and biological tissues. For instance, incision in porcine and chicken tissues have been recently demonstrated using a continuous wave TDFL (Pierce et al., 1999). The penetration depth of this laser also matches with the subcutaneous depth of the pain nerve receptors in the skin which results in minimal damage and pain when used as power source for research and treatment (Opsommer et al., 2001). El-Sherif and King reported a Q-switched TDFL for soft and hard tissue ablation (El-Sherif & King, 2003).

For Thulium ions, energy transition from $^3F_4$ to $^3H_6$ results in quantum efficiency near 2 μm due to cross-relaxation energy transfer between Thulium ions. During this process, two ground-level Thulium ions are excited to the upper lasing level of $^3H_6$ by absorbing only one pump photon near 790 nm. This suggests that one excited Tm^{3+} ion at the $^3H_4$ level generates two Tm^{3+} ions at the $^3F_4$ upper laser level. However, commercial high power diodes required for the excitation in this wavelength range are difficult to obtain as well as very costly. Pumping Thulium-doped fibers at another pumping wavelength of 1200 nm or 1600 nm is complicated because semiconductor laser diodes with sufficient power are not commercially available. Another solution is to co-dope the Thulium fiber with Ytterbium ions so that it can be pumped by commercially available laser diodes operating at 905−980 nm. This is made possible by the energy transfer from Thulium to Ytterbium ions similar to the case of Yb^{3+} sensitized Er^{3+}-

doped fibers (Jackson, 2004). The sensitization of Tm^{3+} doped fibers with Yb^{3+} is possible due to $^3H_5$ level of Tm^{3+} which is (quasi-) resonant with the excited Yb^{3+} level ($^2F_{5/2}$). The up-conversion system has long been proposed based on Tm^{3+}-Yb^{3+} co-doped glass and fibers (Halder et al., 2012), but only more recently the concept is used for the 2-μm fiber laser application (Harun et al., 2011).

In this chapter, a thorough study on both Erbium-Ytterbium and Thulium-Ytterbium co-doped fiber lasers is presented. Both lasers are based on low cost cladding pumping and thus they utilize a double-clad fiber as a gain medium. Multi-wavelength fiber lasers are also demonstrated based on both gain media.

3.2 Erbium-Ytterbium co-doped fiber laser

In this section, the lasing characteristic of a cladding pumped Erbium-Ytterbium co-doped fiber laser (EYDFL) is investigated based on the simplest setup as shown in Fig. 3.1. The EYDFL uses a commercial double clad EYDF as the gain medium. The fiber has a multi lobed pump guide with a core, inner and outer cladding diameters of 5 μm, 105 μm and 125 μm respectively. Inset Fig. 3.1, shows the cross-section image of the EYDF, which has a multi lobed pump guide structure. The core has a numerical aperture (NA) 0.21, whereas the pump guide (inner cladding) has the numerical aperture of 0.25. The inner cladding has an absorption coefficient of approximately 1.0 dB/m at around 980 nm for Ytterbium ion. The erbium peak absorption is 40 dB/m at wavelength of 1535 nm. Pump beams from 980nm multimode laser diode are launched into the EYDF via multimode combiner (MMC) with a NA of around 0.15. The splice region between the EYDF and MMC is covered by low-index gel so that the multimode pump beam is effectively guided into the cladding of the EYDF.

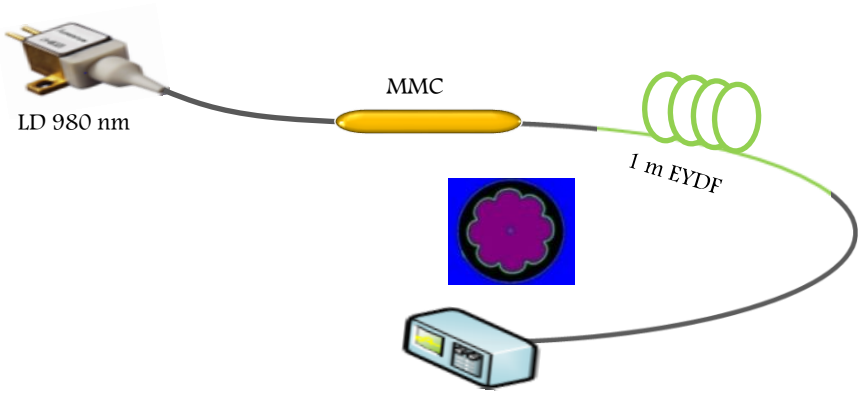

Figure 3.1: EYDFL in open linear cavity configuration. Inset shows the cross section image of the EYDF with a multi lobed pump guide structure.

The EYDF's end is spliced to a standard single-mode fiber to filter out the residual cladding pump light so that the single-mode operation of the output laser can be assured. The fiber at both ends of the laser is perpendicularly cleaved to provide feedback for the laser. The linear laser cavity is formed by the 4% Fresnel reflection from the perpendicular cleaved fiber end on both sides. This allows the generation of amplified spontaneous emission (ASE) light, which oscillates in the linear cavity to produce laser at 1550 nm region. The output power and spectrum of the EYDFL are characterized by using power meter and optical spectrum analyser (OSA) with spectral resolution 0.07 nm, respectively. The temporal measurement was carried out using an oscilloscope in conjunction with a fast photo detector (Thor Labs, DET01CFC, InGaAs based detector).

By pumping the EYDF with the laser diode, the ytterbium and erbium ions are excited to their $^2F_{5/2}$ and $^4I_{11/2}$ levels, respectively. Then the excited ytterbium ions decay down to $^2F_{7/2}$ to release energy, of which a portion is used to emit photons near 1050 nm. Another energy portion is transferred to the erbium ions, which are excited to their $^4I_{11/2}$ level. These erbium ions undergo a non-radiative transition to their metastable state $^4I_{13/2}$ and form a population inversion with the state $^4I_{15/2}$. The population inversion emits an amplified spontaneous emission (ASE) in 1.5 μm region and oscillates in the

linear cavity to generate laser. The performance of the laser is investigated for three different EYDF lengths. It is observed that the threshold pump power for the lasing is at around 140 mW for all the lasers.

Fig. 3.2 shows the output spectra of the EYDFL when the 980 nm pump power is fixed at 500 mW. The laser operates at 1535.4 nm, 1544.3 nm and 1545.6 nm with EYDF lengths of 1, 4 and 5 m, respectively. The operating wavelength is found to increase with the increasing gain medium length. This is attributed to the optimum gain of the active fiber, which occurs at longer wavelength with the increase of the active fiber length. In longer fiber, the ASE at shorter wavelength will be absorbed to emit at longer wavelength and thus improves the gain at the longer wavelength. Fig. 3.3 shows the measured output power as a function of the 980 nm pump power for three different EYDF lengths. The EYDFLs start to lase at 140 mW, 130 mW and 142 mW at fiber lengths of 1m, 4m and 5m, respectively. Above these thresholds, the output powers of all laser increase in a linear trend with increasing pump power. The slope efficiencies of 4.3%, 15.0% and 18.4% are obtained for the EYDFLs configured with 1m, 4m and 5m, respectively. This shows the optimum fiber length of the EYDFL operation is 5 m or longer with the maximum output power of 537 mW is obtained at the maximum pump power of 3100mW. However, the lowest threshold is achieved at 4m long fiber.

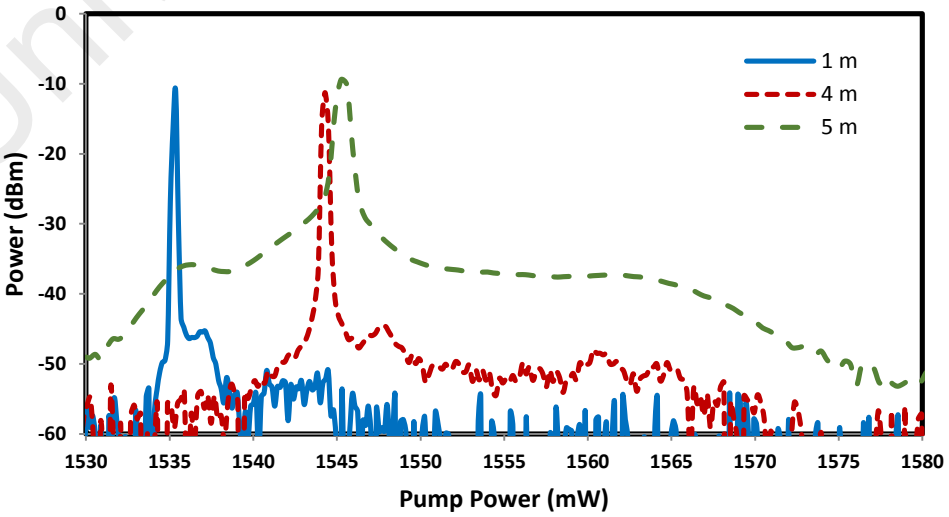

Figure 3.2: Output spectra of the EYDFL configured with linear configuration at three different fiber lengths.

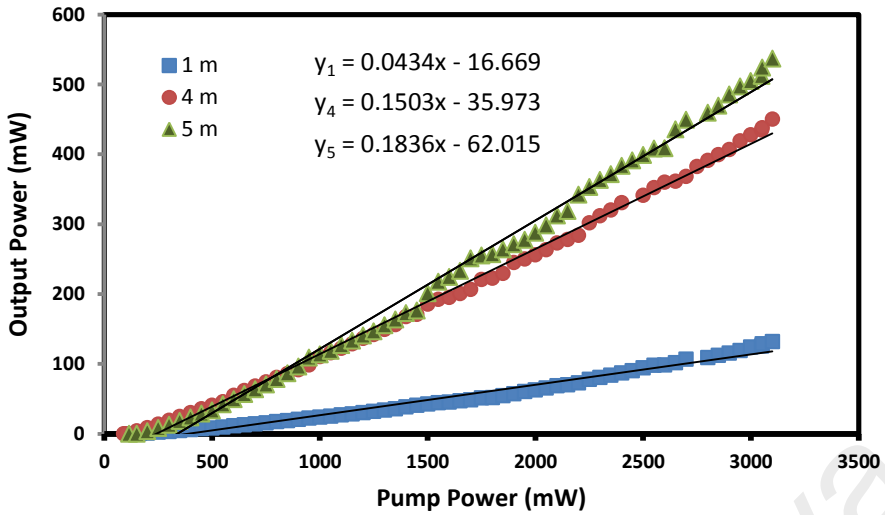

Figure 3.3: Output power against pump power at three different fiber lengths for the EYDFL configured with linear configuration.

3.3 Ring EYDFL

In this section, the performance of a ring EYDFL is investigated at different active fiber lengths. Fig. 3.4 shows the configuration of the proposed EYDFL, which consists of a double-clad EYDF as a gain medium, a multimode combiner (MMC) and an 80/20 output coupler in a ring configuration.

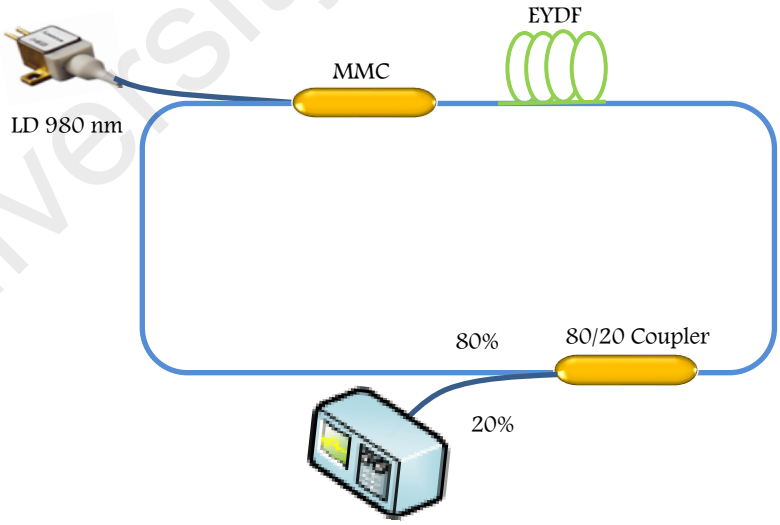

Figure 3.4: EYDFL Ring Cavity Configuration.

The EYDF used is similar with the linear setup in the previous section. The fiber is pumped by a 980 nm multimode laser diode via the MMC. The output of the laser is taken out of the cavity through an 80/20 coupler while keeping 80% of the light to

oscillate in the ring cavity to generate laser. The OSA is used to inspect the spectrum of the EYDFL whereas the power meter is used to measure the output power.

By pumping the EYDFL with a 980 nm pump, it generates an ASE operating at 1.5 µm region through an energy transfer from Yb^{3+} to Er^{3+}. The ASE is then oscillated in the ring cavity to generate laser at around 1550nm region. The operating wavelength of the laser is determined by the gain characteristic of the fiber and the cavity loss. Fig. 3.5 shows the output power of the laser against the pump power at three different lengths of the active fiber. The laser starts at the threshold pump powers of 90 mW, 60 mW and 50 mW for EYDF lengths of 1m, 4m and 5m, respectively. It shows that the threshold reduces with the increasing length of the active fiber. This is due to the population inversion which is higher with longer fiber. Due to a higher number of both Yb^{3+} and Er^{3+} at longer length, the slope efficiency of the laser is also improved with the increase of the length. As shown in Fig. 3.5, the slope efficiencies of 0.8%, 3.1% and 4.6% are obtained at active fiber lengths of 1m, 4m and 5m, respectively. Compared to the linear cavity, the proposed ring cavity demonstrates a significant lower efficiency due to the higher cavity loss.

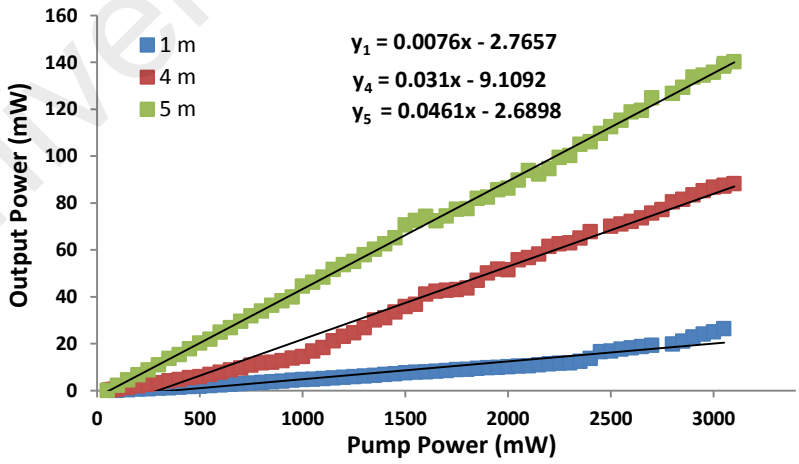

Figure 3.5: Output power against pump power at three different fiber lengths for the EYDFL configured with ring configuration.

Fig. 3.6 shows the output spectra of the EYDFL at pump power of 200 mW for three different active fiber lengths. It is shown that the laser operates at 1544.5 nm with

the employment of 1m long EYDF as the gain medium. The operating wavelength shifts at extended L-band region of around 1611 nm as the gain medium length is changed to 4 or 5m. This is attributed to excess length, which allows the energy transfer from C-band to L-band region. The generated C-band laser is absorbed to emit at 1611 nm region. The random multi-wavelength operation is observed at L-band due to the high nonlinearity of the fiber, which initiates nonlinear polarization rotation (NPR) and four-wave mixing (FWM) effects. These effects are responsible for multi-wavelength generation. A weak Kelly sideband is also observed at 1544.5 nm laser due to the NPR effect. However, no pulse train is observed at the output in the current setup. Optimization of this effect will enable the generation of mode-locking laser, which will be discussed in the next chapter.

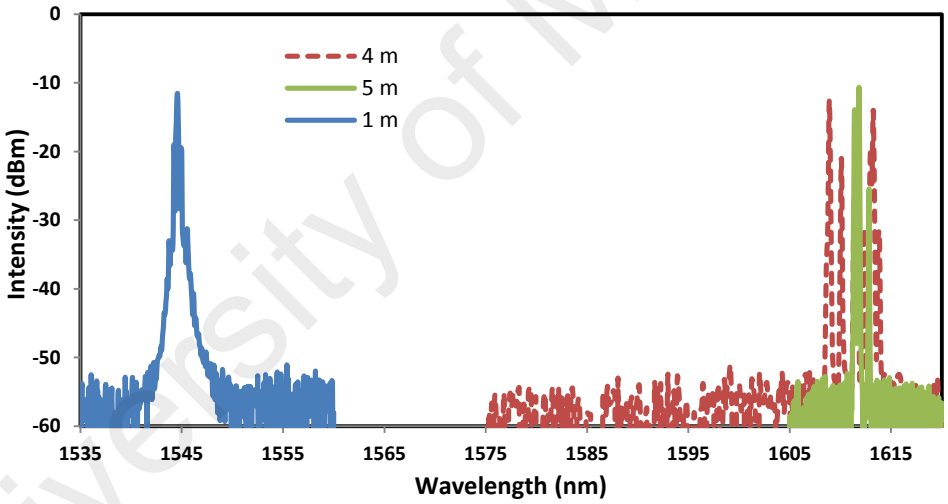

Figure 3.6: Output spectra of the EYDFL configured with ring configuration at three different fiber lengths.

3.4 Thulium-Ytterbium co-doped fiber laser

A quantum efficiency in laser output near 2 μm can be achieved by 790 nm pumping through Thulium ions $^3F_4$ to $^3H_6$ transition, because of the so-called cross-relaxation energy transfer process between Thulium ions (Jackson, 2004). However, the availability of high power diodes in this wavelength at >200mW level from commercial supplies is relatively poor as well as very costly. Pumping Tm^{3+}-doped fibers at 1200 nm or 1600 nm is complicated by the need for an intermediate laser source, since high-

power laser diode are not commercially available at this wavelength. Therefore, an alternative approach with cheaper pump source should be explored for pumping the Thulium fiber.

In this section, a fiber laser operating at 2 μm region is demonstrated using a newly developed double-clad Thulium-Ytterbium co-doped fiber (TYDF) as a gain medium. Here, the Thulium fiber is co-doped withYb^{3+} so that it can be pumped with a well-established multimode laser diode operating in the range from 900 nm to 980 nm. Since, the Tm^{3+} ion has a level ($^3H_5$), which is (quasi-) resonant with the excited Yb^{3+} level ($^2F_{5/2}$), the sensitization of Tm-doped fiber with Yb^{3+} is allowed, similar to the case of Yb^{3+}-sensitized Erbium-doped fibers studied earlier (Pal et al., 2010).

3.4.1 Fabrication of double-clad Thulium-Ytterbium co-doped octagonal-shape fiber

A double-clad octagonal-shaped TYDF was fabricated with a modified chemical vapour deposition technique combined with a solution doping method. A pure silica glass tube of outer/inner diameters 20/17 mm was used for depositing two porous un-sintered SiO_2 soot layers to make a preform, while maintaining a suitable deposition temperature at ~ 1550^{o}C. An alcoholic solution containing such doping elements as Thulium, Ytterbium, Yttrium and Aluminium was used to soak the porous layer for about 30 min and achieve efficient doping. Then dehydration and oxidation were performed at about 900–1000^{o}C. Unsintered layers were sintered by slowly increasing the temperature from 1500 to 2000^{o}C and using a conventional modified chemical vapour deposition technique. Upon completion of sintering and oxidation, a tube was slowly collapsed to be converted into optical preform. The dopant concentration inside the preform was analyzed with an electron probe micro-analyser. It was found that the optical preform thus fabricated consisted of Aluminium Oxide (Al_2O_3), Yttrium Oxide

(Y_2O_3), Thulium Oxide (Tm_2O_3) and Ytterbium Oxide (Yb_2O_3) dopants, with the corresponding average weight percentages of 5.5, 3.30, 0.70 and 4.0, respectively. The presence of Al_2O_3 and Y_2O_3 served to decrease the phonon energy of alumino-silica glass, which prevented clustering of Yb and Tm ions into the core glass matrix and, therefore, increased the probability of radiative emission.

The circular preform fabricated in the above manner was given an octagonal shape after grinding followed by polishing. This geometrically modified preform was then drawn at 2050^{o}C to fabricate an octagonal-shaped double-clad fiber with the outer cladding diameter of about 125 µm. The double-clad fiber was finally coated with a low-refractive index polymer to increase robustness of the fiber. As opposed to a conventional core pumping technique, the pump light in our case propagated in the first cladding of the fiber and then absorbed by Yb dopants in the regions where the clad was overlapped with the core. The octagonal geometry was chosen for improving the pump absorption efficiency. The doping levels of Tm^{3+} and Yb^{3+} ions in the TYDF were measured to be around 4.85 x 10^{19} ions/cc and 27.3 x 10^{19} ions/cc, respectively, by using an electron probe micro-analyzer. The Tm^{3+} and Yb^{3+} cladding absorptions of the fiber were found to be 0.325 and 3.3 dB/m respectively at 790 and 976 nm. Fig. 3.7 displays a microscopic view of TYDF cross- section, which has an octagonal-shaped inner cladding. The core diameter and the numerical aperture of our TYDF are equal to 5.96 µm and 0.23, respectively.

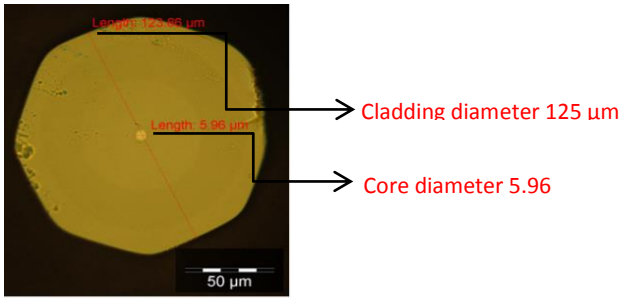

Figure 3.7: Microscopic cross-sectional view of the homemade homemade double-clad octagonal-shaped TYDF.

3.4.2 Lasing characteristics of TYDF

Lasing characteristics of the TYDF have been studied for both ring and linear configurations. Fig. 3.8 shows the experimental setup of our ring TYDFL. It consists of a piece of the newly developed TYDF that serves as a gain medium, a multimode combiner (MMC), a 10 dB output coupler, and a 905 nm multimode laser diode as an optical pump source. The performance of the laser is investigated for three different fiber lengths (5, 10 and 15 m). It has turned out that an ASE centered nearby 1950 nm is generated after the fiber is pumped by the multimode laser diode. The power of this emission increases with increasing pump power. The amplified spontaneous emission oscillates in the ring cavity, resulting in a lasing that occurs at ~ 1.95 μm. The laser output is then tapped from the 10 dB coupler for further characterization. The coupler allows for 90% of the light to oscillate in the laser cavity while tapping out the remaining 10% of the light. Notice that our laser device contains no adjustable parts and can only be controlled externally by the amount of pump power applied to TYDFs of three different lengths.

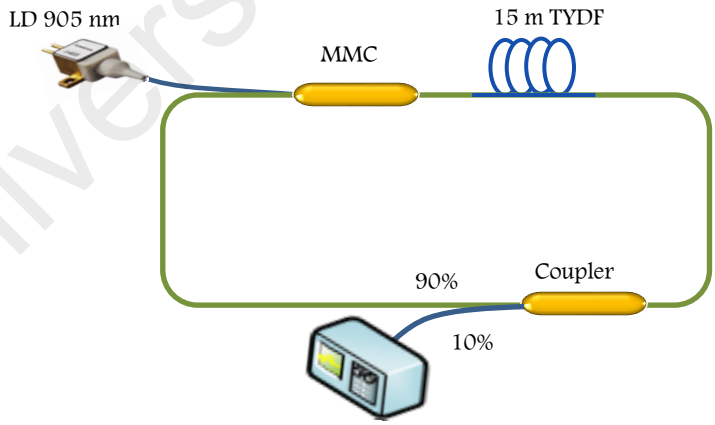

Figure 3.8: Experimental setup of our TYDFL in the ring configuration.

Fig. 3.9 shows the dependences of output power on the pump power for the three different fiber lengths. The output power increases linearly with increasing pump power, with the slopes 0.29, 0.88 and 0.77% characteristic for the TYDF lengths 5, 10

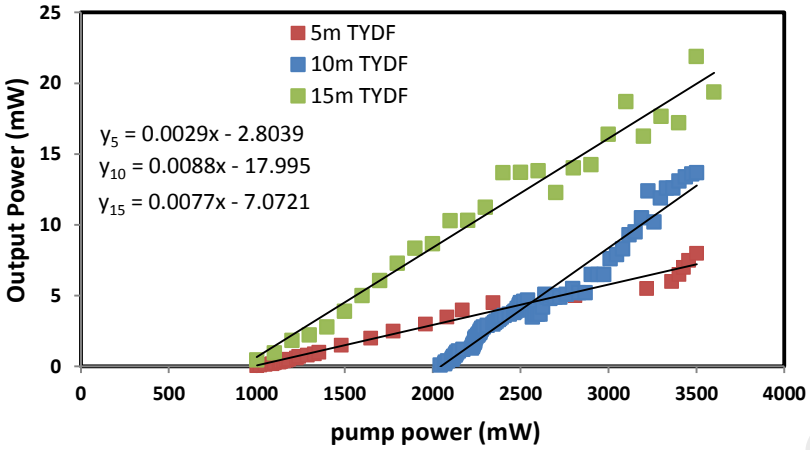

Figure 3.9: Output power of our ring TYDFL versus the pump power as measured at three different TYDF lengths.

and 15 m, respectively. As said above, the TYDFL operates based on the energy transfer from Ytterbium to Thulium ions. As the 905 nm pump photons are absorbed by the Ytterbium ions, they excite the ions from the ground state $^2F_{7/2}$ onto the $^2F_{5/2}$ level. As the ion relaxes to its ground state, the energy transfer proceeds to a neighboring Thulium ion. When the Thulium ions in their ground state ($^3H_6$) absorb the donated photons they get elevated to the $^3H_5$ level before irradiatively relaxing to $^3F_4$. The Thulium ions populating this level drop to the ground state again, generating the amplified spontaneous emission in the vicinity of 1.95 µm, which oscillates in the ring cavity and brings about a laser light. We have obtained the threshold pump powers for our laser as low as 1000, 2044 and 1000 mW for the 5, 10 and 15 m long TYDFs, respectively. The corresponding maximal output powers are 8, 13.7 and 21.9 mW, as measured at the maximal pump power of 3.6 W. The efficiency of our laser is the highest (0.88%) for the 10 m long TYDF, while the 15 m long fiber provides the highest output power (21.9 mW), which is attributed to the lowest threshold pump power. These facts indicate that the optimal length of the fiber in the ring TYDFL is somewhere in the region of 10–15 m.

The output spectra of the ring TYDFL have been studied for the same three

different TYDF lengths. The results are shown in Fig. 3.10 where the multimode 905 nm pump power is fixed at 3.6 W. It is seen that the output spectrum shifts to longer wavelengths with increasing TYDF length. This is attributed to increased absorption of the 905 nm photons, which takes place with increasing fiber length and so results in increased number of the emitted photons. These photons are re-absorbed by Thulium ions along the fiber length, imposing the amplified spontaneous emission at a longer wavelength, which oscillates in the cavity and leads to the lasing effect. With the 5 m long TYDF, the laser produces three lines (1914.5, 1934.7 and 1953.6 nm), with the peak powers being equal respectively to 6.3, 1.6 and 1.7 dBm. On the other hand, the laser operates at a single wavelength (1961.4 nm), with the peak power of 4.8 dBm, as the TYDF length increases to 10 m. Further increase in the TYDF length up to 15 m yields in a dual-wavelength output (1562.7 and 1990.3 nm). These results indicate that the optimal TYDF length for our ring cavity is about 10 m, when the side modes are significantly suppressed, allowing a single-wavelength operation. We have also observed that the operating wavelength shifts toward longer wavelengths with increasing pump power.

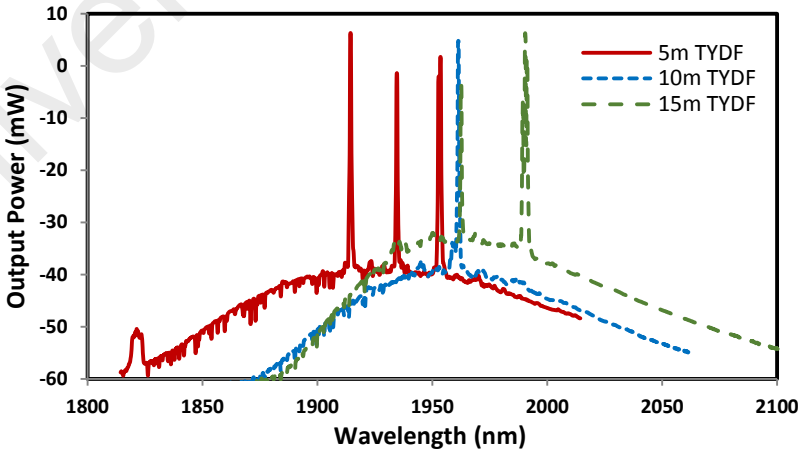

Figure 3.10: Output spectra of our ring TYDFL as measured for different TYDF lengths.

The lasing characteristics of the TYDF have also been studied for the case of linear cavity configuration (see Fig. 3.11). In this experiment, a linear cavity is formed

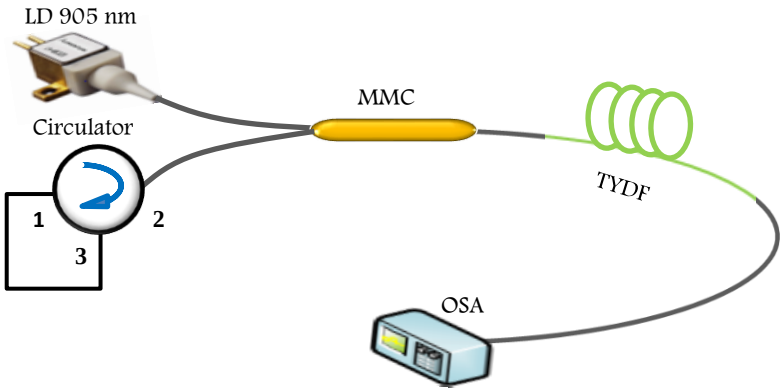

Figure 3.11: Experimental setup of our TYDFL in the linear configuration. OSA is optical spectrum analyzer.

in between an optical circulator, which is used to re-route the back-propagating light back into the cavity, and a splicing point located between the other end of TYDF and a standard single-mode fiber. Ports 3 and 1 of the circulator are spliced together so that the circulator can reflect back the incoming light from port 2. The mode mismatch between the TYDF and the single-mode fiber reflects a small portion of light (~ 3%) back into the cavity due to Fresnel reflection. By cladding pumping of the double-clad TYDF, the ASE is generated in the vicinity of 1950 nm. It oscillates in the linear cavity and produces laser light. The device starts to lase above some threshold pump power that depends on the fiber length. Fig. 3.12 shows the output power of the laser versus the pump power at three different gain-medium lengths. As seen from Fig. 3.12, the output laser power increases almost linearly with increasing pump power. The threshold pump powers 1300, 1400 and 1500 mW are typical for the 10, 15 and 5 m long fibers, respectively. The maximal output power (17.6 mW) is achieved when the pump power is equal to 3.56 W (for the case of 10 m long fiber).

The data of Fig. 3.12 testifies that, among the three fiber lengths under test, the 10 m long TYDF provides both the maximal output power and the minimal threshold. The slope efficiencies 0.75, 0.42 and 0.04% are peculiar for the 10, 15 and 5 m long fibers, respectively. Therefore the optimal gain medium for linear TYDFL is 10 m.

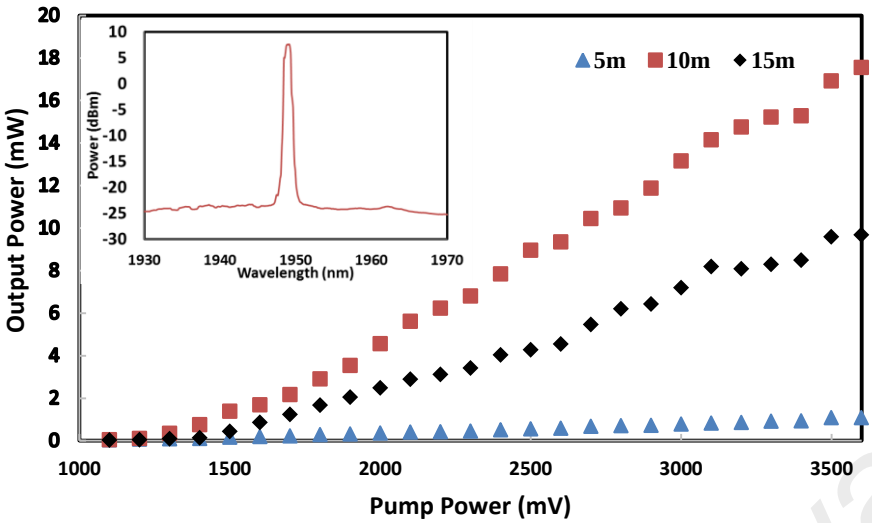

Figure 3.12: Output power versus pump power of linear TYDFL as measured at three different TYDF lengths. Inset shows the output spectrum of the TYDFL configured with 10 m long gain medium.

Nonetheless, the efficiency thus obtained is lower if compared to that typical of the ring TYDFL. This is because the 'mirrors' are built on simply using the Fresnel reflections, thus increasing significantly the cavity losses. Optimization of the output reflector is expected to improve the attainable efficiency and so the output power of our laser.

The inset in Fig. 3.12 displays the output spectrum of our linear TYDFL for the case when the TYDF length is fixed at 10 m. As seen from Fig. 3.12, the laser operates at 1949.2 nm, with the signal-to-noise ratio higher than 30 dB. Notice also that the operating wavelength is slightly shorter than that obtained for the ring cavity. This is attributed to higher losses for the linear cavity, when compared to the ring one. Indeed, higher losses shift the operating wavelength toward shorter wavelengths which have a higher gain to compensate for those losses.

3.4.3 Multi-wavelength TYDFL based on nonlinear polarization rotation effect

There is a growing interest in developing multi-wavelength fiber lasers with constant wavelength spacing. The multi-wavelength lasers have attracted extensive interest for many years, because of their wide potential applications in spectroscopy,

optical communication, optical instrument testing, and optical fiber sensors. Up to date, various techniques have been exploited to realize multi-wavelength fiber laser. Most of the techniques are based on nonlinear optical effect such as polarization hole burning (PHB), stimulated Brillouin scattering and nonlinear polarization rotation (NPR). Among these techniques, NPR is the most promising due to the controllable wavelength spacing. The NPR induces the intensity-dependent loss in the laser cavity so that the mode competition in the gain medium can be effectively suppressed. This allows the generation of a stable and broad bandwidth multi-wavelength laser source.

In this section, a multi-wavelength laser operating at 2 μm regions is demonstrated using a newly developed double-clad Thulium Ytterbium co-doped fiber (TYDF) as gain medium in conjunction with NPR approach. Here, the TYDF is employed in an opened linear cavity to generate an efficient multi-wavelength laser based on NPR assisted by FWM effect. Fig. 3.13 shows the experimental setup of the proposed multi-wavelength TYDFL with an opened linear cavity configuration.

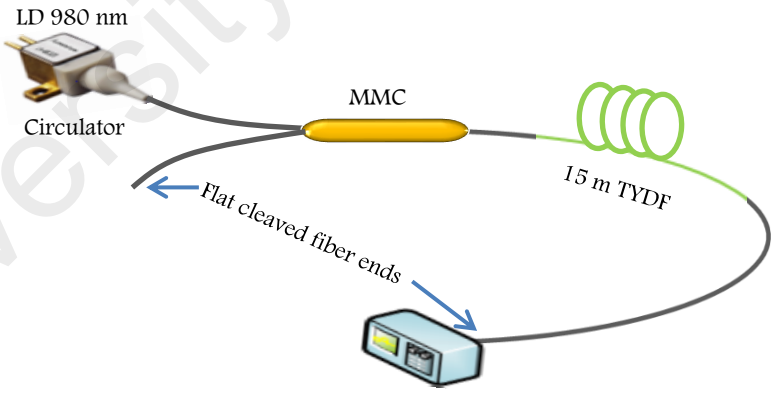

Figure 3.13: Experimental setup of the multi-wavelength TYDFL with an opened cavity configuration.

It consists of a 15 m long TYDF, which is pumped by a multimode 980 nm laser diode via a multimode combiner (MMC). 980 nm pump is used instead of 905nm to improve the efficiency of the laser. The TYDF is a homemade double-clad octagonal shaped fiber TYDF. A short standard single-mode fiber (SMF) is fusion spliced at the output

end of the TYDF to block the residual pump power. The linear laser cavity is formed by the 4% Fresnel reflection from the perpendicular cleaved fiber ends on both sides. The laser output is measured by using an optical spectrum analyzer (OSA) with a resolution of 0.02 nm and an optical power meter (OPM).

The laser is operated based on the TYDF gain and the resonance between 4% Fresnel reflection from both perpendicular cleaved fiber ends. When the TYDF is pumped by 980 nm laser to generate population inversion of Ytterbium ions, the emitted energy is then transferred to Thulium ions to generate an ASE in 2 μm region via spontaneous and stimulated emission process. It is observed that the opened linear cavity TYDFL starts to generate an ASE and stable multi-wavelength lasing as the 980 nm pump power hits the threshold at 700mW and 1800 mW, respectively. Fig. 3.14 shows the output spectra from the TYDFL at various 980 nm pump power as recorded by an OSA. With increasing power of the pump, ASE is generated at 1970 nm region. The ASE oscillates in the linear cavity to generate laser when the gain overcomes the total cavity loss. The multi-wavelength laser starts to be generated as the pump power is increased above 1800 mW. This is due to the effect of the TYDF birefringence, which induced round-trip phase variation in the linear laser cavity based on nonlinear polarization rotation (NPR) effect.

The NPR induces intensity and wavelength dependent loss to suppress mode competition caused by homogeneous gain broadening in the gain medium. As a result, some of the modes will be excited and some will be suppressed. This aspect determines the number of generated wavelengths. As shown in Fig. 3.14, the TYDFL operates at triple wavelengths of 1982.12 nm, 1986.69 nm and 1991.26 nm with a signal to noise ratio of more than 30 dB at the pump power of 2.05 W. The wavelength spacing between two lines is 4.57 nm. As the pump power is further increased to 2.75 W, the laser operates at shorter wavelengths of 1970.60 nm and 1973.12 nm with a smaller

spacing of 2.52 nm. The signal to noise ratio of the dual-wavelength laser is more than 40 dB.

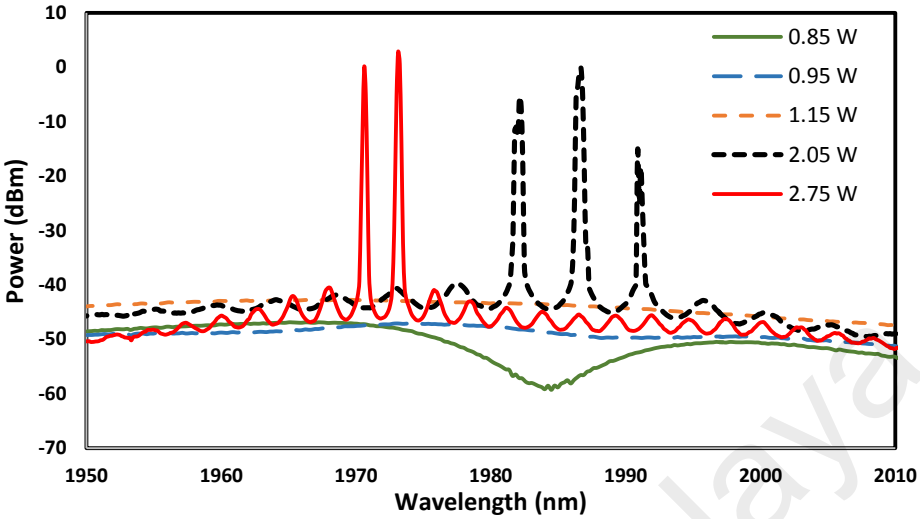

Figure 3.14: Output spectra of the proposed TYDFL with variation of pump power of multimode 980 nm laser diode from 0.85 to 2.75 W.

The relation between the output powers of the multi-wavelength laser against the multimode pump power is shown in Fig. 3.15. The TYDFL starts to produce ASE at 1970 nm region.

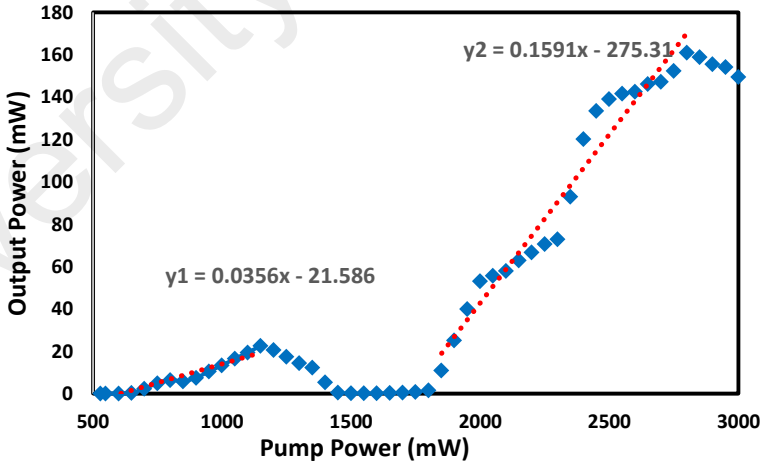

Figure 3.15: Output power against the 980 nm pump power for the proposed multi-wavelength TYDFL.

The ASE power increases linearly with the increase of pump power at a slope efficiency of 3.6%. The ASE oscillates in the linear cavity to generate a multi- wavelength as the pump power reached the threshold pump power of 1800 mW through a stimulated emission process. The output power of the laser is observed to increase linearly with the

increment of multimode pump power up to pump power of 2850mW with a slope efficiency of 15.9 %. The maximum output power of 159 mW with dual-wavelength lasing is obtained at pump power of 2850 mW. Since, the TYDF used in the cavity has a reasonably high nonlinearity, it produces sufficient NPR and four-wave mixing (FWM) induced intensity dependent loss effect in the laser cavity. In this case, the transmission term varies too fast with the power and thus allows at least two wavelengths to oscillate in the linear cavity. At 2800 mW pumping the output power saturates and further increase in pump power increases the noise thus reduces the output power.

3.5 Summary

Both EYDFL and TYDFL operating in CW modes are successfully demonstrated based on both double-clad fiber in conjunction with multimode pumping. At first, cladding pumped EYDFL is investigated based on both linear and ring configurations. The EYDF used has a core composition of SiO_2- GeO_2 - Al_2O_3 – Er_2O_3 - Yb_2O_3 with NA of 0.20 and the cut-off wavelength of 980 nm. In linear configuration, the laser operates at 1535.4 nm, 1544.3 nm and 1545.6 nm with slope efficiencies of 4.3%, 15.0% and 18.4% at EYDF lengths of 1, 4 and 5 m, respectively. This shows the optimum fiber length of the EYDFL operation is 5 m or longer with the maximum output power of 537 mW is obtained at the maximum pump power of 3100mW. The threshold pump power is about 140 mW for all lasers.. In ring configuration, the slope efficiencies of 0.8%, 3.1% and 4.6% are obtained at active fiber lengths of 1m, 4m and 5m, respectively. Compared to the linear cavity, the proposed ring cavity demonstrates a significant lower efficiency due to the higher cavity loss. The lasing performance of a newly developed Thulium-Ytterbium co-doped octagonal shaped double-clad fiber is also investigated and demonstrated based on the cladding pump technique. The fiber is fabricated using a modified chemical vapor deposition (MCVD) in conjunction with

solution doping technique. It has Tm^{3+} and Yb^{3+} cladding absorptions of 0.325 and 3.3 dB/m at 790 nm and 976 nm respectively. A triple wavelength fiber laser operating at 1914.5 nm, 1934.7 nm and 1953.6 nm is successfully demonstrated using a 5 m long fiber as the gain medium in ring configuration pumped with 905 nm laser diode. With 15 m long fiber, the ring laser produces the highest output power of 21.9 mW at pump power of 3600 mW with the lowest threshold pump power of 1000 mW. The maximum efficiency of 0.88% operating at 1961.4 nm is achieved when the gain medium is fixed at 10 m. The characteristics of TYDF are also studied in linear cavity configuration using an optical circulator with 5, 10 and 15 m long gain mediums. The laser operates around 1950 nm, with efficiencies of 0.75, 0.42 and 0.04 % corresponding to 10, 15 and 5 m long TYDF respectively. The TYDF fiber is observed to be less efficient in linear configuration, attributed to the mirrors. Optimization of the output mirrors could improve the efficiency. A multi-wavelength TYDFL operating at 2 μm region is also demonstrated based on NPR effect using the same octagonal shaped double-clad TYDF as gain medium. The proposed laser employs an opened linear cavity configuration to generate the multi-wavelength output lines as the 980nm multimode pump power is increased above a threshold value of 1800 mW. It generates triple-wavelength outputs at 1982.12 nm, 1986.69 nm and 1991.26 nm when the 980 nm multimode pump power is about 2.05 W. At pump power of 2.75 W, the laser lines reduces to two (1970.60 nm and 1973.12 nm) with a signal to noise ratio of more than 40 dB. The slope efficiency of the multi–wavelength laser is about 15.9 %. The maximum output power of 161 mW is obtained at pump power of 2800 mW.

CHAPTER 4: Q-SWITCHED ERBIUM-YTTERBIUM AND THULIUM-YTTERBIUM CO-DOPED FIBER LASERS

4.1 Introduction

Lasers operating in CW or quasi-CW regime have limited optical output power, depending on the maximum available pump power. By concentrating the available energy on a single short optical pulse, or in a periodic sequence of optical pulses, higher peak power is attainable. Q-switching is a technique that enables the generation of short optical pulses by means of repeated switching of the cavity loss (Harun et al., 2012; Kobtsev et al., 2008; Y. Wang & Xu, 2007). Compared to CW fiber lasers, high-peak-power Q-switched fiber lasers are practically useful in numerous applications, such as range finding, fiber sensing, industrial processing, communication and medicine (Fan et al., 2004; J. H. Lin et al., 2007). Active Q-switching is typically achieved by inserting a modulator or an ultrafast silicon-based variable optical attenuator into the cavity (Chang et al., 2011). On the other hand, passive Q-switching is attained by employing saturable absorbers (SAs). It is a convenient technique that simplifies the cavity design and eliminates the need for external Q-switching electronics. In this chapter, several new passively Q-switched fiber lasers are proposed and demonstrated using Erbium-Ytterbium and Thulium-Ytterbium co-doped fibers as gain medium to operate at 1550 nm and 1900 nm region, respectively. All the fiber lasers are based on a low cost multimode pumping.

4.2 Q-switched Erbium-Ytterbium co-doped Fiber Laser (EYDFL) using a nonlinear polarization rotation technique

Recently, nonlinear polarization rotation (NPR) technique has been widely used to provide an artificial SA effect in a mode-locked fiber ring laser. Moreover, the NPR

technique provides an intrinsic feature of spectral filter induced by the combination of polarizer and intra-cavity birefringence, which can be used to achieve the wavelength tunable operation in the fiber ring laser. For instance, Luo et. al. (Luo et al., 2010) employed the NPR induced spectral filtering effect to develop wavelength tunable passively mode-locked fiber laser. However there is still a lack of research work on the use of NPR technique in realizing Q-switched pulses. In this section, a Q-switched Erbium-Ytterbium co-doped Fiber Laser (EYDFL) is proposed and demonstrated based on the NPR technique by configuring the laser cavity so that it has sufficiently high cavity loss to prevent mode locking. The gain medium is a double-clad Erbium-Ytterbium co-doped Fiber (EYDF), which is pumped by a multimode 980 nm pump to generate lasing at 1543.5 nm. In this approach, an isolator is used in conjunction with a highly nonlinear EYDF in a ring cavity to induce intensity dependent loss and initiate Q-switching pulse.

4.2.1 Configuration of the NPR based Q-switched EYDFL

Fig. 4.1 shows the configuration of the proposed Q-switched EYDFL, which consists of a 5 m long double-clad EYDF, a multimode combiner (MMC), an isolator, a polarization controller (PC) and 95/5 output coupler in a ring configuration. The EYDF used has a multi lobed pump guide with a core, inner and outer cladding diameters of 5 µm, 105 µm and 125 µm respectively. Inset of Fig. 4.1 shows the cross-section image of the EYDF, which has a multi lobed pump guide structure. The core has a numerical aperture (NA) of 0.21 whereas the pump guide (inner cladding) has the NA of 0.25. The fiber is pumped by a 980 nm multimode laser diode via the MMC. The PC is used to adjust the polarization state of the oscillating light and the birefringence inside the ring cavity. The isolator is incorporated in the laser cavity to ensure unidirectional propagation of the oscillating laser as well as to function as an artificial SA when

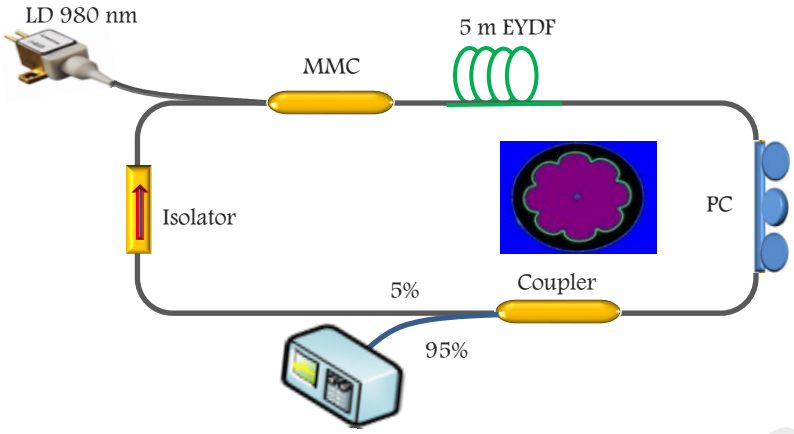

Figure 4.1: Schematic diagram of the proposed Q-switched EYDFL based on NPR technique. Inset shows a cross-section image of the EYDF with a multi lobed pump guide structure.

combined with the intra-cavity birefringence. The output of the laser is taken out of the cavity through a 95/5 coupler while keeping 5% of the light to oscillate in the ring cavity. The optical spectrum analyzer is used to inspect the spectrum of the EYDFL whereas the oscilloscope is used to observe the output pulse train via a 1.2 GHz bandwidth photo-detector.

The total cavity length of the ring resonator is measured to be around 10 m. In order to avoid passive mode-locking, it is worth noting that we intentionally use a 95/5 coupler, which allow only 5 % of the light to oscillate in the cavity. This induces a cavity loss of more than 15 dB in the laser cavity, which is sufficient enough to avoid mode-locking. When the pump power is above the threshold, stable Q-switching pulse is generated when the PC is adjusted in such a way so that the light could not oscillate in the cavity as there is no feedback. At the same time, population inversion builds up leading to high stored energy in the gain medium. After some time the gain medium will be saturated and amplification will take place where Q-switch pulse is formed.

4.2.2 Q-switching performance

In our experiment, NPR technique was applied to implement Q-switching opera-

tion. The combination of PC and isolator acted as an artificial saturable absorber due to the NPR effect so that the intensive waves transmitted in the laser cavity while the weak ones were suppressed. During experiment, when the pump power was increased to about 300 mW, the fiber laser can be easily tuned to operate in the Q-switching state via appropriately adjusting the PC. The optical spectrum and temporal waveform of the laser beam is shown in Figs. 4.2 and 4.3, respectively at pump power of 500 mW. As shown in Fig. 4.2, the EYDFL operates at 1543.51 nm with a 3 dB bandwidth of 0.27 nm.

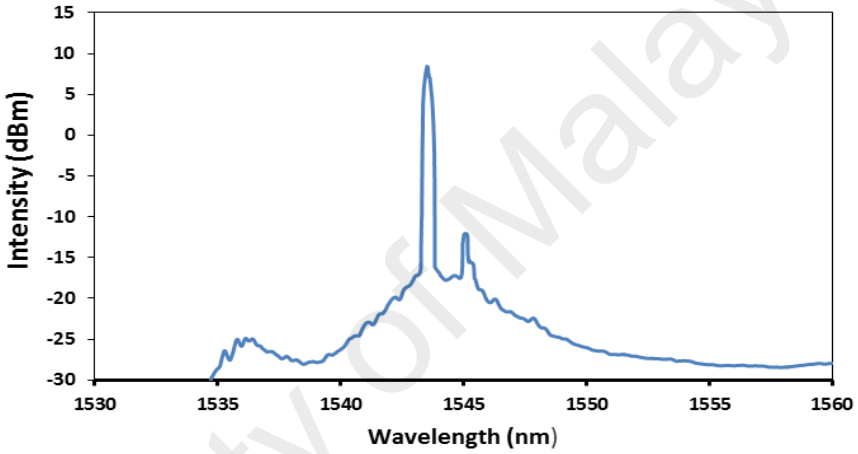

Figure 4.2: The spectral characteristic of the proposed Q-switched EYDFL at the pump power of 500 mW.

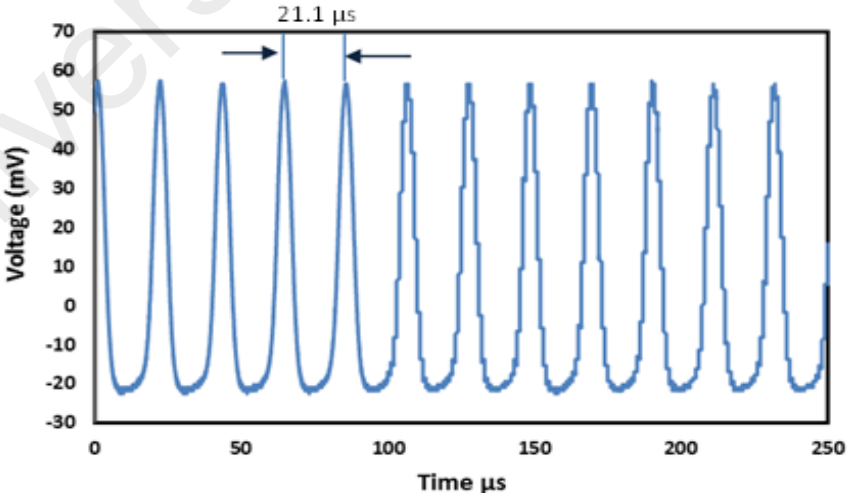

Figure 4.3: The typical pulse train of the proposed Q-switched EYDFL at the pump power of 500 mW.

The spectral broadening is observed in the spectrum due to self-phase modulation (SPM) effect in the laser cavity. The pulses were uniformly sequenced in a train at the

The pulses were uniformly sequenced in a train at the pulse separation of 21.1 μs, which corresponds to repetition rate of 46.95 kHz at this pump power as shown in Fig. 4.3. The pulse width of the pulse train is measured to be around 5.3 μs. By adjusting the polarization state of the oscillating light with the help of PC, the Q-switching pulse is obtained within the pump power range from 300 to 600 mW.

The pump laser creates population inversion in the fiber. As soon as the Erbium ions reach excited state through non radiative energy transfer from Ytterbium ions, some of them undergo spontaneous emission and a fraction of this is guided by the EYDF. Due to the presence of a large number of longitudinal modes which have in general random phase relationships with each other, the light intensity within the ring will have fluctuations. If we consider a portion of light intensity within the ring just before the polarization controller it is linearly polarized and the PC changes it into some elliptical polarization state. Assume that the fibers within the ring maintain the polarization state, then as oscillating light corresponding to low intensity will not be able to pass through the PC as it is adjusted to block the propagation of the elliptically polarized light. Now consider a short pulse of high intensity fluctuations arising out of the interference between various longitudinal modes as it starts from the right end of the fiber, it is linearly polarized and can pass through the PC converted to an elliptically polarized light after losing a portion of light at the output probe of the coupler the rest of the light passes through the isolator and MMC enters the EYDF where it undergoes nonlinear polarization rotation and recovers its linear polarization state, which will employ low loss for the high intensity portion. At the same time the low intensity portion of the pulse will not undergo polarization rotation and thus would be partially blocked by the PC. Hence ring is exhibiting low losses (high Q) for high intensity portion and high losses (low Q) for low intensity portion. This in turn will ensure that the high intensity portions grow in intensity, while the low intensity portions die out,

resulting in the generation of pulses with high energy. Thus the phenomenon of non-linear polarization leads to the generation of high energy pulses.

It comes to our attention that the repetition rate and pulse width of the Q-switched pulses is sensitive to the pump power. In order to further investigate the relationship between them, we fastened the direction of PC, and increased the pump power from 300 to 600 mW. It is observed that the Q-switching pulse disappears as the pump power is increased above 600 mW. The dependence of the repetition rate and pulse width on the input pump power is shown in Fig. 4.4. As shown in the figure, the repetition rate increases almost linearly with the pump power. The result coincides well with the inherent characteristic of the Q switched fiber laser. The pulse repetition rate can be varied from 26.7 to 70.08 kHz as the pump power increases from 300 and 600 mW. On the other hand, the pulse width decreases from 7.5 to 5.3 μs as the pump power increases from 300 to 500 mW. However, with further increase in pump power, an anomalous behavior is observed where the pulse width increases to 6.62 μs at 600mW as shown in Fig. 4.4.

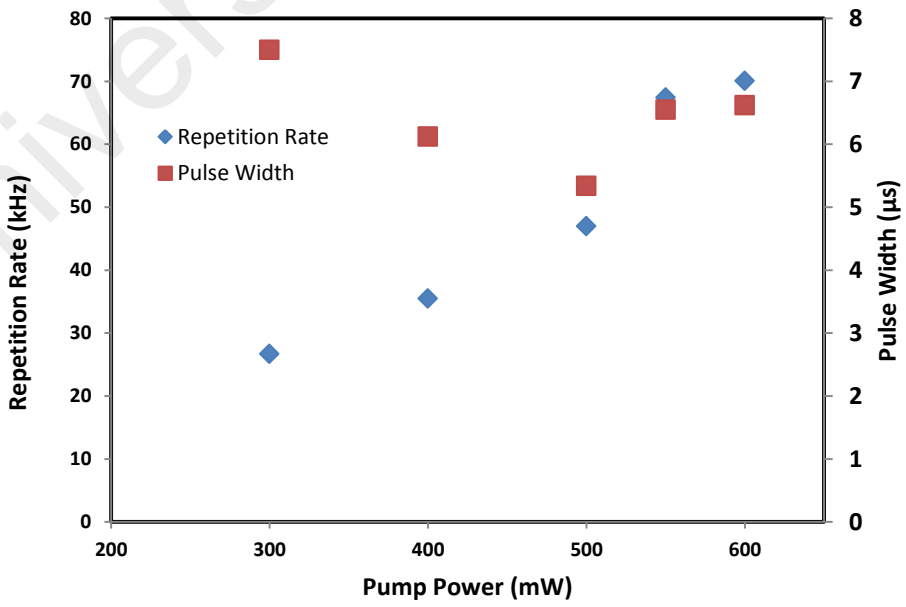

Figure 4.4: Repetition rate and pulse width as functions of 980 nm multimode pump power.

Fig. 4.5 shows the pulse energy and average output power of the Q-switched EYDFL as functions of pump power. Both output power and pulse energy show an increasing trend with the pump power. As shown in the figure, the Q-switched laser has a slope efficiency of 1.39 % with the maximum output power of 5.23 mW, obtained at 600 mW multimode pump power.

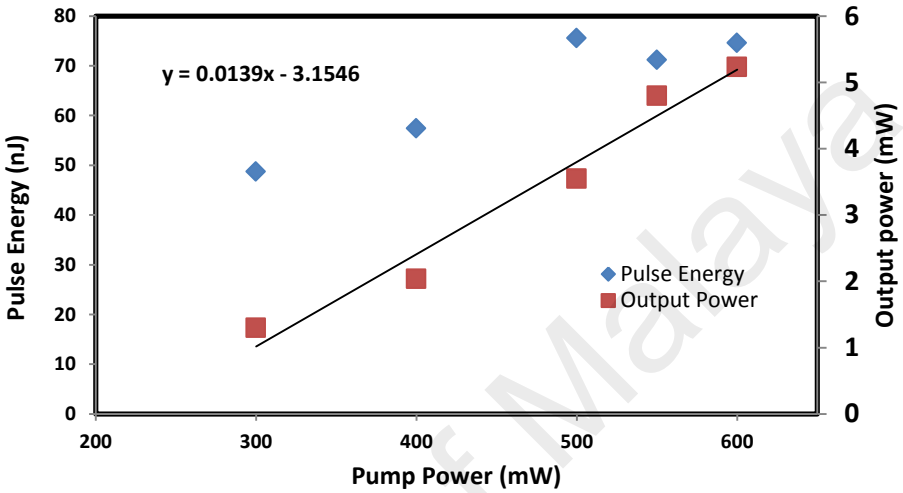

Figure 4.5: Pulse energy and average output power as functions of 980 nm multimode pump power.

On the other hand, the pulse energy increases from 48.7 to the maximum value of 75.6 nJ as the pump power increases 300 to 500 mW. However, the pulse energy starts to saturate as the pump power further increases, this is due to transfer of energy to lattice vibrations, this increass noise, which limits the output energy.

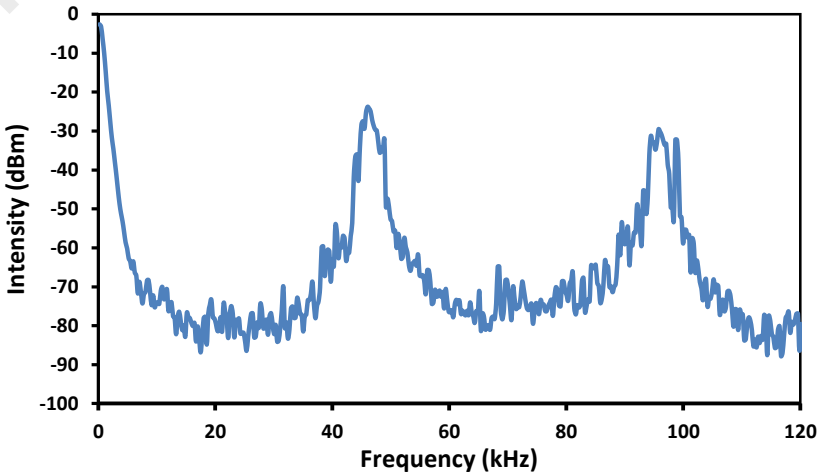

Figure 4.6: RF spectrum of the Q-switched EYDFL at pump power of 500 mW.

Fig. 4.6 shows the radio frequency (RF) spectrum of the Q-switched EYDFL, which was obtained using RF spectrum analyzer via a 1.2 GHz photo-detector. As shown in the figure, the repetition rate is obtained at 46.95 kHz with signal to noise ratio of about 50 dB, which indicates the stability of the Q-switched laser. The harmonics of the Q-switching frequency are present because the modulation of the laser output at the Q-switching frequency is far from sinusoidal. These results indicate that NPR technique has a big potential for Q-switching applications using just simple configuration with cladding pumping. This inexpensive laser is suitable for applications in metrology, environmental sensing and biomedical diagnostics.

4.3 Q-switched EYDFL using Molybdenum disulfide (MoS_2) saturable absorber

Inspired by their unique optical and electronic properties, two-dimensional layered materials have been intensively investigated in recent years, driven by their potential applications for future high speed and broadband electronic and optoelectronic devices. Particularly, the existence of quantum confinements, the absence of inter-layer interactions and the strong intra-layer covalent or ionic bonding, allow researchers to fabricate compact, functional, flexible and efficient photonic devices. For instance, graphene, the most representative two-dimensional nano-material with Dirac-like electronic band structure, has become one of the most heavily studied targets among optical researchers in the past few years (Bao et al., 2009; Yamashita, 2012; Han Zhang et al., 2009). It possesses some unique optical advantages, such as ultra-fast photo-response and ultra-wideband response ranging from ultraviolet (UV) to terahertz (Zheng et al., 2012) Besides these merits, unfortunately, graphene holds two intrinsic disadvantages, the zero band gap and the weak absorption co-efficiency (~2% of incide-ncident light per layer), significantly limit its light modulation ability and potential app-

lications in optics related fields that may require strong light-matter interaction.

Recently 2D transition metal dichalcogenides (TMDs) have also got researchers attentions due to their exceptional optical properties that may complement with graphene and other 2D materials like insulating hexagonal boron nitride, and even overcome the short comings of graphene. Many works have also been reported on generating Q-switched and mode-locked fiber lasers using TMD materials (K. Wang et al., 2013; H Zhang et al., 2014) For instance, the saturable absorption of molybdenum disulfide (MoS2), was demonstrated using the Z-scan technique at 800 nm (H Zhang et al., 2014). By inserting the MoS_2 SA into erbium-doped fiber laser (EDFL), a ~710 fs pulse centered at 1569 nm wavelength with a repetition rate of 12.09 MHz was demonstrated (H. Liu et al., 2014). On the other hand, multi-wavelength fiber laser have also wide applications in optical communications, sensors and instrumentations. In this section, a multi-wavelength Q-switched EYDFL using a few-layer MoS_2 saturable absorber (SA) is demonstrated. The few-layer MoS_2 was prepared by the liquid phase exfoliation (LPE) method and sandwiched between two fiber ferrules with a fiber adapter to form a fiber-compatible MoS_2-based SA. The SA is integrated into a ring cladding pumped laser cavity to produce a stable multi-wavelength Q-switched laser operating at wavelength around 1563 nm.

4.3.1 Preparation and characteristics of MoS_2

Up to date, several approaches have been reported to exfoliate a few-layer MoS_2 from the bulk materials such as micromechanical cleavage, chemical vapour deposition (CVD) and solution based methods. Among these methods, liquid phase exfoliation (LPE) is considered to be the most efficient and cost effective approach since it does not require any post-chemical treatments of the prepared solvents and permits large scale production. The LPE process for MoS_2 was carried out based on two steps. At first, the

bulk MoS_2 crystal powder was added with Dimethylformamide (DMF) solvent with an initial concentration of 5 mg/ml. DMF was used since it has a similar surface energy with MoS_2 (~75 $mJ \cdot m^{-2}$) (Cunningham et al., 2012). Secondly, the solution is ultrasonicated for 24 hours to break the weak Van der Walls force between the atomic layers using a bath ultrasonicator. The suspension is then centrifuged at 3000 rpm for 60 minutes and the supernatant is extracted from the suspension to obtain the few-layer MoS_2. The free-standing MoS_2–polymer composite film is prepared by mixing 10 ml of the few-layer MoS_2 dispersion with 20 ml of aqueous polyvinyl alcohol (PVA) solution with concentration of 10 mg/ml. The solution was obtained by dissolving 200 mg of PVA in 20 ml of deionized water. The MoS_2-PVA solution mixture, which is now 30 ml, is then stirred using a magnetic stirrer and heated continuously at a temperature of 80 °C till the solution is reduced to approximately 10 ml. This process takes approximately 7 hours to complete. The reduced MoS_2–PVA mixture is then poured into a glass substrate and dried in an oven at ~80 °C for another 4 hours to form a ~40 μm thick free-standing composite film.

Raman spectroscopy measurement was then carried out for the fabricated MoS_2–PVA film sample to confirm the presence of few-layer MoS_2 nanosheets inside the thick composite film. In the experiment, Renishaw's Raman analyzer with an excitation wavelength of 514 nm and laser power of 10 mW was used. Fig. 4.7 shows the generated Raman spectrum, which exhibited two Raman characteristic bands at 407 cm^{-1} and 383 cm^{-1} (Tongay et al., 2012; Yim et al., 2014), corresponding to the A_{1g} and E^1_{2g} modes, respectively. It should be noted that the peak frequency difference between the in-plane (E^1_{2g}) and out-of-plane (A_{1g}) vibration modes can be used to identify the number of MoS_2 layers. The frequency difference of the MoS_2 sample was 24 cm^{-1}, corresponding to a layer number of 2~5 (Li et al., 2012). The absence of a noticeable shift in the peak positions from those measured for the exfoliated MoS_2 indicates that

the material structure is unaffected by its inclusion in the composite.

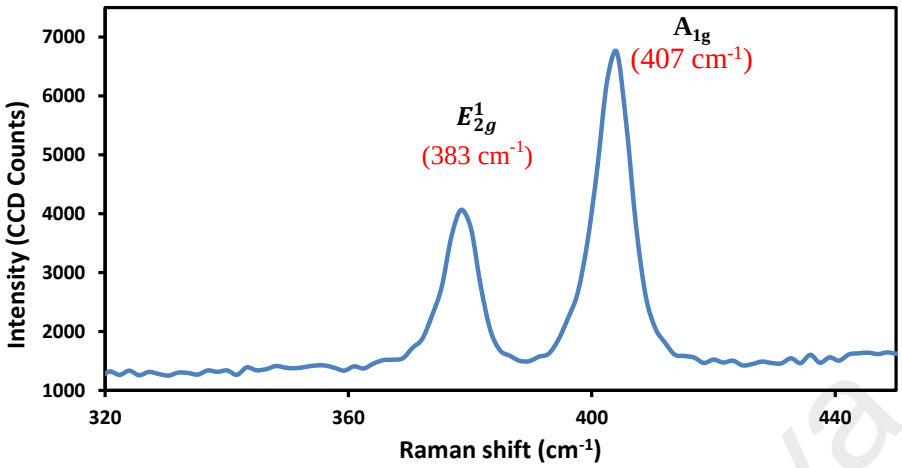

Figure 4.7: Raman spectrum of the MoS_2-polymer composite film.

4.3.2 Experimental setup for MoS_2 based Q-switched EYDFL

The fabricated MoS_2–PVA film was then used to build a pulsed fiber laser working at the main telecommunication window of 1.55 µm. Cladding pumped EYDFL is selected in our experiment, as it has a simple and compact design, efficient heat dissipation, and high-quality pulse generation. The layout of our designed fiber laser is schematized in Fig. 4.8. A 5 m long double-clad EYDF is utilized as the gain medium.

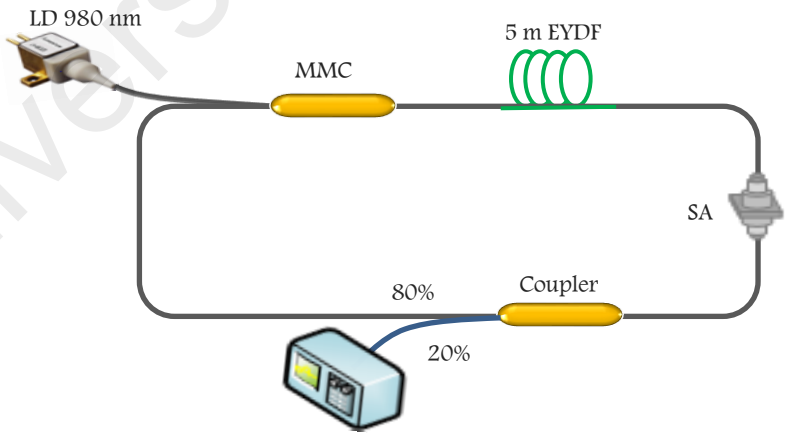

Figure 4.8: Experimental setup of Q-switched EYDFL in ring configuration.

Medium is pumped by a multimode 980 nm laser diode (LD) via a MMC. The MoS_2-PVA SA is integrated into the fiber laser cavity by sandwiching a ~1 × 1 mm^2 piece of the fabricated film between two fiber connectors, adhered with index matching gel. An

80/20 coupler is used to extract the 20 % of light from the cavity for measurements. The total cavity length is ~11 m.

4.3.3 Performance of the MoS_2 based Q-switched EYDFL

Q-switching operation began at a multimode pump power of 100 mW, and stable Q-switched pulses were maintained up to pump power of 1250 mW. Fig. 4.9 shows typical oscilloscope trace of the Q-switched pulse train at pump power of 600 mW. It shows a pulse period of 26.6 µs, which translates to a pulse repetition rate of 37.6 kHz. There is no distinct amplitude modulation in the entire Q-switched envelope in the spectrum, which leads to a knowledge that the self-mode locking effect on the Q-switching is weak. The pulse width is measured to be around 7.12 µs. To verify that the passive Q-switching was attributed to the MoS_2 SA, the ferrule filled with MoS_2 film was replaced with a common clean ferrule.

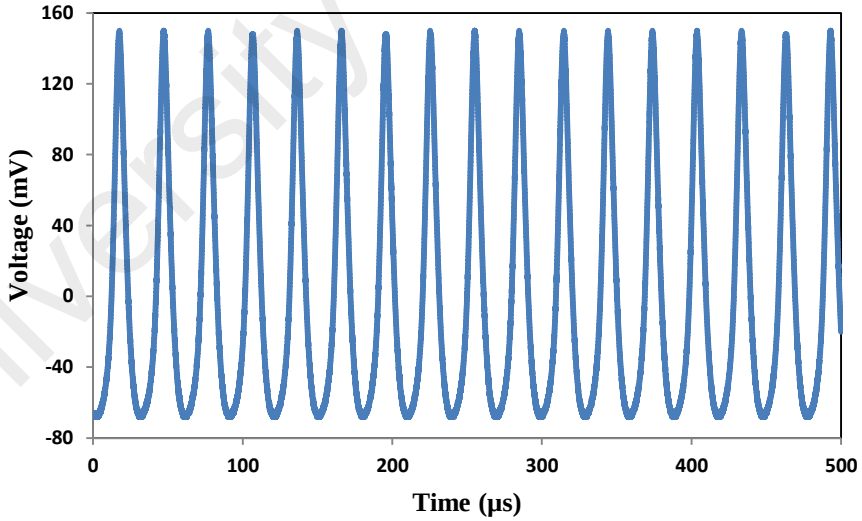

Figure 4.9: Pulse train of Q-switched EYDFL at 600 mW pump power.

In this case, no Q-switched pulses were observed on the oscilloscope even when the pump power was adjusted over a wide range. This finding has confirmed that the MoS_2 film was responsible for the passively Q-switched operation of the laser.

Fig. 4.10 shows the optical spectrum of the Q-switched pulses at three different pump powers. All the spectra show a stable multi-wavelength oscillation centered at wavelengths of 1563.8 nm, 1563.1 nm and 1562.5 nm when the multimode 980 nm pump power is fixed at 250 mW, 750 mW and 1250 mW, respectively. The presence of the MoS_2 thin film in the cavity, induces higher birefringence to the cavity. Moreover, the inhomogeneous loss of the MoS_2 film assisted to suppress the mode competition in EYDF. Thus, the stable multi-wavelength is achieved. As shown in Fig. 4.10, the center wavelength of the multi-wavelength comb shifts to a shorter wavelength as the pump power increases. This is attributed to the peak gain of the EYDF, which shifts towards 1560 nm region as the pump power increases.

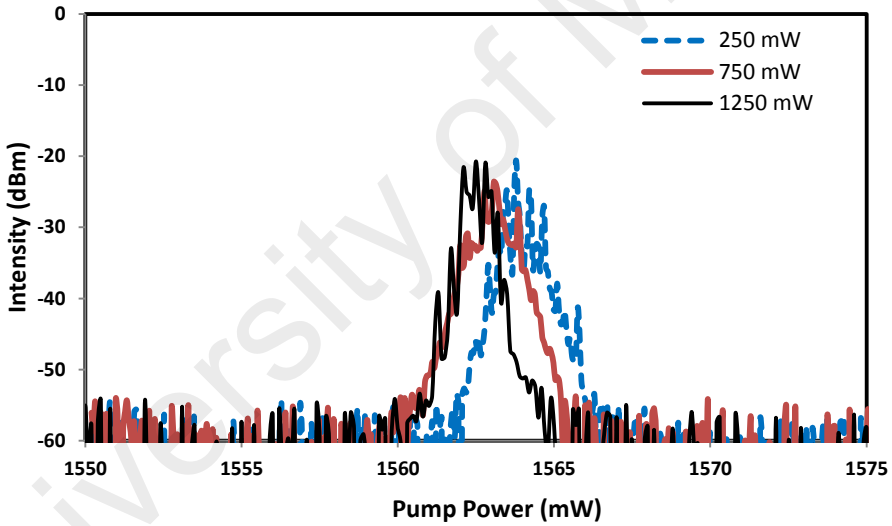

Figure 4.10: Optical spectrum of Q-switched EYDFL at three different pump powers.

Fig. 4.11 shows the pulse repetition rate and pulse width of the Q-switched fiber laser as a function of the incident pump power. In the experiment, the Q-switching pulse is obtained within the pump power range from 100 to 1250 mW. At the threshold pump power of 100mW, the laser produces Q-switched pulse with an average output power of 0.204 mW, repetition rate of 6.4 kHz and pulse width of 29.18 µs. Beyond 1250 mW pump power the laser starts producing continuous wave output.

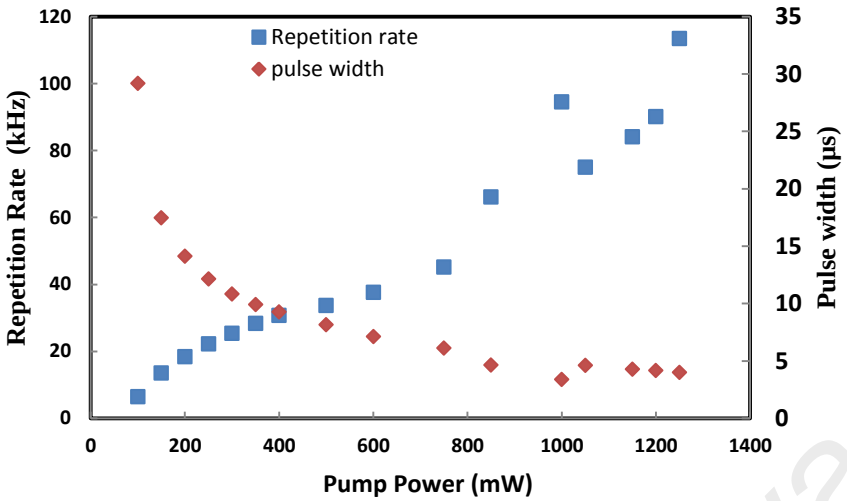

Figure 4.11: Repetition rate and pulse width of Q-switched EYDFL within 100 mW to 1250 mW.

Unlike the fixed repetition rate of a mode-locked fiber laser (Z. Tian et al., 2015) the pulse repetition rate in our laser increased with the pump power, from 6.4 to 113.4 kHz, which is a typical feature of passive Q-switching operation. On the other hand, the pulse width decreased from 29.18 µs near the pump threshold to 3.99 µs at a pump power of 1250 mW. It is observed that the pulse repetition rate can be controlled by varying pump power. A down chirp is observed in repetition rate at the pump power of 1050 mW. This is attributed to the effects of chromatic dispersion and nonlinearities such as self-phase modulation due to optical Kerr effect. For a passively Q-switched laser, the pulse duration or pulse width τ can be evaluated using the following equation (Zayhowski & Kelley, 1991):

$$\tau = \frac{3.5TR}{\Delta T} \qquad (4.11)$$

where TR is the cavity round-trip time and ΔT is the modulation depth of the SA. Therefore, the minimum pulse duration obtained in our experiment could be further narrowed by shortening the cavity length and improving the modulation depth of the few-layer MoS_2.

Fig. 4.12 shows the dependence of the average output power of the Q-switched fiber laser versus the pump power. Based on the measured average output power and the

repetition rate, the pulse energy was calculated, which is also displayed in Fig. 4.12. When the pump power exceeded the threshold, the average output power and pulse energy increased almost linearly with the pump power up to pump power of 600 mW and 500 mW, respectively. Both output power and pulse energy drop as the pump power is further increased. The maximum average output pump power and pulse energy are recorded at 12.43 mW and 96.67 nJ, respectively.

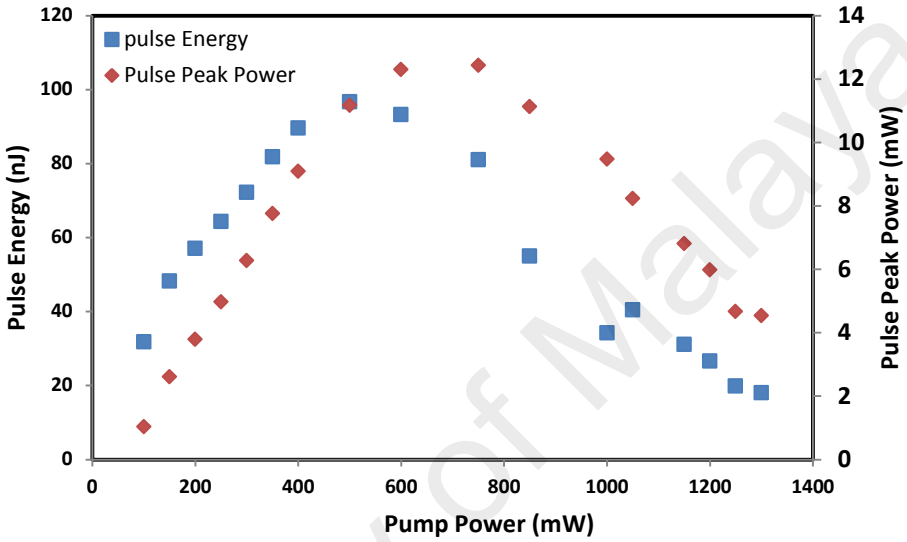

Figure 4.12: Pulse energy and pulse peak power of Q-switched EDFL within 100 mW to 1250 mW.

4.4 Q-switched TYDFL using Multi-walled Carbon Nanotubes Passive saturable absorber

Thulium (Tm) doped fiber lasers (TDFLs) are useful for generating coherent emission in the “eye-safe” wavelength range. Their emission band extends over a wide range of wavelength from 1.6 μm to over 2 μm, and they can be efficiently pumped at ~790 nm, ~1200 nm, or ~1600 nm (Geng et al., 2007; Z. Zhang et al., 2011). These features make Tm doped fiber lasers attractive for a variety of applications in defense (Eichhorn, 2010), medicine (Theisen-Kunde et al., 2007), spectroscopy (Baudelet et al., 2010), and material processing (Mingareev et al., 2012). Interest in the 2 μm lasers for medical field is mainly due to their radiation which has a strong absorption in water and

biological tissues. For instance, incision in porcine and chicken tissues have been recently demonstrated using a continuous wave TDFL (Pierce et al., 1999). The penetration depth of this laser also matches with the subcutaneous depth of the pain nerve receptors in the skin which results in minimal damage and pain when used as power source for research and treatment (Opsommer et al., 2001). El-Sherif and King reported a Q-switched TDFL for soft and hard tissue ablation(El-Sherif & King, 2003).

There are also growing interest in compact Q-switched laser sources that operate in the mid-infrared spectral region around 2 micron. This is mainly driven by the applications in spectroscopy, communication, material processing, manufacturing, sensing, medicine and nonlinear optical research (Lu et al., 2013; Q. Wang et al., 2012). Unlike active Q-switching, passive Q-switching is more convenient and cost-effective in achieving high energy pulses as it does not require additional switching electronics (Rüdiger Paschotta, 2008; Webb & Jones, 2004). Passive Q-switching of TDFLs has so far been realized by a number of techniques including multiple quantum wells, Cr:ZnS and Cr:ZnSe crystals (Qamar & King, 2005; Tang et al., 2008). However, all of these implementations require the use of additional bulk components such as mirrors or lens pairs, thus compromising the key benefits of fiber lasers, i.e. their compactness and alignment-free operation. The most common passive Q-switching approach is the one using semiconductor saturable absorbers (SESAMs) but it suffers the drawback of their complex fabrication and narrow tuning range (Chernysheva et al., 2014). Single-walled carbon nanotubes (CNTs) material has become popular among researchers in recent years due to its ultrafast recovery time, wide operating bandwidth as well as easy integration with fiber optic systems. It has also been used to construct saturable absorbers (SAs) for laser application (Martinez & Sun, 2013; Set et al., 2004).

More recently, a new member of carbon nanotubes family called multi-walled carbon nanotubes (MWCNTs) has also attracted much attention for nonlinear optics

applications due to its lower production cost, which is 50% - 80% cheaper than the SWCNT material. Compared with SWCNTs, the MWCNTs have higher mechanical strength, photon absorption per nanotube and better thermal stability due to its higher mass density (Goze et al., 1999). Previously, Lin et. al. demonstrated a mode-locked Neodymium-doped Yttrium Orthovanadate (Nd:YVO) laser operating in 1 micron region using a MWCNTs SA (X. C. Lin et al., 2013). It was reported that MWCNTs-SA has a modulation depth of 4.7 % and the recovery time of about 330 fs. In this thesis, a Q-switched Thulium Ytterbium co-doped fiber laser (TYFL) is demonstrated using a homemade saturable absorber based on MWCNTs embedded in polyvinyl alcohol (PVA) composite for the first time. The active medium is also a homemade double clad Thulium Ytterbium co-doped fiber (TYDF) drawn from a preform which was manufactured based on modified chemical vapor deposition (MCVD) and solution doping processes. The SA is incorporated in the laser cavity by sandwiching the fabricated MWCNTs-PVA film between two fiber connectors.

4.4.1 Preparation and Raman characterization of the MWCNTs-PVA film

At first, the MWCNTs material used for the fabrication of the absorber in this experiment is functionalized so that it can be dissolved in water. The diameter of the MWCNTs used is about 10–20 nm and the length distribution is from 1 to 2 μm. The functionalizer solution was prepared by dissolving 4 g of sodium dodecyl sulphate (SDS) in 400 ml deionized water. 250 mg MWCNT was added to the solution and the homogenous dispersion of MWCNTs was achieved after the mixed solution was sonicated for 60 minutes at 50 W. The solution was then centrifuged at 1000 rpm to remove large particles of undispersed MWCNTs to obtain a stable dispersed suspension. MWCNTs-PVA composite was prepared by adding the dispersed MWCNTs suspension into a PVA solution in one to four ratio. PVA solution was prepared by dissolving 1 g

of PVA (Mw = 89×103 g/mol) in 120 ml of deionized water. The homogeneous MWCNTs-PVA composite was obtained by sonification process for more than one hour. The CNT-PVA composite was casted onto a glass petri dish and left to dry at room temperature for about one week to produce thin film with thickness around 10 µm. The SA is fabricated by cutting a small part of the prepared film (2×2 mm^2) and sandwiched between two FC/PC fiber connectors, after depositing index-matching gel onto the fiber ends. The insertion loss of the SA is measured to be around 3 dB at 1550 nm. A linear transmission curve of the MWCNTs-PVA film was also investigated as shown in Fig. 4.13. The curve indicates that the film has the saturable absorption (modulation depth) of around 4% and non saturable absorption of around 45%. Raman spectroscopy was then performed on the MWCNT-PVA film.

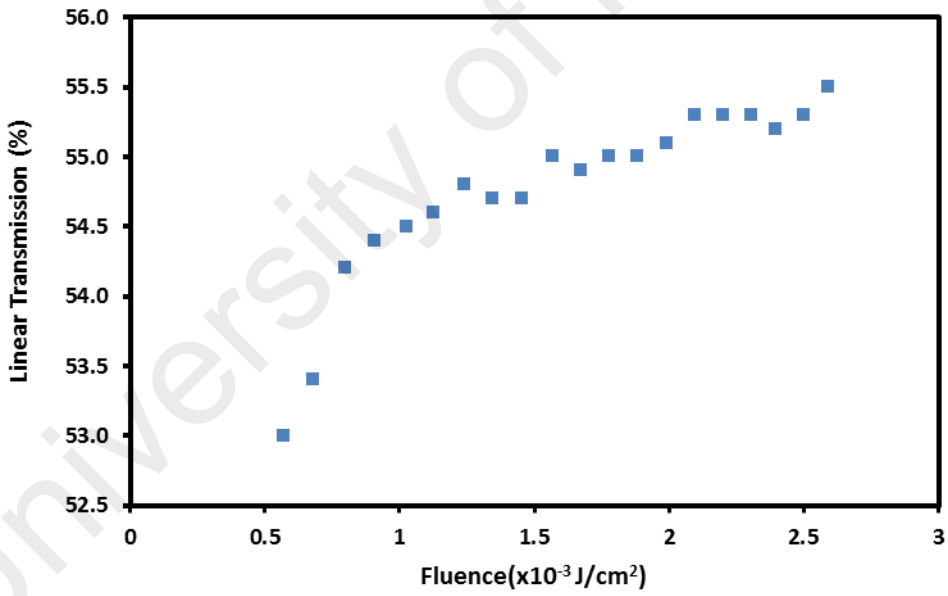

Figure 4.13: Linear transmission curve of the MWCNTs-PVA film, which shows that the saturable absorption and non-saturable absorption of around 4% and 45%, respectively.

The result is shown in Fig. 4.14, which indicates that the fabricated film consists of MWCNTs. The material properties of the MWCNTs are detailed in ref. (Kozma & K˘nya, 2013). The Raman spectrum of the fabricated MWNTs SA shows two main typical graphite bands observed in the Raman spectrum of MWCNTs bundles: the band

at 1585 cm^{-1} (G band) assigned to the in-plane vibration of the C–C bond (G band) and the band at 1400 cm–1 (D band) activated by the presence of disorder in carbon systems. The Raman spectrum also exhibits a band at 2900 cm^{-1} called the G´ band and attributed to the overtone of the D band (Bokobza & Zhang, 2012). An interesting small feature at 848 cm^{-1} is also observed, which is normally observed with armchair (n=8 to 11) single walled nanotubes. All armchair nanotubes with this chirality are assigned as a semiconducting type of nanotubes. In our spectra no radial breathing modes are observed. It can be because of the nanotubes consists of large number of walls (> 20) or because of large inner wall diameter (> 2 nm) (Zdrojek et al., 2004).

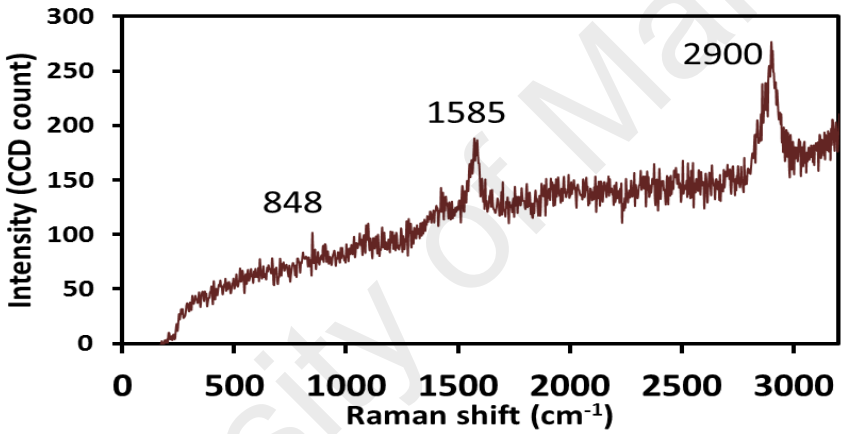

Figure 4.14: The Raman spectrum from the fabricated MWCNTs-PVA film.

4.4.2 Configuration of the Q-switched TYDFL

The schematic of the proposed Q-switched TYDFL is shown in Fig. 4.15. It was constructed using a simple ring cavity, in which a 15 m long laboratory made TYDF was used for the active medium. The fabrication and characteristics of the TYDF are detailed in the previous chapter. An indigenously developed MWCNTs-PVA based SA was used as a Q-switcher. The double-clad TYDF was forward pumped by a 905 nm multimode laser diode via a MMC. The laser output was tapped from a 10 dB output coupler located between the SA and MMC, which allows 10% of the oscillating light to be extracted from the ring cavity. The length of the cavity was approximately 20 m. The

OSA (Yokogawa, AQ6370B) was used to analyze the spectrum of the Q-switched TYDFL with a spectral resolution of 0.05 nm whereas the oscilloscope (OSC, Tektronix, TDS 3052C) was used to observe the output pulse train of the Q-switch operation via a photo-detector (EOT, ET-5010-F). All components used in our setup were polarization independent, i.e. they supported any light polarization. No polarization controller (PC) was used in the laser cavity as we found that a PC did not improve the pulse stability. There was no significant pulse jitter observed through the oscilloscope during the experiment. The lasing threshold was approximately 1.6 W.

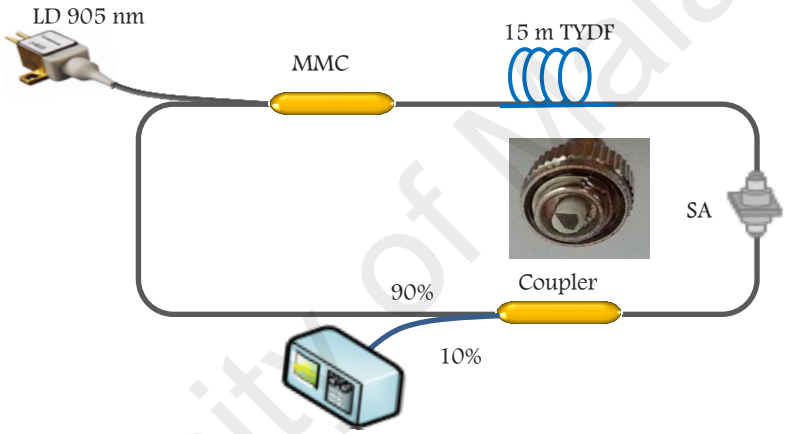

Figure 4.15: Setup of the proposed Q-switched TYDFL with MWCNTs-PVA based SA. Inset shows the image of the film attached onto a fiber ferule.

4.4.3 Q-switching performance of the TYDFL

Initially, the continuous wave (CW) TYDFL was investigated without using the SA and the laser threshold was found to be at 1.0 W pump power. The CW slope efficiency of the laser was also measured to be around 0.8 %. The low efficiency is most probably due to the use of cladding pumping as well as un-optimized fiber geometry and laser cavity. After inserting the SA, stable and self-starting Q-switching operation was obtained just by adjusting the pump power over a threshold value of 1.6 W. This threshold pump power is higher than that of the CW TYDFL due to the SA insertion loss. Fig. 4.16 illustrates the output spectrum of the Q-switched TYDFL at 1.6 W of 905

nm multimode pump power. As seen in the figure, the laser operates at 1977.5 nm with an optical to signal noise ratio (OSNR) of around 30 dB.

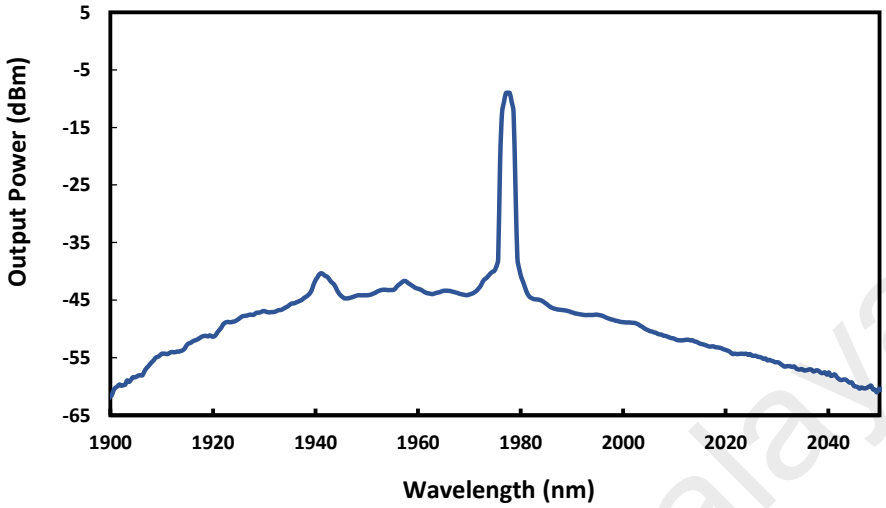

Figure 4.16: Output spectrum of the Q-switched TYDFL at pump power 1.6 W.

Fig. 4.17 (a) and (b) show the oscilloscope trace and the corresponding single pulse envelop of a typical Q-switched pulse train, respectively at pump power of 1.6 W. The spacing between two pulses in Fig. 4.17 (a) is measured to be around 53 µs, which can be translated to a repetition rate of 18.8 kHz. The corresponding pulse width is around 8.6 µs as shown in Fig. 4.17 (b).

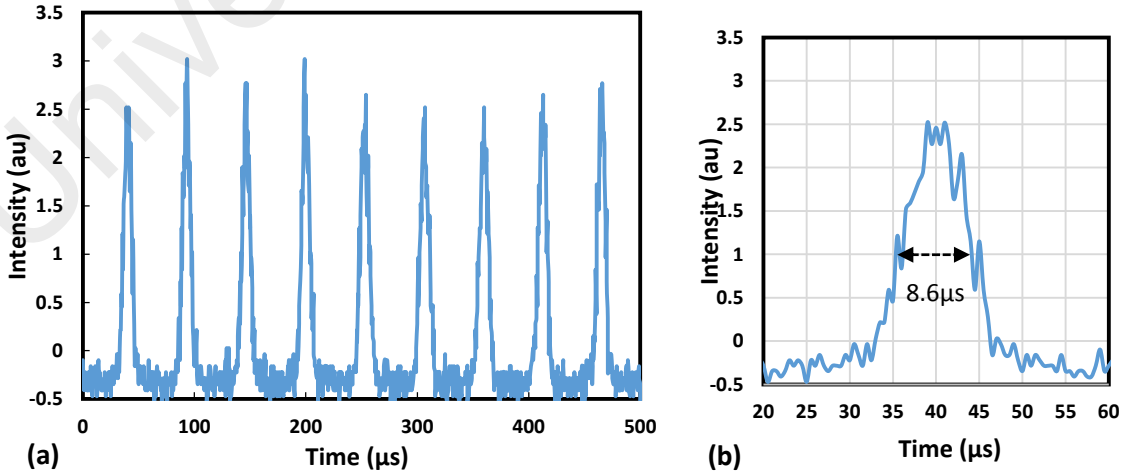

Figure 4.17: (a) A typical pulse trains and (b) a single pulse envelop of the proposed Q-switched TYFL at pump power of 1.6 W. It shows a repetition rate of 18.8 kHz and pulse width of 8.6 µs.

Fig. 4.18 shows the pulse repetition rate and pulse width as a function of the pump power. As the pump power increases from 1.6 to 2.3 W, the repetition rate of the Q-switched pulses grows from 18.8 to 50.6 kHz. At the same time, the pulse duration significantly reduces from 8.6 to 1.0 µs as expected. The pulse duration could be further narrowed by optimizing the parameters, including shortening the cavity length and improving the modulation depth of the MWCNTs Q-switcher. An anomalous increase in the pulse width is observed at 1862 mW pumping, attributed to fiber nonlinearities.

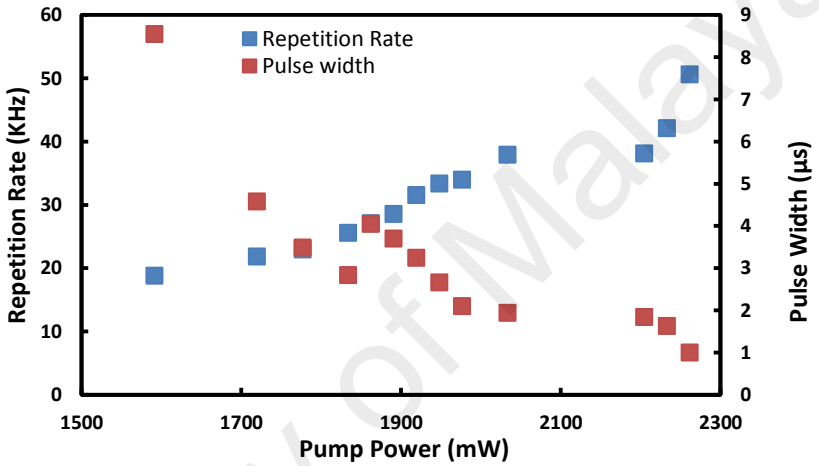

Figure 4.18: Repetition rate and pulse width as a function of 905 nm pump power.

We also measured the average output power and calculated the corresponding single-pulse energy (Fig. 4.19). Both the average output power and pulse energy almost linearly increase with the input pump power from 1.6 W to 2.1 W. However, as the pump power further increases, both the output power and pulse energy becomes saturated and drops. At the pump power of 2.1 W, the maximum output power of 0.21 mW is obtained which corresponds to the maximum pulse energy of 5.71 nJ. A higher pulse energy is attainable by optimizing the characteristics and dimension of the double-clad fiber as well as the cavity design to reduce the cavity loss. The TYDF is under the development phase, we need to optimize the dopant concentration along with minimizing detrimental nonlinear optical effects which are limiting the maximum achievable power from the fiber amplifier. The two nonlinear effects that are of particu-

cular interest, Self-phase modulation (SPM) and Raman gain (Galvanauskas & Sucha, 2003).

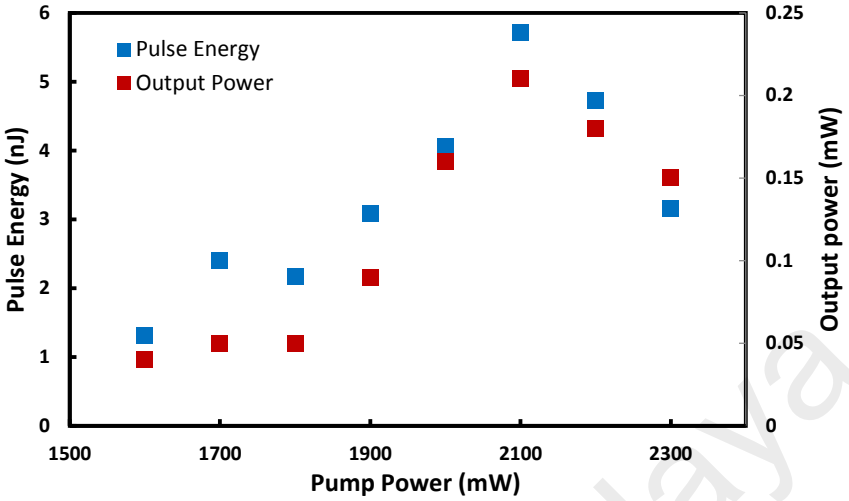

Figure 4.19: Output power and pulse energy as a function of 905 nm pump power.

SPM can be detrimental since it affects the phase of the amplified stretched pulses at high peak pulse intensities, which after recompression manifest as pulse shape distortions affecting both pulse duration and quality. Raman gain at high peak intensities leads to the "shedding" of optical power from the amplified pulse to long wavelength Raman spectral components, thus manifesting itself as a significant power loss at the fiber- amplified pulse wavelength. For future work, the optimizations of gain medium, cavity design and MWCNTs SA will be carried out to improve the pulse energy. Since it has a higher thermal stability, the attainable pulse energy is expected to be higher than that of the conventional SWCNTs and graphene based SAs. The saturable absorber can be easily reproduced and the device performance does not changed with time if the laser cavity is not disturbed.

4.5 Summary

New passively Q-switched fiber lasers have been successfully demonstrated using EYDF and TYDF as a gain medium to operate at 1550 nm and 1900 nm regions, respectively. At first, Q-switched cladding pumped EYDFL has been demonstrated

using a NPR technique to operate at 1543.5 nm. It employs an isolator in conjunction with a highly nonlinear EYDF to induce intensity dependent loss in a sufficiently-high loss ring cavity and thus generates a Q-switching pulse at threshold pump power as low as 300 mW. At 980 nm multimode pump power of 500 mW, the EYDFL generates a sequence of pulses with a repetition rate of 46.95 kHz, pulse width of 5.3 μs and the maximum pulse energy of 75.6 nJ. When the multimode pump power is varied from 300 to 600 mW, the repetition rate can be tuned from 26.7 to 70.08 kHz while the pulse width fluctuates within 7.5 to 5.3 μs. Then, a passively Q-switched ring-cavity EYDFL based on a few-layer MoS_2-PVA SA was successfully demonstrated. The few-layer MoS_2 was prepared by the liquid phase exfoliation method and sandwiched between two fiber ferrules with a fiber adapter to form a fiber-compatible MoS_2-based SA. Stable Q-switched pulses at around 1563 nm were successfully obtained. The laser showed a pump threshold of 100 mW and minimum pulse duration of 3.39 μs. The pulse repetition rate could be varied over a wide range of frequencies, from 6.4 to 113.4 kHz by adjusting the pump power. Our experimental results suggest that few-layer MoS_2 is a promising material for pulsed laser applications. Finally, Q-switched TYDFL was demonstrated using our newly developed octagonal shaped double-clad TYDF in conjunction with a homemade MWCNTs-PVA SA. The MWCNTs-PVA film is fabricated by mixing the MWCNTs homogeneous solution into a PVA polymer solution. The film is sandwiched between two fiber ferrules and incorporated into a laser ring cavity for Q-switching pulse generation. The repetition rate of the Q-switching pulse can be tuned from 18.8 to 50.6 kHz while the pulse width reduces from 8.6 to 1.0 μs as the 905 nm multimode pump power increases from 1.6 to 2.3 W. The maximum pulse energy of 5.7 nJ is obtained at the pump power of 2.1 W. The proposed Q- switched EYDFL and TYDFL use a simple SA in conjunction with a low cost multi-mode pumping.

CHAPTER 5: MODE-LOCKED ERBIUM-YTTERBIUM AND THULIUM-YTTERBIUM CO-DOPED FIBER LASERS

5.1 Introduction

Mode-locked fiber lasers have generated extreme interest in recent years because of their usefulness in many applications like optical communication, micromachining, metrology and military systems (M. E. Fermann & Hartl, 2013;Nishizawa, 2014; Scholle et al., 2010). Mode-locked lasers can be developed by employing either active or passive techniques. In active methods, an external modulator is required to modulate the intra-cavity loss. On the other hand, passive techniques do not require the external modulator. They use the internal cavity element such as saturable absorber (SA) to change the intra-cavity loss and produce pulse trains. The passively mode-locked fiber lasers are more compact in geometry and simpler in setup as they do not require additional switching electronics such as acousto-optic modulators (F. Wang et al., 2008), and thus they are preferable than the active one for use in generating ultra-short pulse train.

Up to date, various types of SAs have been used for realizing passive mode-locked lasers, such as the ion doped crystals (Qiao et al., 2015; W. Tian et al., 2007), semiconductor saturable absorption mirror (SESAM) (P. Li et al., 2015; J. Liu, Xu, et al., 2012), carbon nanotubes (CNTs) (Xu et al., 2014; Z. Zhang et al., 2013) and graphene (Zhipei Sun et al., 2010; Han Zhang et al., 2009). Among them, SESAMs are the most widely used SA owing to their high flexibility and stability. However, SESAMs are expensive, complicated in fabrication process and have a limited range of optical response, which limits their applications to a great extent. Developing low cost SAs for a broadband operation has always been an objective for laser experts. Recently, both single-walled carbon nanotubes (SWCNTs) and graphene are extensively

investigated for mode-locking applications due to their various advantages, such as fast recovery time, large saturable absorption, and ease of fabrication. Chronologically, SWCNT was first used as an effective SA at 1.55 μm (Set et al., 2004). The phenomenon of saturable absorption is observed in semiconductor type SWCNTs and is widely applied for mode locking fiber lasers (Chiu et al., 2011; Martinez & Sun, 2013; Set et al., 2004; Solodyankin et al., 2008; Z Sun et al., 2012; F. Wang et al., 2008) and solid-state lasers (Chen et al., 2011; Cho et al., 2009). Multiwall carbon nanotubes (MWCNTs) based SAs were also reported to produce mode-locked lasers (Azooz et al., 2015; L. Zhang et al., 2011). In CNTs energy band gap strongly depends on nanotube's diameter (Kataura et al., 1999), therefore it is required to precisely control the CNT diameter to tune the absorption band of CNT SAs for mode locking laser at a specific wavelength. However, broadband CNT-SAs can be made in use of different diameters and chirality of nanotubes, e.g., Wang et al. (F. Wang et al., 2008) extend the operation bandwidth to 300 nm.

Graphene, a single layer of carbon in a hexagonal lattice, has been intensively researched due to its wonderful optical properties (Han Zhang et al., 2009). It is superior to CNTs in broadband saturable absorption due to its gapless linear dispersion of Dirac electrons (Avouris & Freitag, 2014; Bonaccorso et al., 2010). Since the demonstrations of mode-locked lasers using graphene as SAs (Bao et al., 2009; Hasan et al., 2009), the extremely broad and flat absorption spectrum of grapheme (Avouris & Freitag, 2014) allows the researchers to generate passively mode-locked laser pulses over the whole (near 1 μm to 2 μm) IR wavelength. To date, many works have been reported on the integration of a graphene polyvinyl alcohol (PVA) SA into fiber laser system for ultra-short pulse generation. For instance, a single Graphene saturable absorber is used to modelock Yb, Er and Tm doped fiber lasers, demonstrating its broadband operation (Fu et al., 2014).

In this chapter, passively mode-locked fiber lasers are proposed and demonstrated using Erbium-Ytterbium and Thulium-Ytterbium co-doped fiber as a gain medium to operate at 1550 nm and 1900 nm region, respectively. Both lasers are realized using a graphene based SA as a mode-locker in conjunction with multimode pumping. The graphene is synthesized by electrochemical exfoliation of graphite at room temperature in 1% sodium dodecyl sulfate (SDS) aqueous solution. Graphene flakes obtained from the process are mixed with PVA as the host polymer to produce free standing composite thin film which acts as a passive mode-locker in the ring laser cavity. The SA is integrated in the fiber lasers by sandwiching the graphene film between two fiber connectors, which resulting a stable mode-locking pulse train with a fixed repetition rate.

5.2 Fabrication and characterization of Graphene PVA film

In this work, the key part of mode-locking generation is the fabrication of SA film based on graphene sheet in PVA host. The PVA is a water-soluble synthetic polymer with monomer formula C_2H_4O, which has excellent film forming, emulsifying, and adhesive properties. It also has high tensile strength, flexibility, high oxygen and aroma barrier, although these properties are dependent on humidity. First, graphene flakes were produced using electrochemical exfoliation process. In this process, a constant voltage difference of 20 V was applied to two electrodes (graphite rods) placed 1 cm apart in an electrolysis cell filled with electrolyte (1% Sodium dodecyl sulfate (SDS) in deionized water) as shown in Fig. 5.1(a). During the electrochemical exfoliation process, hydroxyl and oxygen radicals were produced due to electrolysis of the water at the electrode. The chemical reactions involved are;

$$H_2O \rightarrow OH^- + H^+ \quad (5.1)$$

$$CH_3(CH_2)_{11}OSO_3Na \rightarrow CH_3(CH_2)_{11}OSO^{3-} + Na^+ \quad (5.2)$$

When an electrical potential was applied between the electrodes, the negative ions moved towards the anode while the positive ions to the cathode. The SDS ions accumulated at the anode and interacted and attached itself to the surface of the graphite rod. This resulted in the loosening of the graphene layers from the graphite rod. Several minutes after voltage was applied, bubbles were observed at the cathode due to the formation of hydrogen gas as shown in Fig. 5.1(a).

Hydroxyl and oxygen radicals were generated due to electrolysis of the water at the electrode during the electrochemical process. Then oxygen radicals started to corrode the graphite anode. This was followed by the intercalation of anionic surfactant and finally graphene sheets were created in the solution. In our work, black sediments (graphene) started to peel off from the anode after several minutes. The exfoliation process was continued for 2 h to obtain a stable graphene suspension in the SDS solution. After two hours the solution turned darker due to exfoliated graphene flakes, as shown in Fig. 5.1(b). The stable graphene suspension was centrifuged at 3000 rpm for 30 min to remove large agglomerates. Afterward, the supernatant portion of the

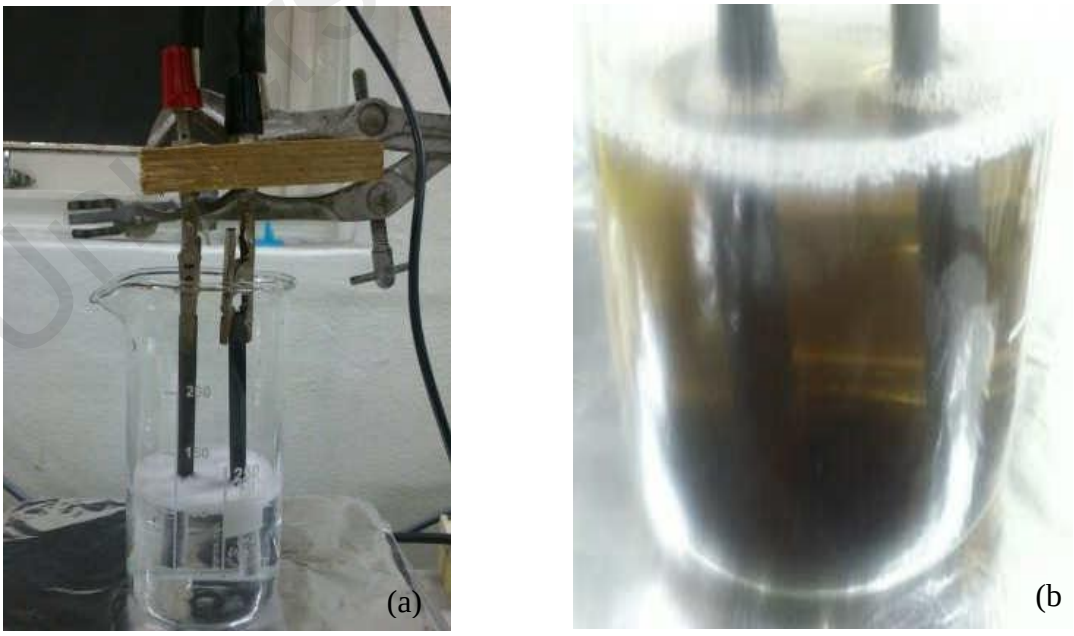

Figure 5.1: Electrochemical exfoliation of graphene (a) after several minutes where bubbles were observed at the cathode due to the formation of hydrogen gas (b) after two hours of exfoliation process.

suspension was decanted. The concentration of the centrifuged graphene was estimated from the weight of the suspension used.

To fabricate the composite, 1g of PVA (Mw=89x103 g/mol, Sigma Aldrich) was dissolved in 120 ml of deionized water. The centrifuged graphene suspension was then mixed with the PVA solution at ratio of 2:3 (in ml) to form the precursor and the mixture was stirred using ultrasonic cleaner for about one hour. This step helped us get precursor with enough viscosity so that it could be easily used in forming a film. Finally, suitable amounts of precursor were spread thinly on the glass substrate, and let dry in an oven with temperature of 56^{o}C to form the graphene PVA film, which is then used to construct a SA. The thickness of the film is about 50 µm.

Raman spectroscopy was performed to confirm the presence of graphene layer in the fabricated graphene PVA film. It is a non-destructive technique that is widely used to obtain structural information about carbon-based materials (Guo et al., 2012). Fig. 5.2 shows the Raman spectrum of the graphene PVA film, which was obtained using a 532-nm laser excitation. The Raman spectrum reveals two prominent features of graphene at 1350 cm^{-1} and 1600 cm^{-1} which are assigned to D and G bands, respectively.

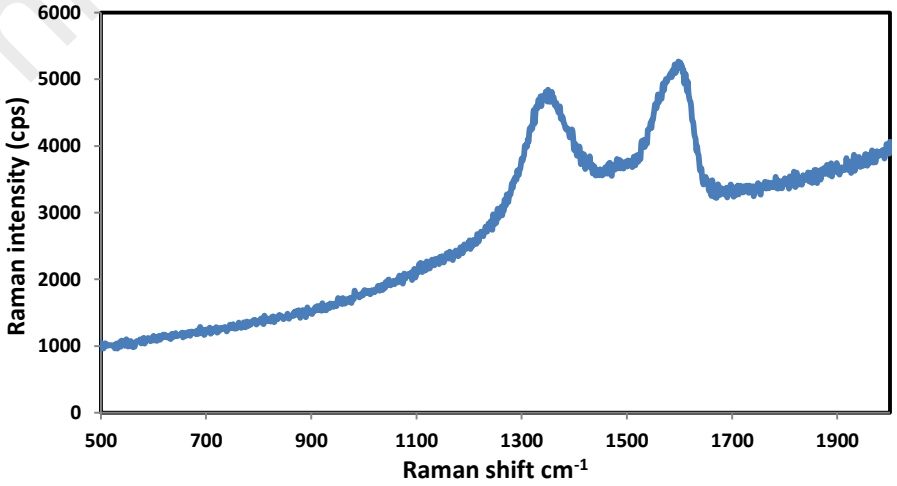

Figure 5.2: Raman spectrum of the graphene PVA film.

The D band is caused by the structural imperfections, which were created by the attachment of hydroxyl and epoxide groups on the carbon basal plane. G band is related to the in-plane vibration of sp^2-bonded carbon atoms.

Twin detector measurement technique was then employed to characterize the nonlinear optical response of this fabricated graphene PVA film sample. In the experiment, a stable self-constructed passively mode-locked fiber laser operating at 1560 nm with a frequency repetition rate of 26 MHz and pulse duration of 600 fs was used as the input pulse light source. The output powers from both detectors were recorded as we gradually increased the output power value. From the result, the absorption was calculated and later, was fitted using the following saturation model formula (Garmire, 2000):

$$\alpha(I) = \frac{\alpha_s}{1+I/I_{sat}} + \alpha_{ns} \qquad (5.3)$$

where $\alpha(I)$ is the absorption rate, α_s is the modulation depth, I is the input light intensity, I_{sat} is the saturation intensity, and α_{ns} is the non-saturable absorption. The absorptions at various input intensities were recorded and plotted as shown in Fig. 5.3 after curve fitting using the above saturation model formula. The saturation intensity,

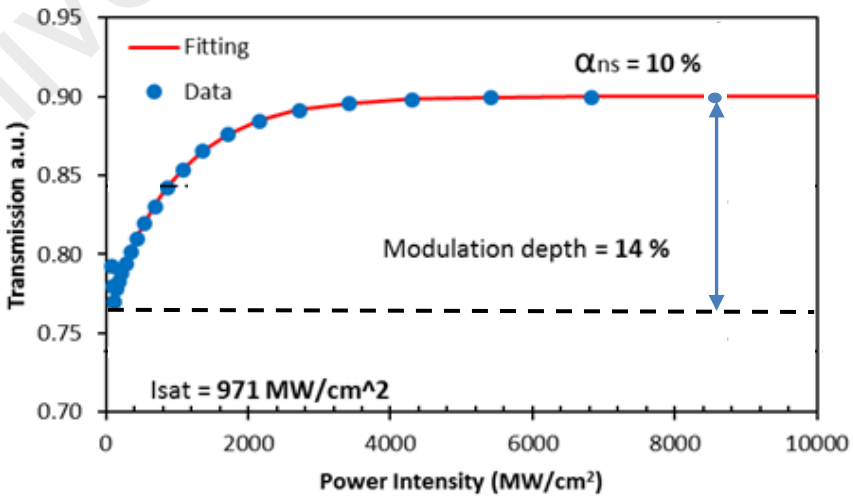

Figure 5.3: Measured saturable absorption of the fabricated graphene PVA film.

nonsaturable absorption and modulation depth of the saturable absorber are 971 MW/cm^2, 10% and 14 %, respectively. Taking into account its nonlinear optical response may lead to absorption saturation at relatively low fluence, the graphene film is expected to function very well as a passive SA in a fiber laser setup.

5.3 Mode-locked EYDFL

In this section, a mode-locked EYDFL is demonstrated using the fabricated graphene PVA film as a SA. The configuration and mode-locking performance of the laser are presented.

5.3.1 Configuration

The experimental setup of the proposed mode-locked Erbium Ytterbium co-doped fiber laser (EYDFL) is shown in Fig. 5.4, which employs Erbium Ytterbium co-doped fiber (EYDF) as the gain medium.

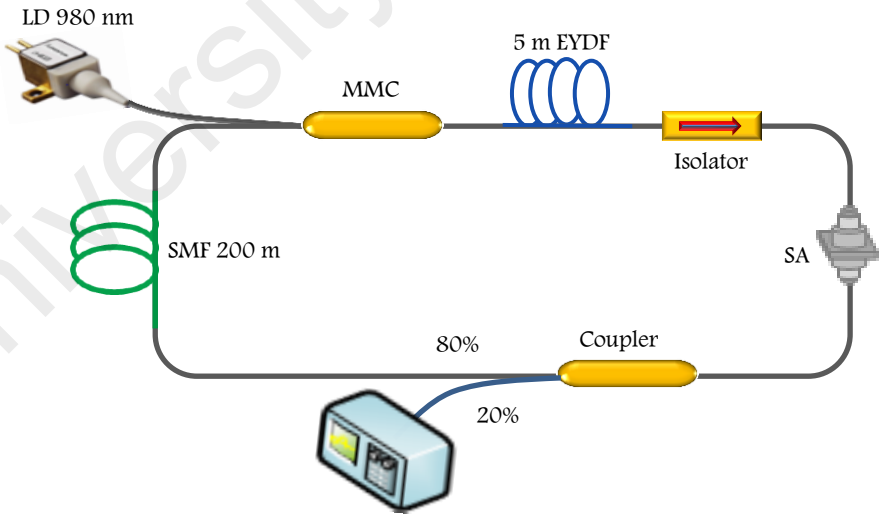

Figure 5.4: Configuration of passively mode-locked EYDFL based on graphene SA.

The laser resonator consists of a 5 m long EYDF, a multimode combiner (MMC), an isolator, a graphene PVA film based SA, a 200 m long additional single-mode fiber (SMF) and 20:80 output coupler in a ring configuration. The SA is fabricated by cutting

a small part of the earlier prepared film (2×2 mm^2) and sandwiching it between two FC/PC fiber connectors, after depositing index-matching gel onto the fiber ends. The insertion loss of the SA is measured to be around 1.5 dB at 1550 nm. The EYDF used is a double-clad fiber with a core, inner and outer cladding diameters of 5 µm, 105 µm and 125 µm respectively. It has a core and inner cladding with numerical apertures of 0.21 and 0.25, respectively. The EYDF is cladding pumped by a 980 nm multimode laser diode via the MMC. An isolator is incorporated in the laser cavity to ensure unidirectional propagation of the oscillating laser. The output of the laser is tapped out of the cavity through 20% port of the output coupler while keeping 80% of the light to oscillate in the ring cavity. The optical spectrum analyzer (OSA) is used to analyze the spectra of the mode-locked EYDFL with a spectral resolution of 0.07 nm whereas the oscilloscope is used to observe the output pulse train of the mode-locked operation via a 460 kHz bandwidth photo-detector (Thor lab, PDA50B-EC). Additional 200 m long standard SMF was added into the cavity to tailor the total group velocity dispersion (GVD) as well as to increase the nonlinearity effect so that mode-locked output pulse can be realized. The mode-locked EYDFL has total cavity length of 217.5 m, which consists of 5 m long EYDF and 212.5 m long SMF, with group velocity dispersion (GVD) of -21.0 ps^2/km, and -21.7 ps^2/km, respectively. The cavity operates in anomalous fiber dispersion of -4.571 ps^2, and thus traditional soliton tends to be formed in the fiber laser.

5.3.2 Mode-locking performance

With the addition of SMF, the balance between the GVD and nonlinearity effect inside the ring cavity allows the generation of a stable mode-locking pulse. The stable self-starting mode-locked pulse begins when the pump power reaches 200 mW. Fig. 5.5 shows the output spectrum at the maximum pump power of 300 mW.

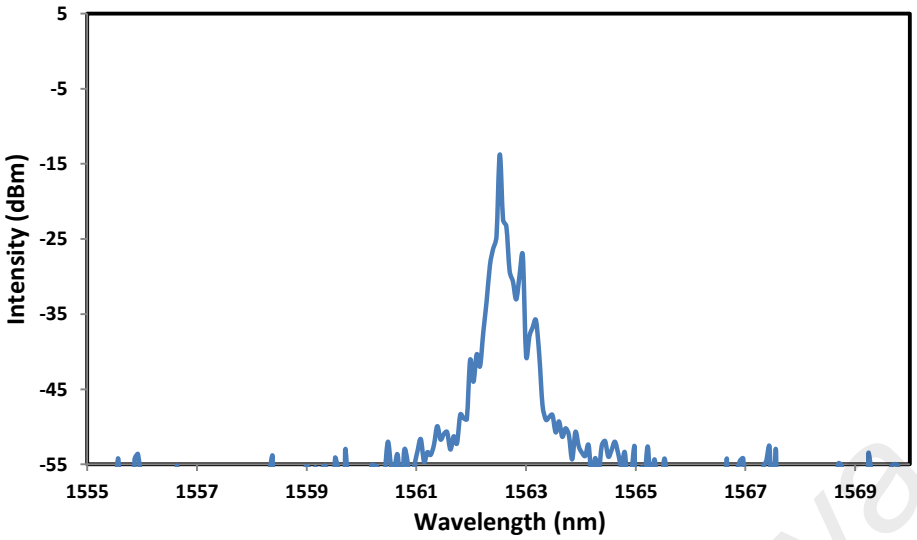

Figure 5.5: Output optical spectrum at input pump power of 250 mW.

At this pump power, the spectrum shows the soliton pulse with the sideband indicated that anomalous dispersion and nonlinearity occurs in the ring cavity. Inter-correlation between dispersion and nonlinearity in the ring cavity produces a good generation of soliton pulses. The stable self-starting mode-locked could be initiated without any adjustment to the polarization state of the cavity. This indicates that the mode-locked pulses are polarization independent, no PC is required to control the polarization. The laser operates at 1562.5 nm with 3 dB spectral bandwidth of less than 0.1 nm. Fig. 5.6 shows the oscilloscope trace at 250 mW pump power, which indicates a stable mode-locked pulse. The pulse train is uniform and no distinct in amplitude is observed for each envelope spectrum. The peak to peak period of the pulse train is measured to be 1082 ns, which correspond to the repetition rate of 0.92 MHz. The obtained repetition rate matches with the cavity length of about 217.5 m. Fig. 5.7 shows a single envelop of the mode-locked pulse with a pulse duration of about 387 ns and the time-bandwidth product is calculated to be 4760, which indicates that the optical pulse is heavily chirped. Since time band width value is very large as compared to 0.315 for a $sech^2$ shaped pulse it shows that the pulse is up chirp that is its repetition rate increased . Fig. 5.8 shows the measured average output power as a function of input pump power.

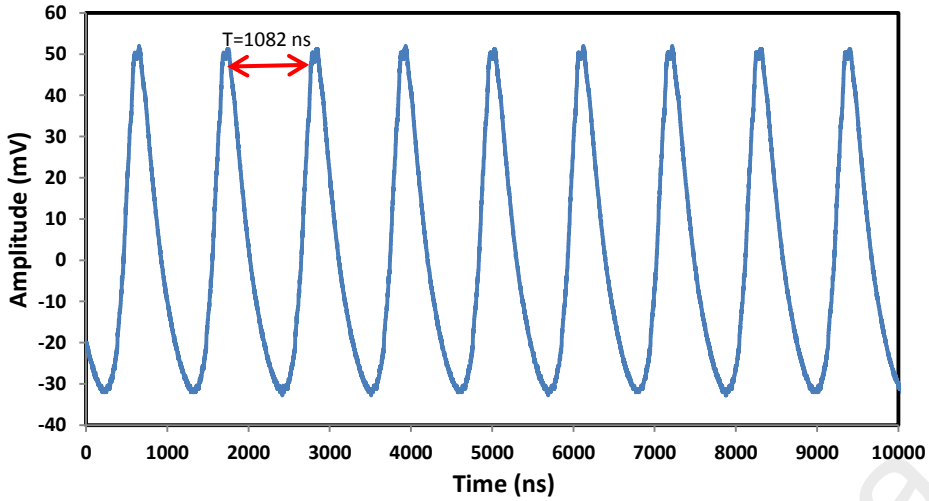

Figure 5.6: Typical mode-locked pulse train at input pump power of 250 mW.

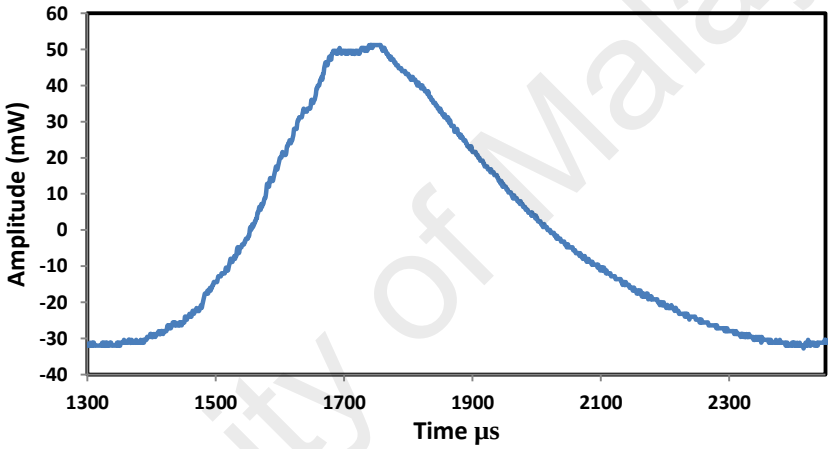

Figure 5.7: Typical single envelop of the mode-locked pulse train at input pump power of 250 mW.

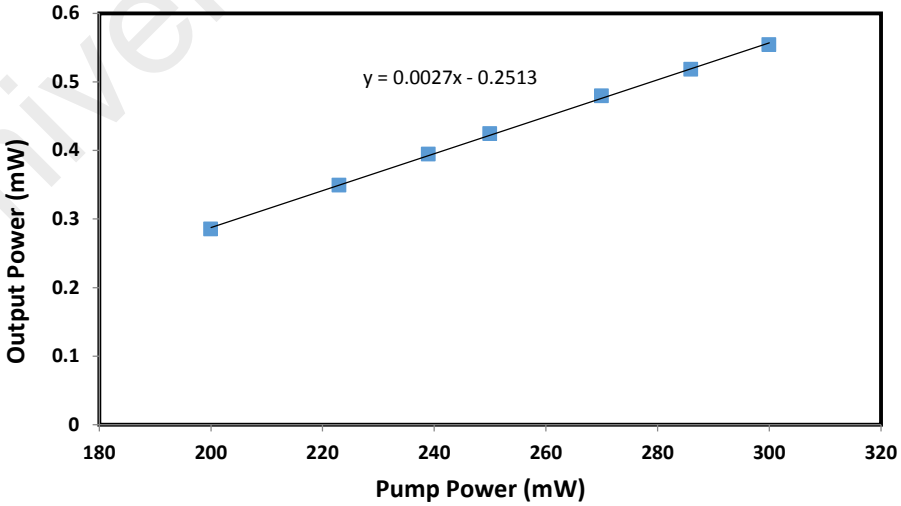

Figure 5.8: Average output power against the pump power.

It is clearly shown that the output power increases from 0.29 mW to 0.55 mW as the corresponding pump power is tuned from threshold power of 200 mW to the pump

power of 300 mW. As the pump power is further increased above 300 mW, the mode-locked operation mode is switched to a CW mode. This is most probably due to the fact that the SA cannot recover in time after the pulse and gain population excited for the next pulse. The optical-to-optical efficiency is relatively lower (0.27%) because of the inefficiency of cladding pumping as well as high cavity loss. Fig. 5.9 shows the calculated peak power and single pulse energy against the pump power.

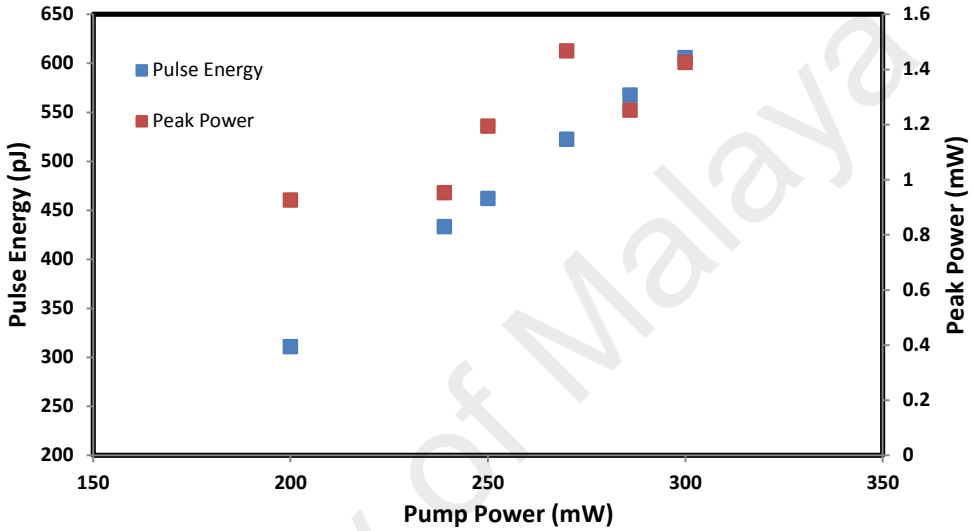

Figure 5.9: Single pulse energy and peak power against the pump power.

It is clearly shown that the peak power fluctuates within 0.93 to 1.47 mW due to birefringence, as the multimode pump power is varied from 200 to 300 mW. On the other hand, the calculated pulse energy also almost linearly increases with the pump power. The maximum pulse energy of 605 pJ is obtained at 300 mW pump power. In order to examine the stability of the laser, the radio frequency (RF) spectrum is also obtained using a RF spectrum analyzer at input pump power of 250 mW. The result is plotted in Fig. 5.10, which shows the fundamental frequency of 0.92 MHz. This frequency matches to the pulse period (peak to peak duration) of the oscilloscope trace. The RF spectrum has a high signal to noise ratio (SNR) up to 57 dB, further indicating the stability of the obtained pulse train. Further work on reducing the film loss and optimizing the EYDFL cavity is important especially for the high power operation.

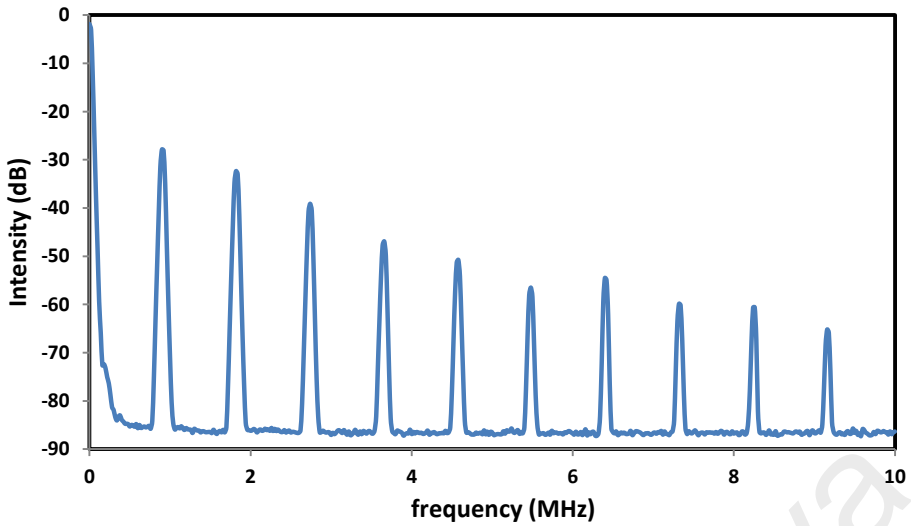

Figure 5.10: The measured RF spectrum at pump power of 250 mW.

5.4 Mode-locked TYDFL

Mode-locked Thulium-doped fiber lasers (TDFLs) have attracted intense interest in recent years for a number of potential applications, including atmospheric measurements, material processing, communication, laser radar, biomedical and medical applications, and longer-wavelength laser pumping (Bouma et al., 1998; Henderson et al., 1993; J. Liu, Wang, et al., 2012; McAleavey et al., 1997; Polder & Bruce, 2012; Sorokina et al., 2014; Spiers et al., 2011). In Chapter 3, a new approach was proposed to enhance Thulium-doped fiber emission at 2 µm wavelength by co-doping the fiber with Yb^{3+} ions as a sensitizer to the Tm^{3+} ions. This approach is feasible due to the fact that the Yb^{3+} emission at 1200 nm wavelength is one of the absorption bands of Tm^{3+}. The excited Yb^{3+} ions at $^2F_{5/2}$ release their energy, which is (quasi-) resonant to the Tm^{3+} energy level of $^3H_5$. In addition, the high absorption of Yb^{3+} ions and the uniqueness of the energy level of Yb provide sufficient contribution to the high power laser application. The low quantum defect of the Yb enables pumping at high power.

Up to now, most ultra-short pulse fiber lasers have adopted passive mode-locking technology, in which SAs act as a key part (Ahmed et al., 2014; J. Wang et al.,

2016) In the previous section, a mode-locked EYDFL was demonstrated using a graphene PVA SA. In this section, a mode-locked Thulium-Ytterbium co-doped fiber laser (TYDFL) is demonstrated by using the similar graphene PVA film as an SA. The SA is constructed by sandwiching the graphene film between two fiber connectors.

5.4.1 Configuration of the proposed mode-locked TYDFL

Fig. 5.11 shows the experimental setup for the proposed graphene based mode-locked TYDFL. It uses a homemade double-clad Thulium-Ytterbium co-doped fiber (TYDF) as gain medium in the ring oscillator.

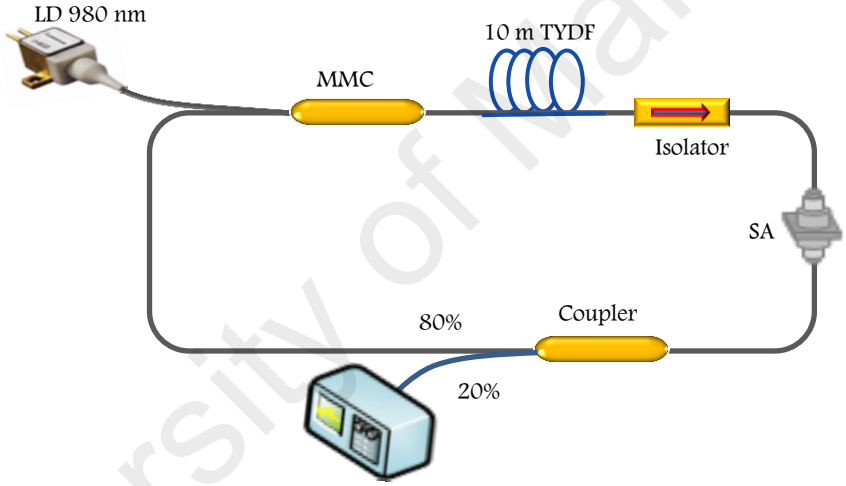

Figure 5.11: The schematic setup of the mode locked TYDFL employing the fabricated graphene PVA film based SA.

The fiber has an octagonal shaped pump inner cladding with a core diameter of 5.96 µm and an NA of 0.23. The selected fiber length of 10 m provides more than 90% pump absorption. The TYDF was pumped by a 980 nm multimode laser diode through a multimode combiner (MMC). The graphene PVA film was prepared by mixing the graphene solution in PVA solution. The graphene solution was obtained from the flakes produced using electrochemical exfoliation process. A free-standing graphene PVA film was obtained after drying as explained in the previous section. The fiber-type SA device was constructed by inserting this film between two ferules. The output pulses are

coupled out of the oscillator from a 20% port of the 80/20 dB output coupler while allowing 80% of the light to oscillate in the ring cavity. The length of total cavity is set at around 17 m so that the net cavity dispersion is anomalous for facilitating self-starting mode locked laser. For the measurements of the laser output, an InGaAs photodetector with a response time of approximately 28 ps connected to a 500 MHz digital oscilloscope was used to measure the pulse train and pulse waveforms. The spectrum of the output pulse was measured by an optical spectrum analyzer (OSA).

5.4.2 Mode-locking performance of the TYDFL

Mode-locking was self-started by increasing the pump power above the threshold of 1487 mW. The mode-locked operation was maintained as the pump power is increased up to the maximum power of 1964 mW. Fig. 5.12 shows the output spectrum of the mode-locked pulse train when the pump power is fixed at 1610 mW.

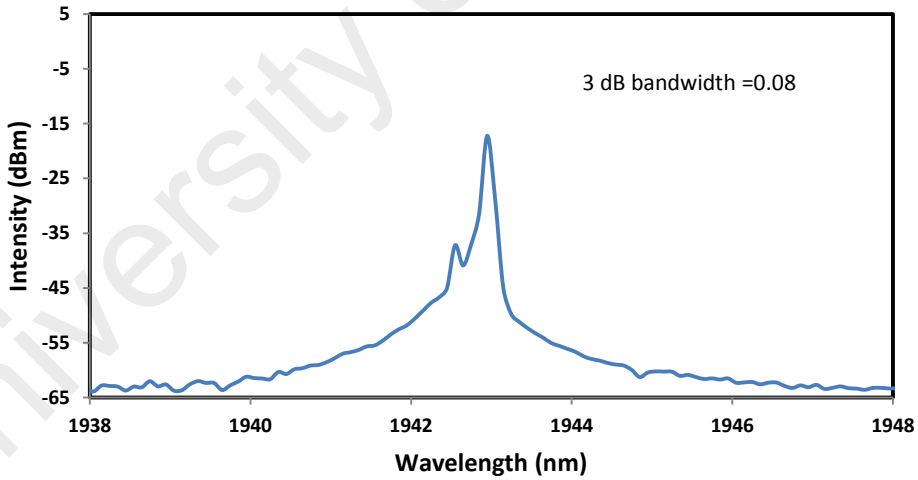

Figure 5.12: Output spectrum of the mode-locked TYDFL.

As shown in the figure, the spectrum was centered at 1942.95 nm with 3 dB bandwidth of 0.08 nm. Without the SA, the CW TYDFL was observed to operate at 1943.50 nm. It is found that the operating wavelength shifts to a shorter wavelength with the insertion of the SA into the cavity due to the change in cavity loss. The oscillating laser shifts to shorter wavelength to acquire more gain to compensate for the insertion loss of the SA.

With the SA, the presence of soliton is also confirmed with a weak side band at 1942.54 nm as shown in Fig. 5.12. It shows that this mode-locked fiber laser is operating in the anomalous dispersion regime. The typical pulse train of the proposed graphene PVA film based passively mode-locked TYDFL is shown in Fig. 5.13 at pump power of 1627 mW. It has a pulse-to-pulse separation of 85 ns, corresponding to a pulse repetition rate of 11.76 MHz, which matches the cavity roundtrip time with a cavity length of 17 m.

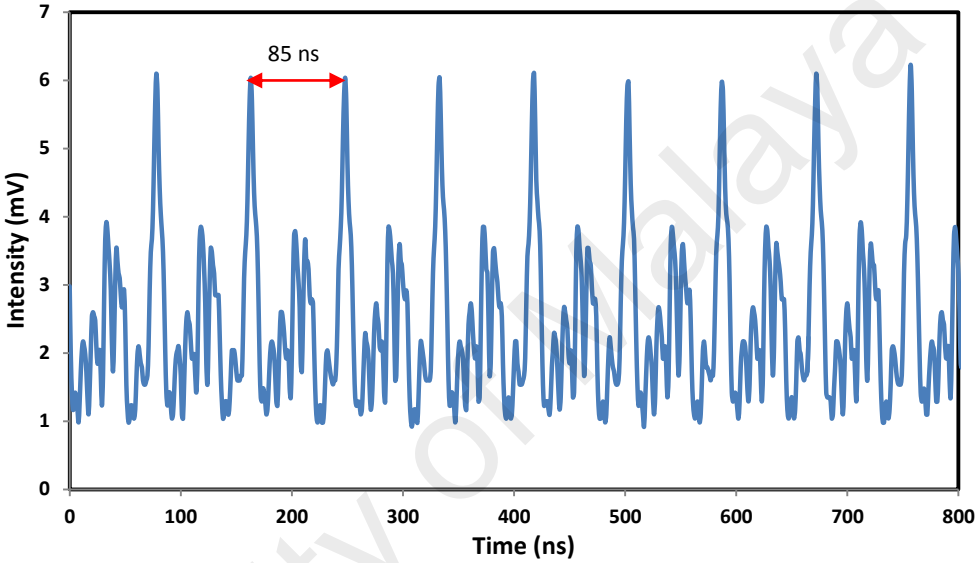

Figure 5.13: Typical pulse train for the mode-locked TYDFL at pump power of 1627 mW.

This indicates that the well dispersed graphene in the PVA film exhibits sufficient saturable absorption for mode-locking operation. The modulation of the pulse amplitude is an artifact caused by the limited sampling points on the sampling oscilloscope, since the pulse duration is too narrow and the sampling rate of our oscilloscope is only 1 Gs/s. Fig. 5.14 shows the repetition rate against the pump power. It is found that the repetition rate was retained at 11.76 MHz as the pump power was varied from 1487 to 1964 mW. The oscilloscope trace analysis indicates that the pulse width of the laser should be less than 9 ns. The actual pulse width is expected to be much smaller than 9 ns, but due to the limitations of the oscilloscope resolution it couldn't be accurately measured.

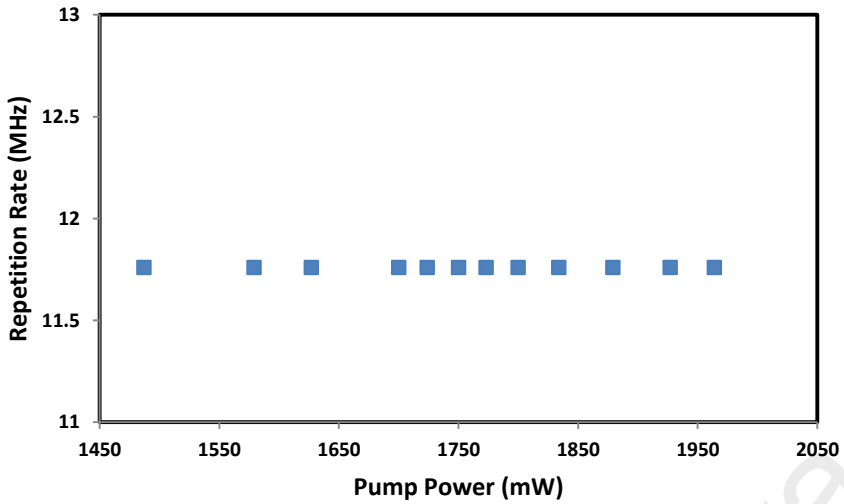

Figure 5.14: Repetition rate of the mode-locked laser at various pump powers.

The total length of the laser cavity was measured to be approximately 17 m, comprising 10 m long of TYDF and 7 m long of single mode fiber (SMF) with estimated dispersions of −0.083 ps^2/m and −0.034 ps^2/m, respectively, at 1943 nm. Therefore, the mode-locked laser is expected to operate in anomalous dispersion regime. On the other hand, the pulse width can be measured using an auto-correlator or can be calculated mathematically using Time Bandwidth Product (TBP). Since Auto-correlator in 2 µm range is not available, it is calculated mathematically by assuming TBP is around 0.315 for $sech^2$ pulse profile. The minimum possible pulse width is estimated about 52.85 ps since the 3dB bandwidth of the optical spectrum is about 0.075 nm (5.96 GHz). We also calculate the repetition rate by using the formula c/1.5L, found to be 11.76 MHz. This is equal to the observed repetition rate of this laser as shown in Fig. 5.14. The output power of the laser is also measured and the measurement is then used to calculate the single pulse energy at various pump power. The maximum output power of 14 mW is observed at 1750 mW pump power. The pulse energy increases linearly up to pump power of 1750 mW before it decreases because of energy converted to noise as shown in Fig. 5.15. The calculated pulse energy is in the range of 756.048 to 1190.476 pJ.

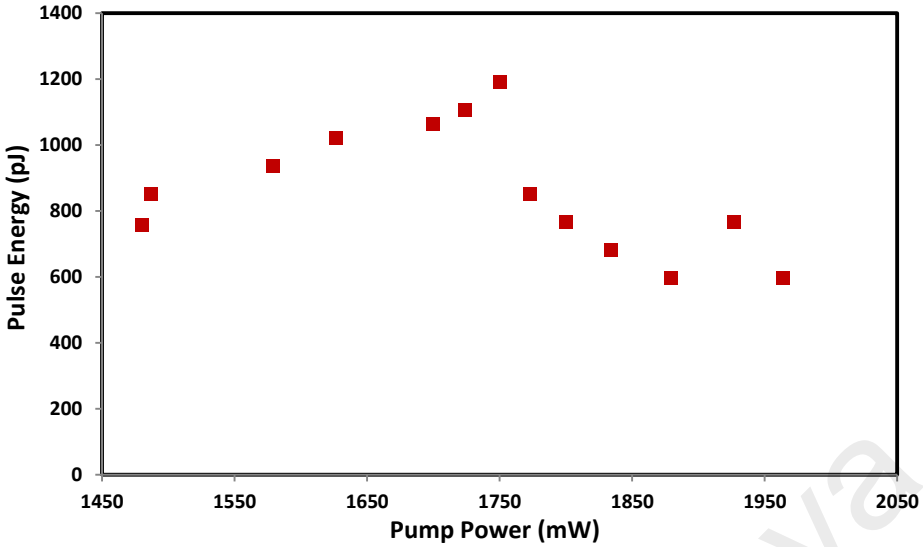

Figure 5.15: The calculated pulse energy against the input pump power.

The RF spectrum of the mode-locked pulses is also measured and the result is shown in Fig. 5.16. Its fundamental mode peak locates at the frequency of 11.76 MHz and has an SNR of 36.5 dB, which confirms the stability of the mode-locking operation. The peak of harmonic decreased moderately, so this identifies the mode locked laser has a narrow pulse width. At all pump power levels, no presence of fundamental frequency is observed when the graphene SA is removed.

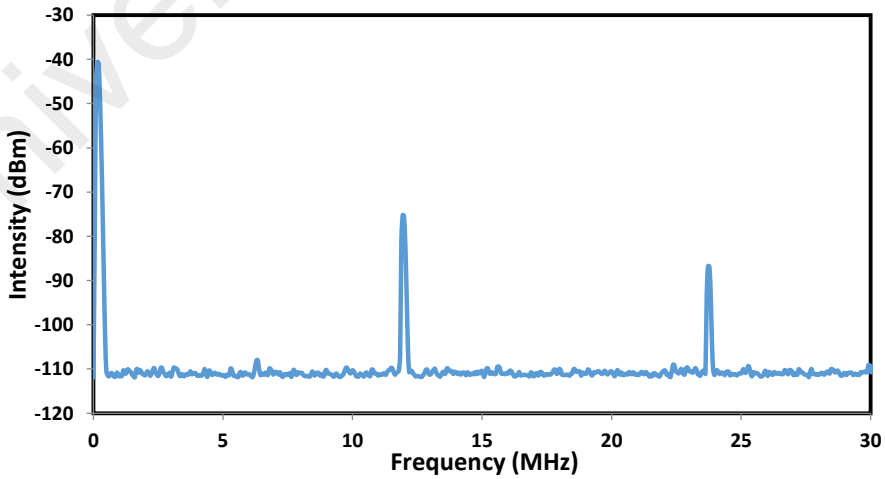

Figure 5:16: RF spectrum of the mode-locked TYDFL.

Further work on reducing the film loss and optimizing the TYDFL cavity is important especially for the high power operation of the laser. The mode-locked pulses

are generated since the longitudinal modes inside the cavity are forced to lock together. All the modes are either in phase or different in a multiple number of 2π. Since many modes are circulating in the cavity randomly, but the length of the cavity is inappropriate to bring them in a relationship that can produce constructive interference between different modes. So, 200 m long SMF is added in EYDFL to create a fixed relationship that can bring some modes in a constant relationship in time and space to generate constructive interference so that mode-locking pulses can be generated. Whereas in TYDFL, the cavity length is appropriate and thus the extra fiber is not required to lock the circulating modes in the laser cavity.

5.5 Summary

New passively mode-locked fiber lasers have been successfully demonstrated using double-clad EYDF and TYDF as a gain medium in conjunction with multimode pumping at 980 nm to operate at 1550 nm and 1900 nm region, respectively. It uses a newly developed graphene PVA SA as the mode-locker. The SA film was prepared from precursor which was obtained by mixing the dispersed graphene suspension into a PVA solution. It has the modulation depth of 14 % at 1550 nm. At first, mode-locked EYDFL has been demonstrated using a 5 m long EYDF as the gain medium in a ring configuration with anomalous dispersion of -4.72 ps^2. The CW light is converted to nanosecond pulses with the incorporation of 200m long SMF in the cavity to balance the total GVD as well as to increase the nonlinear effect. The mode-locked EYDFL operates at 1562.5 nm with a repetition rate of 0.92 MHz and pulse width of 387 ns. The maximum pulse energy is 605 pJ at 300 mW pump power. The laser is very stable as RF spectrum shows an SNR of 57 dB. Then, mode-locked TYDFL was demonstrated using the similar SA. The laser operates at 1942.95 nm with repetition rate of 11.76 MHz. The pulse width is calculated to be around 52.85 ps. The maximum pulse energy

of 1190.5 pJ is achieved at pump power of 1750 mW. These results indicate that the proposed graphene PVA film could be useful as a simple, low-insertion-loss, low-cost, ultrafast SA device for ultrafast laser generation applications in both 1.5 and 2 μm regions.

CHAPTER 6: CONCLUSION AND FUTURE OUTLOOK

6.1 Conclusion

Lasers with emission in the 1.5 and 2 micron spectral regions can be achieved using Erbium-doped fiber (EDF) and Thulium doped fiber (TDF) via energy transition of $^4I_{13/2} \rightarrow {}^4I_{15/2}$ and $^3F_4 \rightarrow {}^3H_6$, respectively as the gain medium. Q-switched and mode-locked fiber lasers operating in both wavelength regions have gained a tremendous research interest in recent years for their potential applications in optical communication, fiber sensor, laser processing, laser marking, etc. Compared with the actively ones, passively pulsed lasers have attracted much attention due to their advantages of compactness, low cost, flexibility and simplicity of design. Most of the pulsed lasers are based on core pumping and there are not many reports on Q-switched and mode-locked double-clad fiber lasers, which are based on more efficient and cheaper cladding pumping scheme. The main objective of this research is to design and construct an efficient and low cost Q-switched and mode-locked fiber lasers using Erbium-Ytterbium co-doped fiber (EYDF) and Thulium-Ytterbium co-doped fiber (TYDF) as the gain medium to operate in 1.5 and 2.0 μm regions, respectively. Both EYDF and TYDF are double-clad fibers and thus they can be pumped by a low cost multimode laser diode operating within 900 to 980 nm.

CW fiber lasers have been successfully demonstrated by using a double-clad EYDF and TYDF as the gain medium to operate at 1.5 and 2 micron region, respectively. In linear configuration, the cladding pumped EYDF laser (EYDFL) operates at 1535.4 nm, 1544.3 nm and 1545.6 nm with slope efficiencies of 4.3%, 15.0% and 18.4% as the fiber lengths are fixed at 1, 4 and 5 m, respectively. This shows that the optimum fiber length of the EYDFL operation is 5 m or longer. At 5m long EYDF, the laser produced 537 mW output power at the maximum pump power of 3100

mW. The threshold pump power was about 140 mW. In ring configuration, the laser produced a significantly lower efficiency due to the higher cavity loss. The ring EYDFL has an efficiency of 4.6% at fiber length of 5m. The TYDF laser (TYDFL) produced a triple wavelength output operating at 1914.5 nm, 1934.7 nm and 1953.6 nm using a 5 m long fiber as the gain medium in ring configuration. At 15 m long fiber, the laser produced the highest output power of 21.9 mW at pump power of 3600 mW with the lowest threshold pump power of 1000 mW. The maximum efficiency of 0.88% operating at 1961.4 nm is achieved when the gain medium is fixed at 10 m. A multi-wavelength TYDFL operating at 2 μm region is also demonstrated based on nonlinear polarization rotation (NPR) effect. The laser generated triple-wavelength outputs at 1982.12 nm, 1986.69 nm and 1991.26 nm when the 980 nm multimode pump power is about 2.05 W. At pump power of 2.75 W, the laser lines reduces to two (1970.60 nm and 1973.12 nm) with a signal to noise ratio of more than 40 dB.

Various types of passive saturable absorber based on Molybdenum disulfide **(**MoS_2), multi-walled carbon nanotubes (MWCNTs) and graphene have been successfully fabricated and characterized for use in developing Q-switched and mode-mode-locked fiber lasers. At first, a few-layer MoS_2 was prepared by the liquid phase exfoliation method. The nanomaterial was then embedded into polyvinyl alcohol (PVA) film before it is sandwiched between two fiber ferrules with a fiber adapter to form a fiber-compatible MoS_2-based SA. Raman spectroscopy measurement confirmed that the fabricated thick composite SA film sample has few-layer MoS_2 Nano sheets. The absence of a noticeable shift in the peak positions indicates that the material structure is unaffected by its inclusion in the PVA composite. Secondly, the MWCNTs-PVA film was fabricated by mixing the MWCNTs homogeneous solution into a PVA polymer solution. The film was sandwiched between two fiber ferrules and incorporated into a laser ring cavity for Q-switching pulse generation. The MWCNTs-PVA film has an

insertion loss of around 3 dB at 1550 nm, the saturable absorption (modulation depth) of around 4% and non saturable absorption of around 45%. Raman spectroscopy was also performed, which confirmed the existence of MWCNT in the film. Finally, graphene based SA was prepared by embedding into the PVA to function as a mode-locker in this study. The SA film was prepared from precursor which was obtained by mixing the dispersed graphene suspension into a PVA solution. It has the modulation depth of 14 % at 1550 nm.

Q-switched EYDFLs and TYDFL have been successfully demonstrated using various passive techniques. At first, Q-switched cladding pumped EYDFL operating at 1543.5 nm was demonstrated based on NPR technique. The laser was designed by incorporating an isolator in a sufficiently-high loss ring cavity so that Q-switching pulse can be generated with the help of highly nonlinear EYDF to induce intensity dependent loss. The EYDFL generated a sequence of pulses with a repetition rate from 26.7 to 70.08 kHz, corresponding to pulse width range of 7.5 to 5.3 μs and the maximum pulse energy of 75.6 nJ at pump power of 500 mW. The second Q-switched EYDFL was achieved based on a few-layer MoS2-PVA SA. It operates at around 1563 nm with pump threshold of 100 mW and minimum pulse duration of 3.39 μs. The pulse repetition rate could be varied over a wide range of frequencies, from 6.4 to 113.4 kHz by adjusting the pump power. Finally, Q-switched TYDFL was demonstrated using the prepared MWCNTs-PVA SA. The repetition rate of the Q-switching pulse can be tuned from 18.8 to 50.6 kHz while the pulse width reduces from 8.6 to 1.0 μs as the 905 nm multimode pump power increases from 1.6 to 2.3 W. The maximum pulse energy of 5.7 nJ is obtained at the pump power of 2.1 W. All the proposed Q-switched lasers use a simple SA in conjunction with a low cost multimode pumping.

New passively mode-locked EYDFL and TYDFL have been successfully demonstrated using the newly developed graphene PVA SA as the mode-locker. The

mode-locked EYDFL was achieved in a ring cavity configured with 5 m long EYDF and 200m long SMF. The cavity has an anomalous dispersion of -4.72 ps^2. The mode-locked EYDFL operated at 1562.5 nm with a repetition rate of 0.92 MHz and pulse width of 387 ns due to the balance between the total group velocity dispersion and the nonlinear effect. The laser produced the maximum pulse energy of 605 pJ at 300 mW pump power. The RF spectrum shows a signal to noise ratio (SNR) of 57 dB, which indicates the stability of the output pulse. The mode-locked TYDFL operating at 1942.95 nm was also demonstrated using the similar SA. The laser has a repetition rate of 11.76 MHz with calculated pulse width of around 52.85 ps. The maximum pulse energy of 1190.5 pJ is achieved at pump power of 1750 mW.

These results indicate that CW, Q-switched and mode-locked fiber lasers have been successfully demonstrated using double-clad EYDF and TYDF as a gain medium in conjunction with multimode pumping at 980 nm to operate at 1550 nm and 1900 nm region, respectively. New SAs films were also successfully developed. These films could be useful as a simple, low-insertion-loss, low-cost, ultrafast SA device for ultrafast laser generation applications in both 1.5 and 2 μm regions.

6.2 Future outlooks

Much work has been carried out on the generation of pulsed and multi-wavelength lasers based on Ytterbium co-doped fibers. However, it can be further explored and investigated in future, especially on improving the lasing characteristics and ultra-short pulse generation. The performances of Q-switched fiber lasers based on SA can be improved while mode-locked pulse generation can also be explored using other types of SA based on other nanomaterials. Future work should also focus on exploring new nanomaterials such as zero dimensional materials, quantum dots (QDs), and two dimensional materials, Black phosphorous, topological insulators, etc.

The pulse generation can be further investigated using more enhanced configurations with a better control of cavity dispersion and nonlinear effect. The investigation should also focused to reduce further the length of gain medium or to replace the gain medium with higher dopant active fiber that can maintain high gain per length coefficient of compact lasers. The short cavity laser has potential to produce a high repetition rate, which is useful for certain, applications. The repetition rate is expected to be increased because of the repetition rate is usually fixed by the length of the laser cavity, and the pulse width will be decreased since the repetition rate is inversely proportional to the pulse width. With the advancement of ultrafast laser system, the cavity length can also be reduced to several meters to allow hundreds of Mega-Hertz and also Giga-Hertz repetition rate for applications in high capacity telecommunication systems and photonic switching devices. Future works should focus on improving fabrication of the saturable absorbers and optimizing of laser cavity to improve the quality of output pulse train. The fabrication techniques for both MWCNTs, MoS_2 and graphene based SAs should also be optimized. These materials could also be used for developing other photonic devices such as photo detectors and modulators.

REFERENCES

Agrawal, G. P. (2007). *Nonlinear fiber optics* (fourth ed.): Academic press, ISBN 13: 978-0-12-369516-1.

Ahmed, M., Ali, N., Salleh, Z., Rahman, A., Harun, S., Manaf, M., & Arof, H. (2014). All fiber mode-locked Erbium-doped fiber laser using single-walled carbon nanotubes embedded into polyvinyl alcohol film as saturable absorber. *Optics & Laser Technology, 62*, 40-43.

Avouris, P., & Freitag, M. (2014). Graphene photonics, plasmonics, and optoelectronics. *IEEE Journal of Selected Topics in Quantum Electronics, 1*(20), 6000112.

Azooz, S., Ahmad, F., Ahmad, H., Harun, S., Hamida, B., Khan, S., . . . Bhadra, S. K. (2015). Mode-locked 2 μm fiber laser with a multi-walled carbon nanotube as a saturable absorber. *Chinese Optics Letters, 13*(3), 030602-030602.

Bao, Q., Zhang, H., Ni, Z., Wang, Y., Polavarapu, L., Shen, Z., . . . Loh, K. P. (2011). Monolayer graphene as a saturable absorber in a mode-locked laser. *Nano Research, 4*(3), 297-307. doi: 10.1007/s12274-010-0082-9

Bao, Q., Zhang, H., Wang, Y., Ni, Z., Yan, Y., Shen, Z. X., . . . Tang, D. Y. (2009). Atomic-layer graphene as a saturable absorber for ultrafast pulsed lasers. *Advanced Functional Materials, 19*(19), 3077-3083.

Barnes, W., Poole, S. B., Townsend, J., Reekie, L., Taylor, D., & Payne, D. N. (1989). Er 3+-Yb 3+ and Er 3+ doped fiber lasers. *Journal of Lightwave Technology, 7*(10), 1461-1465.

Baudelet, M., Willis, C. C., Shah, L., & Richardson, M. (2010). Laser-induced breakdown spectroscopy of copper with a 2 μm thulium fiber laser. *Optics Express, 18*(8), 7905-7910.

Bedö, S., Lüthy, W., & Weber, H. (1993). The effective absorption coefficient in double-clad fibres. *Optics Communications, 99*(5), 331-335.

Blixt, P., Nilsson, J., Carlnas, T., & Jaskorzynska, B. (1991). Concentration-dependent upconversion in Er/sup 3+/-doped fiber amplifiers: Experiments and modeling. *IEEE Photonics Technology Letters, 3*(11), 996-998.

Bokobza, L., & Zhang, J. (2012). Raman spectroscopic characterization of multiwall carbon nanotubes and of composites. *Express Polym. Lett, 6*(7), 601-608.

Bonaccorso, F., Sun, Z., Hasan, T., & Ferrari, A. (2010). Graphene photonics and optoelectronics. *Nature Photonics, 4*(9), 611-622.

Bouma, B. E., Nelson, L. E., Tearney, G. J., Jones, D. J., Brezinski, M. E., & Fujimoto, J. G. (1998). Optical coherence tomographic imaging of human tissue at 1.55 μm and 1.81 μm using Er-and Tm-doped fiber sources. *Journal of Biomedical Optics, 3*(1), 76-79.

Burshtein, Z., Blau, P., Kalisky, Y., Shimony, Y., & Kikta, M. (1998). Excited-state absorption studies of Cr 4+ ions in several garnet host crystals. *IEEE journal of quantum electronics, 34*(2), 292-299.

Chang, Y. M., Lee, J., Jhon, Y. M., & Lee, J. H. (2011). Active Q-switching in an erbium-doped fiber laser using an ultrafast silicon-based variable optical attenuator. *Optics Express, 19*(27), 26911-26916.

Chen, H.-R., Wang, Y.-G., Tsai, C.-Y., Lin, K.-H., Chang, T.-Y., Tang, J., & Hsieh, W.-F. (2011). High-power, passively mode-locked Nd: GdVO 4 laser using single-walled carbon nanotubes as saturable absorber. *Optics Letters, 36*(7), 1284-1286.

Chernysheva, M. A., Krylov, A. A., Arutyunyan, N. R., Pozharov, A. S., Obraztsova, E. D., & Dianov, E. M. (2014). SESAM and SWCNT mode-locked all-fiber thulium-doped lasers based on the nonlinear amplifying loop mirror. *IEEE Journal of Selected Topics in Quantum Electronics, 20*(5), 448-455.

Chiu, J.-C., Chang, C.-M., Hsieh, B.-Z., Lin, S.-C., Yeh, C.-Y., Lin, G.-R., . . . Cheng, W.-H. (2011). Pulse shortening mode-locked fiber laser by thickness and concentration product of carbon nanotube based saturable absorber. *Optics Express, 19*(5), 4036-4041.

Cho, W. B., Schmidt, A., Yim, J. H., Choi, S. Y., Lee, S., Rotermund, F., . . . Mateos, X. (2009). Passive mode-locking of a Tm-doped bulk laser near 2 μm using a carbon nanotube saturable absorber. *Optics Express, 17*(13), 11007-11012.

Clarkson, W., Barnes, N., Turner, P., Nilsson, J., & Hanna, D. (2002). High-power cladding-pumped Tm-doped silica fiber laser with wavelength tuning from 1860 to 2090 nm. *Optics Letters, 27*(22), 1989-1991.

Cunningham, G., Lotya, M., Cucinotta, C. S., Sanvito, S., Bergin, S. D., Menzel, R., . . . Coleman, J. N. (2012). Solvent exfoliation of transition metal dichalcogenides: dispersibility of exfoliated nanosheets varies only weakly between compounds. *ACS nano, 6*(4), 3468-3480.

Digonnet, M. J. (2001a). *Rare-earth-doped fiber lasers and amplifiers, revised and expanded* (2nd ed.): CRC press.

Digonnet, M. J. (2001b). *Rare-earth-doped fiber lasers and amplifiers, revised and expanded* (2nd ed.): CRC press.

Dong, J. (2003). Numerical modeling of CW-pumped repetitively passively Q-switched Yb: YAG lasers with Cr: YAG as saturable absorber. *Optics Communications, 226*(1), 337-344.

Eichhorn, M. (2010). *Pulsed 2 μm fiber lasers for direct and pumping applications in defence and security.* Paper presented at the Security+ Defence.

El-Sherif, A., & King, T. (2003). Soft and hard tissue ablation with short-pulse high peak power and continuous thulium-silica fibre lasers. *Lasers in medical science, 18*(3), 139-147.

Encyclopedia, W. t. f. https://en.wikipedia.org/wiki/Double-clad_fiber.

Fan, Y.-X., Lu, F.-Y., Hu, S.-L., Lu, K.-C., Wang, H.-J., Dong, X.-Y., . . . Wang, H.-T. (2004). Tunable high-peak-power, high-energy hybrid Q-switched double-clad fiber laser. *Optics Letters, 29*(7), 724-726.

Federighi, M., & Di Pasquale, F. (1995). The effect of pair-induced energy transfer on the performance of silica waveguide amplifiers with high Er/sup 3+//Yb/sup 3+/concentrations. *IEEE Photonics Technology Letters, 7*(3), 303-305.

Fermann, M., Hanna, D., Shepherd, D., Suni, P., & Townsend, J. (1988). Efficient operation of an Yb sensitised Er fibre laser at 1.56 μm. *Electronics Letters, 24*(18), 1135-1136.

Fermann, M. E., & Hartl, I. (2013). Ultrafast fibre lasers. *Nature Photonics, 7*(11), 868-874.

Früngel, F. B. (2014). *Optical Pulses-Lasers-Measuring Techniques*: Academic Press.

Fu, B., Hua, Y., Xiao, X., Zhu, H., Sun, Z., & Yang, C. (2014). Broadband graphene saturable absorber for pulsed fiber lasers at 1, 1.5, and 2 μm. *IEEE Journal of Selected Topics in Quantum Electronics, 20*(5), 411-415.

Galvanauskas, M. F. A., & Sucha, G. (2003). Ultrafast Lasers: Technology and applications: Marcel Dekker Inc, ISBN 0-8247-0841-5.

Garmire, E. (2000). Resonant optical nonlinearities in semiconductors. *IEEE Journal of Selected Topics in Quantum Electronics, 6*(6), 1094-1110.

Geng, J., Wu, J., Jiang, S., & Yu, J. (2007). Efficient operation of diode-pumped single-frequency thulium-doped fiber lasers near 2 μm. *Optics Letters, 32*(4), 355-357.

Goze, C., Vaccarini, L., Henrard, L., Bernier, P., Hemandez, E., & Rubio, A. (1999). Elastic and mechanical properties of carbon nanotubes. *Synthetic Metals, 103*(1), 2500-2501.

Grubb, S., Cannon, R., Windhorn, T., Vendetta, S., Leilabady, P., Anton, D., . . . Townsend, J. (1991). *High power sensitized erbium doped fiber amplifier*. Paper presented at the Proceedings of Optical Fiber Communication, OFC.

Grubb, S., Humer, W., Cannon, R., Windhorn, T., Vendetta, S., Sweeney, K., . . . Townsend, J. (1992). + 21 dBm erbium power amplifier pumped by a diode-pumped Nd: YAG laser. *IEEE Photonics Technology Letters, 4*(6), 553-555.

Guo, Y., Sun, X., Liu, Y., Wang, W., Qiu, H., & Gao, J. (2012). One pot preparation of reduced graphene oxide (RGO) or Au (Ag) nanoparticle-RGO hybrids using chitosan as a reducing and stabilizing agent and their use in methanol electrooxidation. *Carbon, 50*(7), 2513-2523.

Gupta, M. C., & Ballato, J. (2006). *The handbook of photonics*: CRC press, ISBN 13: 978-0-8493-3095-7.

Halder, A., Paul, M. C., Damanhuri, S., Huri, N., Hamzah, A., Harun, S., . . . Bhadra, S. K. (2012). Upconversion luminescence in Tm3+/Yb3+ co-doped double-clad silica fibers under 980 nm cladding pumping. *Journal of Modern Optics, 59*(6), 527-532.

Harun, S., Abdul-Rashid, H., Muhd-Yassin, S., Abd-Rahman, M., Jayapalan, K., & Ahmad, H. (2008). 37.2 dB small-signal gain from Er/Yb Co-doped fiber amplifier with 20mW pump power. *Optics & Laser Technology, 40*(1), 88-91.

Harun, S., Ismail, M., Ahmad, F., Ismail, M., Nor, R., Zulkepely, N., & Ahmad, H. (2012). A Q-switched erbium-doped fiber laser with a carbon nanotube based saturable absorber. *Chinese Physics Letters, 29*(11), 114202.

Harun, S., Saidin, N., Damanhuri, S., Ahmad, H., Halder, A., Paul, M. C., . . . Bhadra, S. K. (2011). Fiber laser at 2 micron region using double-clad thulium/ytterbium co-doped yttria-alumino-silicate fiber. *Laser Physics Letters, 9*(1), 50.

Hasan, T., Sun, Z., Wang, F., Bonaccorso, F., Tan, P. H., Rozhin, A. G., & Ferrari, A. C. (2009). Nanotube–polymer composites for ultrafast photonics. *Advanced Materials, 21*(38-39), 3874-3899.

Haus, H. A. (2000). Mode-locking of lasers. *IEEE Journal of Selected Topics in Quantum Electronics, 6*(6), 1173-1185.

Henderson, S. W., Suni, P. J., Hale, C. P., Hannon, S. M., Magee, J. R., Bruns, D. L., & Yuen, E. H. (1993). Coherent laser radar at 2 μm using solid-state lasers. *IEEE Transactions on Geoscience and Remote Sensing, 31*(1), 4-15.

Jackson, S. D. (2004). Cross relaxation and energy transfer upconversion processes relevant to the functioning of 2 μm Tm 3+-doped silica fibre lasers. *Optics Communications, 230*(1), 197-203.

Jeong, Y., Sahu, J., Soh, D., Codemard, C., & Nilsson, J. (2005). High-power tunable single-frequency single-mode erbium: ytterbium codoped large-core fiber master-oscillator power amplifier source. *Optics Letters, 30*(22), 2997-2999.

Jeong, Y., Yoo, S., Codemard, C. A., Nilsson, J., Sahu, J. K., Payne, D. N., . . . Harker, A. (2007). Erbium: ytterbium codoped large-core fiber laser with 297-W continuous-wave output power. *IEEE Journal of Selected Topics in Quantum Electronics, 13*(3), 573-579.

Jeong, Y. e., Sahu, J., Payne, D., & Nilsson, J. (2004). Ytterbium-doped large-core fiber laser with 1.36 kW continuous-wave output power. *Optics Express, 12*(25), 6088-6092.

Jung, M., Lee, J., Park, J., Koo, J., Jhon, Y. M., & Lee, J. H. (2015). Mode-locked, 1.94-μm, all-fiberized laser using WS 2-based evanescent field interaction. *Optics Express, 23*(15), 19996-20006.

Kashiwagi, K., & Yamashita, S. (2010). *Optical Deposition of Carbon Nanotubes for Fiber-based Device Fabrication*: INTECH Open Access Publisher.

Kataura, H., Kumazawa, Y., Maniwa, Y., Umezu, I., Suzuki, S., Ohtsuka, Y., & Achiba, Y. (1999). Optical properties of single-wall carbon nanotubes. *Synthetic Metals, 103*(1), 2555-2558.

KINCADE, K. (2005). Optoelectronics applications: Biophotonics fiber lasers find new opportunities in medical applications. *Laser focus world, 41*(9).

Kobtsev, S., Kukarin, S., & Fedotov, Y. (2008). High-energy Q-switched fiber laser based on the side-pumped active fiber. *Laser Physics, 18*(11), 1230-1233.

Kozma, G., & Kˇnya, Z. (2013). Multi-Walled Carbon Nanotubes *Springer Handbook of Nanomaterials* (pp. 147-188): Springer, ISBN 978-3-642-20594-1.

Li, D., Shen, D., Li, L., Chen, H., Tang, D., & Zhao, L. (2015). Unidirectional dissipative soliton operation in an all-normal-dispersion Yb-doped fiber laser without an isolator. *Applied optics, 54*(26), 7912-7916.

Li, H., Zhang, Q., Yap, C. C. R., Tay, B. K., Edwin, T. H. T., Olivier, A., & Baillargeat, D. (2012). From bulk to monolayer MoS2: evolution of Raman scattering. *Advanced Functional Materials, 22*(7), 1385-1390.

Li, P., Zhao, Z., Zhang, M., Liang, B., Chi, J., Yang, C., . . . Ma, C. (2015). Subpicosecond SESAM and nonlinear polarization evolution hybrid mode-locking ytterbium-doped fiber oscillator. *Applied Physics B, 118*(4), 561-566.

Lin, J. H., Lin, K.-H., Hsu, C., Yang, W., & Hsieh, W. F. (2007). Supercontinuum generation in a microstructured optical fiber by picosecond self Q-switched mode-locked Nd: GdVO4 laser. *Laser Physics Letters, 4*(6), 413.

Lin, X. C., Zhang, L., Tsang, Y. H., Wang, Y. G., Yu, H. J., Yan, S. L., . . . Hou, W. (2013). Multi-walled carbon nanotube as a saturable absorber for a passively mode-locked Nd: YVO4 laser. *Laser Physics Letters, 10*(5), 055805.

Liu, H., Luo, A.-P., Wang, F.-Z., Tang, R., Liu, M., Luo, Z.-C., . . . Zhang, H. (2014). Femtosecond pulse erbium-doped fiber laser by a few-layer MoS 2 saturable absorber. *Optics Letters, 39*(15), 4591-4594.

Liu, J., Wang, Q., & Wang, P. (2012). High average power picosecond pulse generation from a thulium-doped all-fiber MOPA system. *Optics Express, 20*(20), 22442-22447.

Liu, J., Xu, J., & Wang, P. (2012). High repetition-rate narrow bandwidth SESAM mode-locked Yb-doped fiber lasers. *IEEE Photonics Technology Letters, 24*(7), 539-541.

Lu, B., Chen, H., Jiang, M., Chen, X., Ren, Z., & Bai, J. (2013). Graphene-based passive Q-switching for a 2 μm thulium-doped fiber laser. *Laser Physics, 23*(4), 045111.

Luo, Z.-C., Luo, A.-P., Xu, W.-C., Yin, H.-S., Liu, J.-R., Ye, Q., & Fang, Z.-J. (2010). Tunable multiwavelength passively mode-locked fiber ring laser using intracavity birefringence-induced comb filter. *IEEE Photonics Journal, 2*(4), 571-577.

Martin E. Fermann, A. G., Gregg Sucha. (2003). *Ultra fast lasers, Technology and applications*. New York, Basel: Marcel Dekker, INC, ISBN 0-8247-0841-5.

Martinez, A., & Sun, Z. (2013). Nanotube and graphene saturable absorbers for fibre lasers. *Nature Photonics, 7*(11), 842-845.

Mary, R., Choudhury, D., & Kar, A. K. (2014). Applications of fiber lasers for the development of compact photonic devices. *IEEE Journal of Selected Topics in Quantum Electronics, 20*(5), 72-84.

McAleavey, F. J., O'Gorman, J., Donegan, J. F., MacCraith, B. D., Hegarty, J., & Mazé, G. (1997). Narrow linewidth, tunable Tm 3+-doped fluoride fiber laser for optical-based hydrocarbon gas sensing. *IEEE Journal of Selected Topics in Quantum Electronics, 3*(4), 1103-1111.

McClung, F., & Hellwarth, R. (1962). Giant optical pulsations from ruby. *Journal of Applied Physics, 33*(3), 828-829.

Mindly, J., Barnes, W., Laming, R., Morkel, P., Townsend, J., Grubb, S., & Payne, D. (1993). Diode-Array Pumping of Er3+/Yt> 3+ Co-Doped Fiber Lasers and Amplifiers. *IEEE Photonics Technology Letters, 5*(3).

Mingareev, I., Weirauch, F., Olowinsky, A., Shah, L., Kadwani, P., & Richardson, M. (2012). Welding of polymers using a 2μm thulium fiber laser. *Optics & Laser Technology, 44*(7), 2095-2099.

Myslinski, P., Nguyen, D., & Chrostowski, J. (1997). Effects of concentration on the performance of erbium-doped fiber amplifiers. *Journal of Lightwave Technology, 15*(1), 112-120.

Nayar, B., Lewandowski, J., Wilson, F., Chavez, J., Grudinin, A., Minelly, J., . . . Raven, A. (1998). *High power 1540 nm fibre lasers for surgical applications.* Paper presented at the Lasers and Electro-Optics Society Annual Meeting, 1998. LEOS'98. IEEE.

Nettleton, J. E., Schilling, B. W., Barr, D. N., & Lei, J. S. (2000). Monoblock laser for a low-cost, eyesafe, microlaser range finder. *Applied optics, 39*(15), 2428-2432.

Ngo, N. Q. (2011). *Ultra-fast fiber lasers: principles and applications with MATLAB® models*: CRC Press, ISBN 13: 978-1-4398-1130-6.

Ngo., L. N. B. a. N. Q. (2011). *Ultra-Fast Fiber lasers Principles and Applications with MATLAB® Models*: CRC Press Taylor & Francis Group, ISBN 978-1-4398-1130-6.

Nilsson, J., Jaskorzynska, B., & Blixt, P. (1993). Performance reduction and design modification of erbium-doped fiber amplifiers resulting from pair-induced quenching. *IEEE Photonics Technology Letters, 5*(12), 1427-1429.

Nishizawa, N. (2014). Ultrashort pulse fiber lasers and their applications. *Japanese Journal of Applied Physics, 53*(9), 090101.

Opsommer, E., Weiss, T., Miltner, W., & Plaghki, L. (2001). Scalp topography of ultralate (C-fibres) evoked potentials following thulium YAG laser stimuli to tiny skin surface areas in humans. *Clinical neurophysiology, 112*(10), 1868-1874.

Pal, A., Dhar, A., Das, S., Chen, S. Y., Sun, T., Sen, R., & Grattan, K. T. (2010). Ytterbium-sensitized Thulium-doped fiber laser in the near-IR with 980 nm pumping. *Optics Express, 18*(5), 5068-5074.

Park, N., Wysocki, P., Pedrazzani, R., Grubb, S., DiGiovanni, D., & Walker, K. (1996). High-power Er-Yb-doped fiber amplifier with multichannel gain flatness within 0.2 dB over 14 nm. *IEEE Photonics Technology Letters, 8*(9), 1148-1150.

Paschotta, D. R. from https://www.rp-photonics.com/q_switching.html.

Paschotta, D. R. Encyclopedia of Laser Physics and Technoligy, Q-Switching. https://www.rp-photonics.com/q_switching.html.

Paschotta, D. R. Encyclopedia of Laser Physics and Technology, Rare-earth-doped Fibers. https://www.rp-photonics.com/rare_earth_doped_fibers.html.

Paschotta, R. (2008). *Field guide to laser pulse generation* (Vol. 14): SPIE Press Bellington.

Paschotta, R., Nilsson, J., Barber, P., Caplen, J., Tropper, A. C., & Hanna, D. C. (1997). Lifetime quenching in Yb doped fibres. *Optics Communications, 136*(5-6), 375-378.

Pask, H., Carman, R. J., Hanna, D. C., Tropper, A. C., Mackechnie, C. J., Barber, P. R., & Dawes, J. M. (1995). Ytterbium-doped silica fiber lasers: versatile sources for the 1-1.2 μm region. *IEEE Journal of Selected Topics in Quantum Electronics, 1*(1), 2-13.

Pierce, M. C., Jackson, S. D., Dickinson, M. R., & King, T. A. (1999). Laser–tissue interaction with a high-power 2-μm fiber laser: Preliminary studies with soft tissue. *Lasers in surgery and medicine, 25*(5), 407-413.

Po, H., Snitzer, E., Tumminelli, R., Zenteno, L., Hakimi, F., Cho, N., & Haw, T. (1989). *Double clad high brightness Nd fiber laser pumped by GaAlAs phased array.* Paper presented at the Optical Fiber Communication Conference.

Polder, K. D., & Bruce, S. (2012). Treatment of Melasma Using a Novel 1,927-nm Fractional Thulium Fiber Laser: A Pilot Study. *Dermatologic Surgery, 38*(2), 199-206.

Qamar, F. Z., & King, T. A. (2005). Passive Q-switching of the Tm-silica fibre laser near 2μm by a Cr 2+: ZnSe saturable absorber crystal. *Optics Communications, 248*(4), 501-508.

Qiao, J., Zhao, J., Yang, K., Zhao, S., Li, Y., Li, G., . . . Chu, H. (2015). Diode-pumped Nd: Gd3Ga5O12–KTiOPO4 green laser doubly passively Q-switched mode-locked by GaAs and Cr4+: YAG saturable absorbers. *Japanese Journal of Applied Physics, 54*(3), 032701.

Savastru, D., Miclos, S., & Lancranjan, I. (2012). THEORETICAL ANALYSIS OF A PASSIVELY Q-SWITCHED ERBIUM DOPED FIBER LASER. *Nonconventional Technologies Review/Revista de Tehnologii Neconventionale, 16*(1).

Scholle, K., Fuhrberg, P., Koopmann, P., & Lamrini, S. (2010). *2 μm laser sources and their possible applications*: INTECH Open Access Publisher.

Sen, R., Saha, M., CHOWDHURY, S. D., KUMAR, N., SHEKHAR, D. P., Ghosh, A., . . . Pal, M. (2015). High powder fiber lasers: fundamentals to applications. *Science and Culture*.

Set, S. Y., Yaguchi, H., Tanaka, Y., & Jablonski, M. (2004). Laser mode locking using a saturable absorber incorporating carbon nanotubes. *Journal of Lightwave Technology, 22*(1), 51-56.

Simpson, D. A., Gibbs, W., Collins, S. F., Blanc, W., Dussardier, B., Monnom, G., . . . Baxter, G. W. (2008). Visible and near infra-red up-conversion in Tm 3+/Yb 3+ co-doped silica fibers under 980 nm excitation. *Optics Express, 16*(18), 13781-13799.

Snitzer, E., Po, H., Hakimi, F., Tumminelli, R., & McCollum, B. (1988). *Double clad, offset core Nd fiber laser*. Paper presented at the Optical fiber sensors.

Solodyankin, M. A., Obraztsova, E. D., Lobach, A. S., Chernov, A. I., Tausenev, A. V., Konov, V. I., & Dianov, E. M. (2008). Mode-locked 1.93 μm thulium fiber laser with a carbon nanotube absorber. *Optics Letters, 33*(12), 1336-1338.

Sorokina, I. T., Dvoyrin, V. V., Tolstik, N., & Sorokin, E. (2014). Mid-IR ultrashort pulsed fiber-based lasers. *IEEE Journal of Selected Topics in Quantum Electronics, 20*(5), 99-110.

Spiers, G. D., Menzies, R. T., Jacob, J., Christensen, L. E., Phillips, M. W., Choi, Y., & Browell, E. V. (2011). Atmospheric CO 2 measurements with a 2 μm airborne laser absorption spectrometer employing coherent detection. *Applied optics, 50*(14), 2098-2111.

Sudo, S. (1997). *Optical fiber amplifiers: materials, devices, and applications*: Artech house.

Sun, Z., Hasan, T., & Ferrari, A. (2012). Ultrafast lasers mode-locked by nanotubes and graphene. *Physica E: Low-dimensional Systems and Nanostructures, 44*(6), 1082-1091.

Sun, Z., Hasan, T., Torrisi, F., Popa, D., Privitera, G., Wang, F., . . . Ferrari, A. C. (2010). Graphene mode-locked ultrafast laser. *ACS nano, 4*(2), 803-810.

Taccheo, S., Laporta, P., Svelto, O., & De Geronimo, G. (1998). Theoretical and experimental analysis of intensity noise in a codoped erbium–ytterbium glass laser. *Applied Physics B: Lasers and Optics, 66*(1), 19-26.

Tang, Y., Yang, Y., Xu, J., & Hang, Y. (2008). Passive Q-switching of short-length Tm 3+-doped silica fiber lasers by polycrystalline Cr 2+: ZnSe microchips. *Optics Communications, 281*(22), 5588-5591.

Tanguy, E., Larat, C., & Pocholle, J.-P. (1998). Modelling of the erbium–ytterbium laser. *Optics Communications, 153*(1), 172-183.

Taylor, N. (2002). *LASER: The inventor, the Nobel laureate, and the thirty-year patent war*: Simon and Schuster, 0-7432-1321-1.

Theisen-Kunde, D., Tedsen, S., Herrmann, K., Danicke, V., & Brinkmann, R. (2007). *Partial kidney resection based on 1.94 µm fiber laser system.* Paper presented at the European Conference on Biomedical Optics.

Tian, W., Wang, C., Wang, G., Liu, S., & Liu, J. (2007). Performance of diode-pumped passively Q-switched mode-locking Nd: GdVO4/KTP green laser with Cr4+: YAG. *Laser Physics Letters, 4*(3), 196-199.

Tian, Z., Wu, K., Kong, L., Yang, N., Wang, Y., Chen, R., . . . Tang, Y. (2015). Mode-locked thulium fiber laser with MoS2. *Laser Physics Letters, 12*(6), 065104.

Tongay, S., Varnoosfaderani, S. S., Appleton, B. R., Wu, J., & Hebard, A. F. (2012). Magnetic properties of MoS2: Existence of ferromagnetism. *Applied Physics Letters, 101*(12), 123105.

Upadhyaya, B. (2014). High-power Yb-doped continuous-wave and pulsed fibre lasers. *Pramana, 82*(1), 15-27.

Wang, F., Rozhin, A., Scardaci, V., Sun, Z., Hennrich, F., White, I., . . . Ferrari, A. C. (2008). Wideband-tuneable, nanotube mode-locked, fibre laser. *Nature nanotechnology, 3*(12), 738-742.

Wang, J., Liang, X., Hu, G., Zheng, Z., Lin, S., Ouyang, D., . . . Sun, Z. (2016). 152 fs nanotube-mode-locked thulium-doped all-fiber laser. *Scientific reports, 6*.

Wang, K., Wang, J., Fan, J., Lotya, M., O'Neill, A., Fox, D., . . . Zhao, Q. (2013). Ultrafast saturable absorption of two-dimensional MoS2 nanosheets. *ACS nano, 7*(10), 9260-9267.

Wang, Q., Teng, H., Zou, Y., Zhang, Z., Li, D., Wang, R., . . . Wei, Z. (2012). Graphene on SiC as a Q-switcher for a 2 µm laser. *Optics Letters, 37*(3), 395-397.

Wang, Y., & Xu, C.-Q. (2007). Actively Q-switched fiber lasers: Switching dynamics and nonlinear processes. *Progress in Quantum Electronics, 31*(3), 131-216.

Webb, C. E., & Jones, J. D. (2004). *Handbook of Laser Technology and Applications: Laser design and laser systems* (Vol. 2): CRC Press, ISBN 9780750306072.

Xing, G., Guo, H., Zhang, X., Sum, T. C., & Huan, C. H. A. (2010). The Physics of ultrafast saturable absorption in graphene. *Optics Express, 18*(5), 4564-4573. doi: 10.1364/OE.18.004564

Xu, X., Zhai, J., Li, L., Chen, Y., Yu, Y., Zhang, M., . . . Tang, Z. (2014). Passively mode-locking erbium-doped fiber lasers with 0.3 [emsp14] nm Single-Walled Carbon Nanotubes. *Scientific reports, 4*.

Yahel, E., & Hardy, A. (2003). Efficiency optimization of high-power, Er 3+–Yb 3+-codoped fiber amplifiers for wavelength-division-multiplexing applications. *JOSA B, 20*(6), 1189-1197.

Yamashita, S. (2012). A tutorial on nonlinear photonic applications of carbon nanotube and graphene. *Journal of Lightwave Technology, 30*(4), 427-447.

Yim, C., O'Brien, M., McEvoy, N., Winters, S., Mirza, I., Lunney, J. G., & Duesberg, G. S. (2014). Investigation of the optical properties of MoS2 thin films using spectroscopic ellipsometry. *Applied Physics Letters, 104*(10), 103114.

Zayhowski, J., & Kelley, P. (1991). Optimization of Q-switched lasers. *IEEE journal of quantum electronics, 27*(9), 2220-2225.

Zdrojek, M., Gebicki, W., Jastrzebski, C., Melin, T., & Huczko, A. (2004). *Studies of multiwall carbon nanotubes using Raman spectroscopy and atomic force microscopy.* Paper presented at the Solid State Phenomena.

Zen, D., Saidin, N., Damanhuri, S., Harun, S., Ahmad, H., Ismail, M., . . . Das, S. (2013). Mode-locked thulium–bismuth codoped fiber laser using graphene saturable absorber in ring cavity. *Applied optics, 52*(6), 1226-1229.

Zhang, H., Lu, S., Zheng, J., Du, J., Wen, S., Tang, D., & Loh, K. (2014). Molybdenum disulfide (MoS 2) as a broadband saturable absorber for ultra-fast photonics. *Optics Express, 22*(6), 7249-7260.

Zhang, H., Tang, D., Zhao, L., Bao, Q., & Loh, K. (2009). Large energy mode locking of an erbium-doped fiber laser with atomic layer graphene. *Optics Express, 17*(20), 17630-17635.

Zhang, L., Wang, Y., Yu, H., Sun, L., Hou, W., Lin, X., & Li, J. (2011). Passive mode-locked Nd: YVO4 laser using a multi-walled carbon nanotube saturable absorber. *Laser Physics, 21*(8), 1382-1386.

Zhang, Z., Boyland, A., Sahu, J., Clarkson, W., & Ibsen, M. (2011). High-power single-frequency thulium-doped fiber DBR laser at 1943 nm. *IEEE Photonics Technology Letters, 23*(7), 417-419.

Zhang, Z., Popa, D., Sun, Z., Hasan, T., Ferrari, A., & Ilday, F. (2013). *All-fiber Yb-doped laser mode-locked by nanotubes.* Paper presented at the Lasers and Electro-Optics Europe (CLEO EUROPE/IQEC), 2013 Conference on and International Quantum Electronics Conference.

Zheng, Z., Zhao, C., Lu, S., Chen, Y., Li, Y., Zhang, H., & Wen, S. (2012). Microwave and optical saturable absorption in graphene. *Optics Express, 20*(21), 23201-23214.

ZULKIFLI, A. Z. B. (2015). *Fabrication and Characterization of Graphene Oxide Saturable Absorber for Q-switched Fiber Laser Generation.* (Ph.D), University of Malaya, Kuala Lumpur , Malaysia.

LIST OF PUBLICATIONS

1) I. M. Babar, M. B. S. Sabran, Z. Jusoh, H. Ahmad, S. W. Harun, A. Halder, M. C. Paul, S. Das and S. K. Bhadra; Thulium-Ytterbium co-doped Octagonal Shaped Double-Clad Fiber for Fiber Laser Applications; Ukrainian Journal of Physical Optics, Vol. 15, issue 4, 173-183 (2014).
2) I. M. Babar, M. B. S. Sabran, S. W. Harun, H. Ahmad, M. C. Paul, A. Halder, S. Das and S.K Bhadra; Q-switched Thulium-Ytterbium co-doped fiber laser using newly developed octagonal shaped double-clad active fiber and multi-walled carbon nano tubes passive saturable absorber; IET Optolectronics, Vol. 9, Iss. 3, pp. 131–135, (2015).
3) I. M. Babar, M. B. S. Sabran, A. A. Rahman, M. Manaf, H. Ahmad and S. W. Harun; Multi-lobed double clad Erbium-Ytterbium co doped Q-switched fiber laser based on nonlinear polarization rotation technique; Journal of nonlinear optical physics and materials(JNOPM); Volume 24, Issue 01, (2015).
4) Ibrahim M. Babar, Mukul C. Paul, Shyamal Das, Anirban Dhar, Harith Ahmad1 and Sulaiman W. Harun; Mode-locked Thulium Ytterbium co-Doped Fiber Laser with a Graphene Saturable Absorber; Photonics letters of Poland; vol. 8 (4), 104-106 (2016).
5) I. M. Babar, S. W. Harun, M. Yasin and H. Ahmad; Mode-locking Pulse Generation in Cladding Pumped Erbium-Ytterbium co-doped Fiber Laser With Graphene PVA Film; Optik - International Journal for Light and Electron Optics; Available online 23rd February 2017.